

# A random walk through surface scattering phenomena: Theory and phenomenology

Ingve Simonsen\*

*Department of Physics, Norwegian University of Science and Technology, NO-7491 Trondheim, Norway*

(Dated: October 29, 2018)

No surface is perfectly planar at all scales. The notion of flatness of a surface therefore depends on the size of the probe used to observe it. As a consequence rough interfaces are abundant in nature. Here the old, but still active field of rough surface scattering of electromagnetic waves is addressed. This topic has implications and practical applications in fields as diverse as observational astronomy and the electronics industry. This article reviews the theoretical and computational foundation and methods used in the study of rough surface scattering. Furthermore, it presents and explains the physical origin of a series of multiple scattering surface phenomena. In particular what is discussed are: the enhanced backscattering and satellite peak phenomena, coherent effects in angular intensity correlation functions and second harmonic generated light (a non-linear effect).

Keywords: Wave scattering; random systems; multiple scattering; coherent effects

## Contents

|  |    |
|--|----|
| <b>I. Introduction</b>   | 2  |
| <b>II. Elements of Electromagnetic theory</b>                                  | 4  |
| A. Maxwell's Equations and the Constitutive Equations                          | 4  |
| 1. Maxwell's Equations   | 4  |
| 2. Constitutive Equations  | 5  |
| B. The Electromagnetic Wave Equations  | 6  |
| C. Boundary Conditions   | 7  |
| 1. Boundary Condition at a General One-Dimensional Surface                     | 7  |
| D. Surface Plasmon Polaritons  | 9  |
| 1. SPPs on a plan surface geometry   | 9  |
| 2. SPPs at a planar free electron metal surface                                | 10 |
| E. Characterization of Random Rough Surfaces                                   | 10 |
| F. A Statistical description of Randomly Rough Surfaces                        | 11 |
| 1. Gaussian Random Surfaces  | 12 |
| 2. Non-Gaussian Random Surfaces  | 14 |
| G. Self-affine surfaces  | 14 |
| H. Numerical Generation of Randomly Rough Surfaces                             | 16 |
| <b>III. Quantities and Techniques used in Rough Surface Scattering Studies</b> | 17 |
| A. The Scattering Geometry   | 17 |
| B. The Scattered Field   | 17 |
| 1. Plane Incident Wave   | 18 |
| 2. Finite Width Incident Wave  | 18 |
| C. The mean differential reflection coefficient                                | 19 |
| 1. Plane incident wave   | 20 |
| 2. Finite width incident beam  | 21 |
| D. General Properties of the Scattering Problem                                | 21 |
| 1. Reciprocity   | 21 |
| 2. Unitarity   | 22 |
| 3. Energy Conservation   | 22 |
| E. Derivation of the Reduced Rayleigh Equation                                 | 23 |

---

\*Electronic address: [Ingve.Simonsen@phys.ntnu.no](mailto:Ingve.Simonsen@phys.ntnu.no)

|  |    |
|--|----|
| 1. The Rayleigh Hypothesis   | 23 |
| 2. The Rayleigh Equations  | 24 |
| 3. The Reduced Rayleigh Equations  | 24 |
| 4. The Reduced Rayleigh Equation for Transmission  | 26 |
| F. Small Amplitude Perturbation Theory   | 26 |
| G. Unitary and Reciprocal Expansions   | 29 |
| 1. The Transition Matrix   | 29 |
| 2. The Scattering Potential  | 30 |
| H. Many-Body Perturbation Theory   | 31 |
| I. Numerical Simulation Approach   | 33 |
| 1. The Extinction Theorem  | 33 |
| 2. A Remark on the Accuracy of the Numerical Simulation Approach   | 38 |
| <b>IV. Physical Phenomena in Electromagnetic Rough Surface Scattering</b>                                | 38 |
| A. Coherent Effects in Multiple-Scattered Fields: Weak Localization of Light on a Randomly Rough Surface | 39 |
| 1. Enhanced backscattering   | 39 |
| 2. Satellite Peaks   | 44 |
| 3. A Formal Approach to Enhanced Backscattering and Satellite Peaks                                      | 45 |
| B. Localization  | 46 |
| 1. The Scattering System   | 48 |
| 2. Surfaces that Suppress Leakage  | 48 |
| 3. The Anderson Localization Length for Surface Plasmon Polaritons Localized on a Randomly Rough Surface | 50 |
| C. Angular Intensity Correlations for the Scattered Light from Randomly Rough Surfaces                   | 51 |
| 1. Definition of the Angular Intensity Correlation Functions   | 53 |
| 2. Short Range Correlations for Weakly rough Surfaces  | 54 |
| 3. Long- and Infinite-Range Correlations   | 58 |
| 4. Angular Intensity Correlation Functions for Strongly Rough Surfaces                                   | 59 |
| D. Second Harmonic Generation of Scattered Light   | 61 |
| 1. Strongly Rough Surfaces: A Numerical Simulation Approach to the Second Harmonic Generated Light       | 61 |
| 2. Weakly Rough Surfaces   | 65 |
| <b>V. Directions for Future Research</b>   | 66 |
| <b>Acknowledgement</b>   | 67 |
| <b>A. Matrix Elements</b>  | 67 |
| <b>B. The <math>\chi</math>-functions used in Small Amplitude Perturbation Theory</b>                    | 69 |
| 1. P-polarization  | 70 |
| 2. S-polarization  | 70 |
| <b>References</b>  | 70 |

## I. INTRODUCTION

We are surrounded by waves, and they effect our daily life in a way that many of us are not aware. Sound and light are our main tools for observing our immediate surroundings. Light is for example responsible for you being able to read these lines, and more important, to get access to the vast majority of the knowledge accumulated in writings by man throughout centuries of intellectual activities. X-ray and ultra sound techniques have given tremendous contribution to the success of modern medicine. Radio- and micro-waves are invaluable in modern communication technology including cellular phones and radio and TV broadcastings. Understanding of quantum waves, and their behavior, constitutes the foundation of electronics and semiconductor technologies — an essential ingredient in the past and future progress of computer hardware. The above list is not at all, or intended to be, complete. It could in fact easily been made much longer. However, the bottom line that we want to make here is that with the ubiquitous presence of wave phenomena in various applications, it is not surprising to find that wave phenomena have had, and still have, a prominent position in our studies of the physical world, and even today such phenomena are of out-most importance in science, medicine and technology.

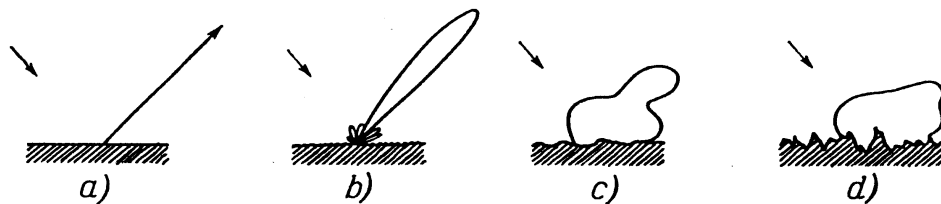


FIG. 1: An illustration showing the transition from specular (Fig. 1a) to diffuse scattering (Fig. 1d) of light from a surface of increasing roughness. The arrows indicate the direction of the incident light (After Ref. [5]).

If you take an average introductory text on wave phenomena, you will find discussions of how plane waves of constant frequency propagates in a homogeneous, isotropic medium. Thereafter, the authors typically discuss the scattering and transmission of such waves at a *planar* interface separating two semi-infinite media of different dielectric properties [11] — the Fresnel formulae. These formulae serve to accurately describe the scattering of light from for example a mirror. However, from our everyday experience, we know that most surfaces are not mirror like, and naturally occurring objects are more complicated than two semi-infinite media. Most naturally occurring surfaces are actually not smooth at all. They are, however, rough in some sense. In fact, all objects, man-made or not, *have* to be rough at atomic scales, but such small length scales are normally not resolved by our probes.

It should be kept in mind that the characterization of a surface as rough or smooth is noticeably not unique, and it is not an intrinsic property of the surface. Instead, however, it depends on the wavelength used to “observe” the surface. If the typical roughness is on a scale much smaller than the wavelength of the probe, this surface is considered as smooth. However, by reducing the wavelength of the light, the same surface might also be characterized as being rough. It is, among other factors, the surface topography and the wavelength of the probe, as we will see below, that together go into the characterization of a surface as being rough<sup>1</sup>.

Let us from now on assume an electromagnetic probe, *i.e.* light. If the surface can be considered as smooth, light is scattered (coherently) into the specular direction. As the roughness of the surface is increased so that the surface becomes weakly rough, a small fraction of the incident light will be scattered into other directions than the specular one. This non-specular scattering is called *diffuse scattering* or by some authors *incoherent scattering*. As the roughness is increased even further, the diffuse (incoherent) component of the scattered light is increased on the expense of the specular component. When the surface roughness is so that the specular component can be more-or-less neglected as compared to the diffuse component, the surface is said to be strongly rough. This transition from a smooth to a strongly rough surface is depicted in Figs. 1.

Due to the practical applications of waves, and the number of naturally occurring surfaces being rough, it is rather remarkable that it took several hundreds years from the birth of optics as a scientific discipline to someone started to consider wave scattering from rough surfaces. As far as we know today, the first such theoretical study was made at the end of the 19th century (probably in the year of 1877) by one of the greatest scientists of its time, the British physicist Lord Rayleigh [1, 2]. He considered the scattering of light incident normally onto a sinusoidal surface.

In 1913 Mandel’shtam studied how light was scattered from liquid surfaces [3]. By doing so, he became the first to consider scattering from *randomly* rough surfaces. This, as it turned out, should define the beginning of an active research area — *wave scattering from randomly rough surfaces* — which still today is an active field. However, it was first after the last world war that the research effort put into the field started to accelerate [4]. Since that time, a massive body of research literature has been generated in the field [5–8].

Up to the mid 1980’s most of the theories used in this field were single scattering theories [5–7]. However, from then on the main focus of the research has been on multiple scattering theories. In addition, advances in experimental techniques has lately enabled experimentalists to fabricate surfaces under well controlled conditions by using a holographic grating technique [9]. This has opened up a unique possibility for direct comparison of theory and experiments in a way not possible a few decades ago.

Inspired by the works of Lord Rayleigh [1, 2] researchers developed a criterion — the Rayleigh criterion — that

<sup>1</sup> When discussing the Rayleigh criterion later in this section we will see that also the angle of incidence of the light will play an important role.

could be used to determine when a given surface was to be considered as rough. Here both the wavelength of the incident light as well as its angle of incidence are incorporated [6].

To illustrate how this comes about, let us consider a rough surface defined by  $x_3 = \zeta(x_1)$ . On this surface we pick two arbitrary points  $(\xi, \zeta(\xi))$  and  $(\xi', \zeta(\xi'))$ . It could now be asked: What is the phase difference between two waves being scattered from these two points? For simplicity we will here only consider the specular direction. Under this assumption it is straight forward to show that the phase difference is given by the following expression

$$\Delta\phi = 2|\mathbf{k}||\zeta(\xi) - \zeta(\xi')| \cos\theta_0, \quad (1)$$

where  $|\mathbf{k}| = 2\pi/\lambda$  is the modulus of the wave vector of the incident light of wavelength  $\lambda$ , and  $\theta_0$  is the angle of incidence of the light as measured from the normal to the mean surface. From Eq. (1) we immediately observe that if the surface is planar, so that  $\zeta(\xi) = \zeta(\xi')$ , the phase difference (in the specular direction) is always zero independent of the angle of incidence. However, if the surface is rough,  $\Delta\phi \neq 0$  in general. If  $\Delta\phi \ll \pi$ , the two waves will be in, or almost in, phase and they will thus interfere constructively. On the other hand, if  $\Delta\phi \simeq \pi$ , they will be (more-or-less) completely out of phase and as a result interfere destructively, and no, or almost no, energy will be scattered into the specular direction. In terms of the phase, a smooth surface would correspond to  $\Delta\phi \ll \pi$ , and a rough one to  $\Delta\phi \simeq \pi$ . Thus,  $\Delta\phi = \pi/2$  might be considered as the borderline between a smooth and a rough surface; if  $\Delta\phi < \pi/2$  the surface is smooth, and otherwise ( $\pi/2 < \Delta\phi \leq \pi$ ) it is rough. The criterion  $\Delta\phi < \pi/2$  is the famous Rayleigh criterion for a smooth surface.

If the surface is randomly rough, it is practical to replace the height difference  $\zeta(\xi) - \zeta(\xi')$  by a typical height fluctuation as provided, for example, by the RMS-height,  $\delta$ , of the surface. Hence, the Rayleigh criterion can be expressed as

$$R_a = |\mathbf{k}|\delta \cos\theta_0 < \frac{\pi}{4}, \quad (2)$$

where  $R_a$  is the so-called Rayleigh parameter. From the Rayleigh criterion,  $R_a < \pi/4$ , it should be observed that in addition to the surface topography itself and the wavelength of the light, also its angle of incidence goes into determining if a surface is rough or not. This is probably the most important lesson to be learned today from the Rayleigh criterion.

The present review consists of basically two main parts — one focus theoretical methods whilst the other one is devoted to rough surface scattering phenomenology. In the first part we try to present an overview of some of the main theories and methods used in the study of wave scattering from randomly rough surfaces. We start in Sect. II by recapitulating the basic results of electromagnetic theory including Maxwell's equations. This section serves among other things to define our notation. Then we continue by describing how to characterize randomly rough surfaces (Sect. II E). Sect. III is devoted to the quantities and main techniques used in the field of electromagnetic wave scattering from randomly rough surfaces. We here review classical theories like small amplitude perturbation theory, many-body perturbation theory as well as numerical simulation approaches. Finally in Sect. IV we discuss some of the phenomena that may occur when light is scattered from rough surfaces. Such effects include the backscattering and satellite peaks phenomena (weak localization), Anderson localization, angular intensity correlation effects and nonlinear effects (second harmonic generation).

## II. ELEMENTS OF ELECTROMAGNETIC THEORY

The present review mainly concern itself with rough surfaces and the scattering of electromagnetic wave from such. In this section we therefor review some of the basic results of electromagnetic theory, including surface polaritons. The present section also serves to define our notation that we will use extensively in the following sections. The style of this review is kept quite brief, since all the material should be well known. A more thorough treatments can be found for example in the classical text on electrodynamics by J. D. Jackson [34].

### A. Maxwell's Equations and the Constitutive Equations

#### 1. Maxwell's Equations

The Maxwell's equations, which unify in one magnificent theory all the phenomena of electricity and magnetism, were put forward by the Scottish physicist James Clerk Maxwell (1831–1879). These equations are the fundamental

| Quantity     | SI-unit  | Name                  |
|--------------|----------|-----------------------|
| $\mathbf{E}$ | $V/m$    | Electric field        |
| $\mathbf{H}$ | $A/m$    | Magnetic field        |
| $\mathbf{D}$ | $C/m^2$  | Electric displacement |
| $\mathbf{B}$ | $Wb/m^2$ | Magnetic induction    |
| $\rho$       | $C/m^3$  | Charge density        |
| $\mathbf{J}$ | $A/m^2$  | Current density       |

TABLE I: Summary of the quantities contained in Maxwell's equations, as well as their SI-units.

equations of electromagnetism, in the same way that Newton's law is to classical mechanics. In fact, the Maxwell's equations are in a way even more fundamental since they are consistent with the theory of special relativity that Einstein develop years later. Because all of electromagnetism is contained within this set of equations, they are definitely among one of the greatest triumphs of the human mind.

Strictly speaking the equations put forward by Maxwell only applies to point charges in vacuum. A dielectric, for example, is a collection of a very huge number of point charges. To deal with them all individually is an impossible task. It is therefore practical to introduce effective fields,  $\mathbf{D}$  and  $\mathbf{H}$ , to represent their collective behavior. This dielectric approach to electromagnetism represents great simplifications for many (near-to-natural) systems. It is based on the following two assumptions [34]: (i) the response of the background medium is dipole like as well as linear in the applied fields, and (ii) the medium is homogeneous (or close to) throughout a given region. The first assumption obviously breaks down if the fields becomes to strong while the latter breaks down on short length scales. Hence the resulting effective field theory, or effective Maxwell theory as we might call it, should be treated as a long-wavelength approximation to electromagnetism for weak fields. In most practical situations the above approximations are fortunately well satisfied, and in particular they are valid for the type of scattering system that we will be considering.

In the SI-system, the (effective) Maxwell's equations take on the following form:

$$\nabla \cdot \mathbf{D} = \rho, \quad (3a)$$

$$\nabla \cdot \mathbf{B} = 0, \quad (3b)$$

$$\nabla \times \mathbf{E} = -\frac{\partial \mathbf{B}}{\partial t}, \quad (3c)$$

$$\nabla \times \mathbf{H} = \frac{\partial \mathbf{D}}{\partial t} + \mathbf{J}. \quad (3d)$$

Here  $\mathbf{E}$  and  $\mathbf{H}$  denote the electric and magnetic field vectors respectively. These field vectors make together up what is known as the electromagnetic field. The field quantities  $\mathbf{D}$  and  $\mathbf{B}$ , known as the electrical displacement and the magnetic induction respectively, are included in order to describe the effect of the electromagnetic field on matter. Finally,  $\rho$  and  $\mathbf{J}$  denote the charge density and the current density respectively. Those two latter quantities act like sources for the electromagnetic field,  $\mathbf{E}$  and  $\mathbf{H}$ , and they fulfill the continuity relation

$$\frac{\partial \rho}{\partial t} + \nabla \cdot \mathbf{J} = 0. \quad (4)$$

The various quantities appearing in the Maxwell's equations, and related formulae, are summarized in Table II A where also their SI-units are given.

## 2. Constitutive Equations

The Maxwell's equations (3) consist of eight scalar equations. However, on the other hand the field vectors,  $\mathbf{E}$ ,  $\mathbf{H}$ ,  $\mathbf{D}$ , and  $\mathbf{B}$ , represent in total 12 (scalar) variables, 3 for each of the 4 vectors. Thus, obviously, the Maxwell's equations alone do not uniquely specify a solution. Therefore, in order to obtain a unique solution to the Maxwell's equations, those are supplemented by so-called constitutive relations also known as material equations. These relations read

$$\mathbf{D} = \varepsilon \mathbf{E}, \quad (5a)$$

$$\mathbf{B} = \mu \mathbf{H}. \quad (5b)$$

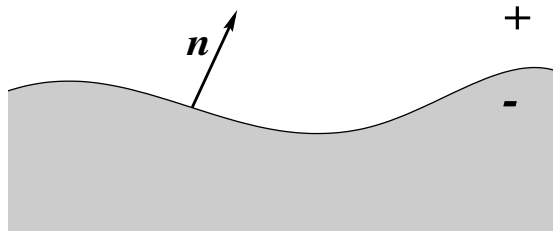


FIG. 2: A sketch of a general interface separating two dielectric media.

Here  $\varepsilon$  and  $\mu$  are the constitutive parameters which are tensors of 2nd order and known as the *permittivity*<sup>2</sup>, and the *permeability* tensor respectively. In general these tensors are rather complicated functions of the spatial variable  $\mathbf{x}$  and the field vectors  $\mathbf{E}$  and  $\mathbf{H}$ . However, for an isotropic and homogeneous medium, these tensors reduce to scalars, and if the field-strengths are not too large, they may be considered as independent of the field vectors. In this latter case we are dealing with linear electromagnetic theory. The fascinating, but complicated nonlinear electromagnetic theory [35] where per definition  $\varepsilon$  and  $\mu$  depend on  $\mathbf{E}$  and  $\mathbf{H}$ , will not be discussed here in any depth.

Eqs. (5) can within linear electromagnetic theory be cast into the equivalent form

$$\mathbf{D} = \varepsilon_0 \mathbf{E} + \mathbf{P}, \quad (6a)$$

$$\mathbf{B} = \mu_0 \mathbf{H} + \mathbf{M}, \quad (6b)$$

where  $\mathbf{P}$  and  $\mathbf{M}$  are the electric and magnetic polarizations respectively. The constants  $\varepsilon_0$  and  $\mu_0$  are the permittivity and permeability of vacuum respectively. In the SI-system they have the following values

$$\varepsilon_0 = 8.854 \times 10^{-12} \text{ F/m}, \quad (7a)$$

$$\mu_0 = 4\pi \times 10^{-7} \text{ H/m}. \quad (7b)$$

## B. The Electromagnetic Wave Equations

Probably the two most important consequences of the Maxwell's equations are the *wave equations* and the existence of solutions to these which are known as *electromagnetic waves* due to the wave-like nature of such solutions. In this section we derive the wave equations in a material medium. For simplicity, and since it is the most relevant case for this review, we will limit ourselves to a region of space which is source free and isotropic.

The derivation of the wave equations for the  $\mathbf{E}$ -field in a source-free region (*i.e.*  $\rho = 0$  and  $\mathbf{J} = \mathbf{0}$ ), is achieved by eliminating the  $\mathbf{H}$ -field from the Maxwell's equations. This is done by taking the curl of Eq. (3c), substituting Eq. (3d), and taking advantage of the constitutive relations (5). The result is

$$\nabla \times (\nabla \times \mathbf{E}) + \varepsilon\mu \frac{\partial^2 \mathbf{E}}{\partial t^2} = 0. \quad (8)$$

By applying the vector identity  $\nabla \times (\nabla \times \mathbf{A}) = \nabla(\nabla \cdot \mathbf{A}) - \nabla^2 \mathbf{A}$  to Eq. (8) and taking advantage of Eq. (3a) we obtain the well-known standard (space-time) wave equation for the electrical field in a source-free, homogeneous and isotropic medium

$$\nabla^2 \mathbf{E} - \mu\varepsilon \frac{\partial^2 \mathbf{E}}{\partial t^2} = 0. \quad (9)$$

In a similar way one can obtain a wave equation for the magnetic field by eliminating the electric field from the Maxwell's equations.

---

<sup>2</sup> This quantity is also known as the dielectric function.

It should be noticed that not every solution to the wave equation is also a solution to the Maxwell's equations. For it to be, it must in addition satisfy Gauss's law,  $\nabla \cdot \mathbf{E} = \mathbf{k} \cdot \mathbf{E} = 0$  in order to also be a solution of Maxwell's equations<sup>3</sup>. As the reader readily may check the wave equation has a solution  $\mathbf{E} = \exp(i\mathbf{k} \cdot \mathbf{r} - i\omega t)$  if  $\omega = ck$ . This solution is the plane wave solution.

### C. Boundary Conditions

In Sect. II A we introduced the Maxwell's equations and the constitutive relations. These equations can be solved for the field vectors in a region of space containing no boundaries. However, no real media are infinite, *i.e.* without boundaries. For practical applications of the electromagnetic theory it is therefore important to know how to treat the boundaries between two media of different electromagnetic properties. It is this question that we will address in this section.

Let us consider the geometry of Figure 2. It shows an arbitrary interface separating the otherwise homogeneous, isotropic and linear media labeled  $\pm$ . We have also introduced a normal vector for the interface,  $\mathbf{n}$ , which is directed into medium  $+$ . The question we now address is: How are the electromagnetic field vectors for the two media in the immediate vicinity of the interface related to each other? The answer to this question should be well-known and can be found in nearly any book on electromagnetic theory, *e.g.* in Refs. [11] and [34]. The results, for which the derivation will not be repeated here, are

$$\mathbf{n} \cdot (\mathbf{B}_- - \mathbf{B}_+) = 0, \quad (10a)$$

$$\mathbf{n} \cdot (\mathbf{D}_- - \mathbf{D}_+) = \rho_s, \quad (10b)$$

$$\mathbf{n} \times (\mathbf{E}_- - \mathbf{E}_+) = 0, \quad (10c)$$

$$\mathbf{n} \times (\mathbf{H}_- - \mathbf{H}_+) = \mathbf{J}_s, \quad (10d)$$

where the vector subscripts,  $\pm$ , are referring to the media where the field vectors are evaluated. In Eqs. (10)  $\rho_s$  and  $\mathbf{J}_s$  denote the surface charge density and the surface current density respectively, while the other quantities have been defined earlier. In many areas of optics one deals with situations where the surface charge density and the surface current density are zero. Under such circumstances the normal component of  $\mathbf{B}$  and  $\mathbf{D}$  are continuous, while the vectors  $\mathbf{E}$  and  $\mathbf{H}$  have continuous tangential components.

It should be stressed that in arriving at the results (10), it has been assumed that the electromagnetic properties take on their bulk values all the way to the surface. This is obviously not true, but is a good approximation whenever the mean field theory applies.

#### 1. Boundary Condition at a General One-Dimensional Surface

Most of this review will concern itself with randomly rough surfaces that are effectively one-dimensional, *i.e.* the surface profile function  $\zeta$  has a non-trivial dependence only on  $x_1$ , say, and does not depend explicitly on  $x_2$ . In this case the boundary conditions (10) simplifies somewhat. This is what we plan to outline in this section.

Let us start by assuming, without loss of generality, that the plane of incidence is the  $x_1x_3$ -plane and that the incident light is either  $p$ - or  $s$ -polarized. In such case, there is only one non-trivial field component needed in order to fully describe the electromagnetic field. For  $p$ -polarization this component is  $H_2$ , while for  $s$ -polarization it is  $E_2$ . Thus the primary field for a one-dimensional interface problem can be written as

$$\Phi_\nu(x_1, x_3|\omega) = \begin{cases} H_2(x_1, x_3|\omega), & \nu = p, \\ E_2(x_1, x_3|\omega), & \nu = s, \end{cases} \quad (11)$$

where a harmonic time-dependence,  $\exp(-i\omega t)$ , has been assumed, but suppressed. This form for the primary field will be used frequently throughout this review. Notice the fact that the primary field can be fully described by a single vector component. This represents a dramatic simplification of the problem since it is reduced from a vector problem down to a scalar one.

---

<sup>3</sup> One explicate example of this is provided by  $\mathbf{E} = \hat{\mathbf{e}}_3 E_0 \cos(kx_3 - \omega t)$  that satisfies the wave-equation, but not  $\nabla \cdot \mathbf{E} = 0$ . It must therefore be discarded as a solution of the Maxwell's equations.

When  $\Phi_\nu(x_1, x_3|\omega)$  is known, the remaining component of the electromagnetic field can be calculated from it alone. These components are given for  $p$ -polarization by

$$E_1(x_1, x_3|\omega) = -\frac{i}{\omega\varepsilon(\omega)}\frac{\partial}{\partial x_3}H_2(x_1, x_3|\omega), \quad (12a)$$

$$E_3(x_1, x_3|\omega) = \frac{i}{\omega\varepsilon(\omega)}\frac{\partial}{\partial x_1}H_2(x_1, x_3|\omega), \quad (12b)$$

and for  $s$ -polarization

$$H_1(x_1, x_3|\omega) = \frac{i}{\omega\mu(\omega)}\frac{\partial}{\partial x_3}E_2(x_1, x_3|\omega), \quad (13a)$$

$$H_3(x_1, x_3|\omega) = -\frac{i}{\omega\mu(\omega)}\frac{\partial}{\partial x_1}E_2(x_1, x_3|\omega). \quad (13b)$$

In the above equations  $\varepsilon(\omega)$  and  $\mu(\omega)$  denoted the dielectric function and the magnetic permeability respectively of the medium where the fields are being evaluated. The relations (12) and (13) are easily derived by using the two curl-equations contained in the Maxwell's equations, Eqs. (3c) and (3d), together with the constitutive relations, Eqs. (6).

Let us now try to focus on the boundary conditions that the primary field  $\Phi_\nu(x_1, x_3|\omega)$  will be subjected to. By construction  $\Phi_\nu(x_1, x_3|\omega)$  is a tangential field independent of polarization. Therefore it follows automatically from Eqs. (10a) and (10d) ( $\rho_s = \mathbf{J}_s = 0$ ) that

$$\Phi_\nu^+(x_1, x_3|\omega)|_{x_3=\zeta(x_1)} = \Phi_\nu^-(x_1, x_3|\omega)|_{x_3=\zeta(x_1)}, \quad (14a)$$

where  $\zeta(x_1)$  denotes the interface separating the two materials of different dielectric properties.

In order to satisfy the remaining boundary conditions expressed in Eqs. (10), we notice that for respectively  $p$ - and  $s$ -polarization we have

$$\begin{aligned} \mathbf{n} \times \mathbf{E} &= \hat{\mathbf{e}}_2 \frac{i}{\omega\varepsilon(\omega)} \partial_n \Phi_p, \\ \mathbf{n} \times \mathbf{H} &= \hat{\mathbf{e}}_2 \frac{i}{\omega\mu(\omega)} \partial_n \Phi_s, \end{aligned}$$

where  $\partial_n$  denotes the normal derivative to the surface. If the one-dimensional interface can be represented as  $x_3 = \zeta(x_1)$ , where  $\zeta(x_1)$  is a single-valued function of  $x_1$  the normal derivative becomes

$$\partial_n = \mathbf{n} \cdot \nabla = \frac{-\zeta'(x_1)\partial_{x_1} + \partial_{x_3}}{\sqrt{1 + (\zeta'(x_1))^2}},$$

where  $\partial_{x_i} = \partial/\partial x_i$  and

$$\mathbf{n} = \frac{\zeta'(x_1)\hat{\mathbf{e}}_1 + \hat{\mathbf{e}}_3}{\sqrt{1 + (\zeta'(x_1))^2}}. \quad (14b)$$

Here  $\hat{\mathbf{e}}_i$  are the standard unit vectors. Hence the remaining boundary conditions can be expressed as

$$\frac{1}{\kappa_\nu^+(\omega)} \partial_n \Phi_\nu^+(x_1, x_3|\omega)|_{x_3=\zeta(x_1)} = \frac{1}{\kappa_\nu^-(\omega)} \partial_n \Phi_\nu^-(x_1, x_3|\omega)|_{x_3=\zeta(x_1)}, \quad (14c)$$

where  $\kappa_\nu^\pm(\omega)$  are defined as

$$\kappa_\nu^\pm(\omega) = \begin{cases} \varepsilon_\pm(\omega), & \nu = p \\ \mu_\pm(\omega), & \nu = s \end{cases}. \quad (14d)$$

Eqs. (14) are the final result for the boundary conditions to be satisfied by the primary field  $\Phi_\nu(x_1, x_3|\omega)$  on a one-dimensional interface  $x_3 = \zeta(x_1)$ .



## D. Surface Plasmon Polaritons

In subsequent sections, we will see that so-called surface plasmon polaritons, or for short just SPPs, will play an important roll for the rough surface scattering problem. We will therefore in this section define and discuss some of the distinguishing properties of such modes.

Before starting our discussion, we have to know what a polariton is: According to its classical definition a polariton is defined to be an elementary electromagnetic wave, and therefore a solution of the Maxwell's equations, that may couple to one of several possible excitations possible in a condensed medium. Examples of such excitations are plasmons, phonons, magnons etc., and in such cases one talks of plasmon polaritons, phonon polaritons and magnon polaritons. With the notion of polariton established, one might definition an SPP as follows: *A surface plasmon polariton is a plasmon polariton where the associated electromagnetic field is confined to the surface separating two dielectric medium.*

### 1. SPPs on a plan surface geometry

To see under which condition SPPs might exist, and to discuss some of their properties, we will consider a planar interface separating two isotropic and homogeneous media. For simplicity, the coordinate system will be chosen so that the interface is located at  $x_3 = 0$ . The materials above ( $x_3 > 0$ ) and below ( $x_3 < 0$ ) this surface will be characterized by frequency dependent dielectric functions  $\varepsilon_+(\omega)$  and  $\varepsilon_-(\omega)$  respectively. For simplistic reasons, which are not essential for the present discussion, we will assume that the imaginary part of the dielectric functions can be neglected. The conclusion that we arrive at herein will, however, be independent of this assumption. Furthermore, we will assume either pure p- or s-polarization of the incident light. Hence the scalar wave equation might be used. A more complete discussion using vector fields can be found in Refs. [36] and [37].

According to the definition of SPP, we are interested in solutions to the Maxwell equations, equivalent in our case to the scalar wave equation, that are wave-like parallel to the surface  $x_3 = 0$  and that decays exponentially with increasing distance from the surface into each of the two media. Such a solution can be represented as

$$\Phi_\nu^\pm(x_1, x_3|\omega) = \mathcal{A}_\nu^\pm e^{\mp\beta_\pm(\omega)x_3} e^{ikx_1}, \quad \nu = p, s, \quad (15)$$

where  $\mathcal{A}_\nu^\pm$  represents the amplitudes (to be determined). The decay constants  $\beta_\pm(\omega)$  are defined as

$$\beta_\pm(\omega) = \sqrt{k^2 - \varepsilon_\pm(\omega) \frac{\omega^2}{c^2}}, \quad (16)$$

and they must be real and positive for Eq. (15) to describe an electromagnetic wave localized to the surface<sup>4</sup>. To investigate if Eq. (15) is an acceptable solution for our scattering system, we have to impose the boundary conditions, given in Eqs. (14), for the two polarizations. By utilizing the continuity of the fields on the flat surface, Eq. (14a), one finds that

$$\mathcal{A}_\nu^+ = \mathcal{A}_\nu^- \equiv \mathcal{A}_\nu,$$

for all locations along the surface. Moreover, the normal derivative condition, Eq. (14c), gives the following condition for the existence for surface plasmon polaritons on a flat surface ( $\partial_n = \partial_{x_3}$ )

$$\left( \frac{\beta_+(\omega)}{\kappa_\nu^+(\omega)} + \frac{\beta_-(\omega)}{\kappa_\nu^-(\omega)} \right) \mathcal{A}_\nu = 0, \quad (17)$$

where we recall the definitions of  $\kappa_\nu^\pm(\omega)$  from Eq. (14d). The most immediate consequence of this relation is the following: Since for s-polarization  $\kappa_s^\pm(\omega) = \mu_0$  (for non-magnetic materials) and  $\beta_\pm(\omega)$  are assumed to be real and *positive*, the only solution to Eq. (17) is  $\mathcal{A}_s \equiv 0$ . Thus, a s-polarized surface plasmon polariton (surface wave) *cannot* exist for the scattering system that we are considering.

However, for p-polarization, where  $\kappa_p^\pm(\omega) = \varepsilon_\pm(\omega)$  a non-trivial solutions might exist. It is given by (assuming that  $\mathcal{A}_p \neq 0$ )

$$\frac{\varepsilon_+(\omega)}{\varepsilon_-(\omega)} = -\frac{\beta_+(\omega)}{\beta_-(\omega)}, \quad (18)$$

---

<sup>4</sup> If we had allowed the dielectric functions of the problem to be complex with  $Im \varepsilon_\pm(\omega) > 0$ , we would have to require that  $Re \beta_\pm(\omega) > 0$ .

which is the dispersion relation for surface plasmon polaritons on a flat interface. For this relation to be satisfied, since  $\beta_{\pm}(\omega)$  are both assumed to be positive, the two dielectric functions of the scattering system have to have different signs due to the presence of the negative sign on the right-hand-side of Eq. (18). Only such combination of materials will support surface plasmon polaritons. An important example of such a system at optical frequencies, is a metal with a planar interface to vacuum.

By squaring both sides of Eq. (18) as well as taking advantage of Eq. (16), the dispersion relation can be expressed as

$$k_{sp}(\omega) = \pm \sqrt{\frac{\varepsilon_+(\omega)\varepsilon_-(\omega)}{\varepsilon_+(\omega) + \varepsilon_-(\omega)} \frac{\omega}{c}}. \quad (19)$$

This equation gives an explicit expression for the wave vector of the surface plasmon polariton. However, this formulae should be used with some care since it may, from the way it is derived from Eq. (18), introduce some spurious solutions. The additional and sufficient requirement that have to be satisfied is that  $\beta_{\pm}(\omega)$  are positive while the two dielectric functions,  $\varepsilon_{\pm}(\omega)$ , have different sign.

## 2. SPPs at a planar free electron metal surface

Let us for illustrative purposes consider a free electron metal with a planar interface to vacuum. For such a metal the dielectric function is known to be [38]

$$\varepsilon_-(\omega) = \varepsilon_{\infty}(\omega) \left( 1 - \frac{\omega_p^2}{\omega^2} \right), \quad (20)$$

while the one for vacuum is  $\varepsilon_+(\omega) = 1$ . In the above equation  $\varepsilon_{\infty}(\omega)$  is the background dielectric constant of the material while  $\omega_p$  is the electronic plasma frequency. With Eq. (20) the frequency of the SPP can be shown to be

$$\omega_{sp}(k) = \left[ \frac{1}{2} \left( \frac{k^2 c^2}{\varepsilon_{\infty}(\omega)} (1 + \varepsilon_{\infty}(\omega)) + \omega_p^2 \right) - \frac{1}{2} \sqrt{\left( \frac{k^2 c^2}{\varepsilon_{\infty}(\omega)} (1 + \varepsilon_{\infty}(\omega)) + \omega_p^2 \right)^2 - 4k^2 c^2 \omega_p^2} \right]^{\frac{1}{2}}. \quad (21)$$

It should be noticed from this equation that

$$\omega_{sp}(k) = \begin{cases} kc, & k \rightarrow 0, \\ \sqrt{\frac{\varepsilon_{\infty}(\omega)}{\varepsilon_{\infty}(\omega) + 1}} \omega_p, & k \rightarrow \infty, \end{cases} \quad (22)$$

This means that in the small wave vector limit the surface plasmon polariton is photon-like, while it in the large wave vector limit it is plasmon-like. In Fig. 3 the dispersion relation, Eq. (21), for a free electron metal is plotted. In this figure we have also included the light-line (dash-dotted line)  $\omega = kc$ , as well as the large wave vector limit (dashed line) of  $\omega_{sp}(k)$ .

From Fig. 3 we see that the dispersion curve for the SPP lies entirely to the right of the light-line,  $\omega = kc$ . The physical consequence of this is that there is no coupling between the surface plasmon polariton and light in vacuum for a flat vacuum-metal interface. Or put another way, light incident onto a planar vacuum-metal interface cannot excite surface plasmon polaritons. Later, however, we will see that if the surface is rough such coupling is possible. This will give rise to many new and interesting multiple-scattering effects, as we discuss in some detail in Sect. IV.

## E. Characterization of Random Rough Surfaces

Almost everyone grows up with some kind of intuitive “feeling” of what is meant by a rough surface. A fractured stone, say, is normally looked upon as being rough, while a piece of paper as being smooth. However, on the micro-scale, where the human eye is not very sensitive, also the paper has some kind of structure. So in a strict sense, both the paper and the stone surface are rough. Paper is made out of fibers which is quite different from the crystals that are seen on the micro scale of the surface of the fractured stone. So the question is: How shall we quantify the difference in roughness between say the paper and the stone surface? One possibility is to measure by some suitable

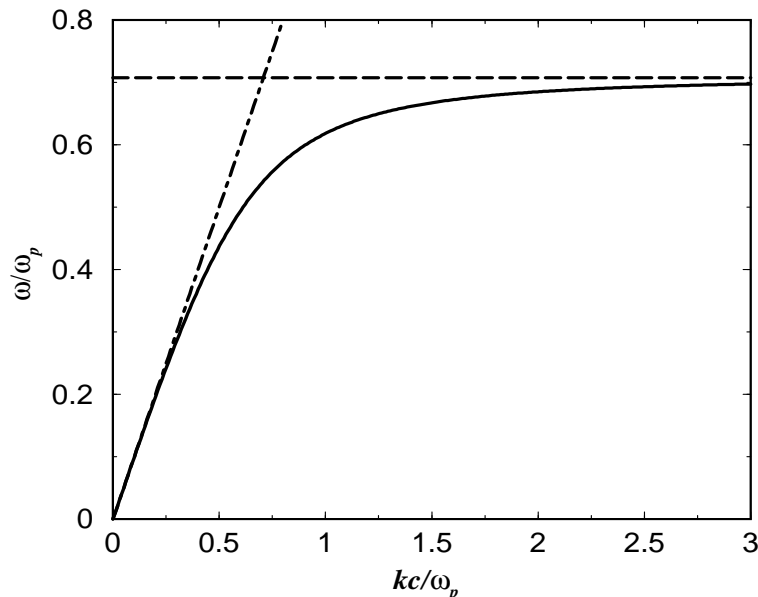


FIG. 3: Dispersion relation curve, Eq. (21), for a surface plasmon polariton (solid line) at a flat interface between a simple metal and vacuum (assuming  $\varepsilon_\infty(\omega) = 1$ ). The dash-dotted line represents the light line  $\omega = kc$ , while the dashed line is the large momentum asymptotic limit  $\omega_{sp} = \omega_p/\sqrt{2}$  (see Eq. (22)).

technique the surface topography. Such measurements will of course produce different results for the paper and stone surface. However, if we move to another area of the fractured stone and measure the surface topography here, we will obviously not get the same result as obtained in the previous measurement taken from another area of the same surface. So, how shall we be able to characterize the rough surfaces at hand, so that we are able to distinguish them from each other? In this section we intend to discuss in some detail how to characterize randomly rough surfaces in a quantitative way.

However, before we do so, let us take a look at what kind of rough surfaces we have. Depending on how the surface height fluctuates around some reference surface, we may categorize them as being deterministic or randomly rough. For random surfaces, one may in addition group them as correlated or uncorrelated surfaces, and they might occur as fractal or non-fractal surfaces depending on under which conditions they were formed. Rough surfaces that are found in nature are normally randomly rough, correlated surfaces. We will therefore proceed by discussing how to characterize such surfaces.

#### F. A Statistical description of Randomly Rough Surfaces

Two randomly rough surfaces are never identical. Thus the knowledge of the surface topography alone is therefore not enough to be able to say if two rough surfaces were generated by the same underlying process, and therefore have to be looked upon as being identical. However, if we assume that the randomly rough surface can be considered as a continuous random process [12–17], then a statistical description might be relevant and useful. We will now introduce this method of characterization.

Under experimental conditions, the surface topography is measured relative to some reference surface. In our case we will assume that this reference surface is a planer surface. Other choices might be practical in some cases, but this will not be discussed here. Furthermore, it is convenient to choose our coordinate system so that this planar surface is located at  $x_3 = 0$ . In this case the randomly rough surface is just the roughness that perturb the plane  $x_3 = 0$ . For simplicity, we limit our discussion to one-dimensional surfaces. The extension to (isotropic) two-dimensional surfaces is trivial. For the purpose of this introduction it will be assumed that the surface does not possess any overhangs<sup>5</sup>, that is to say that the surface profile function, that we will denote by  $\zeta(x_1)$ , is a single-valued function of the lateral

<sup>5</sup> Such surfaces are also known as reentrant surfaces.

coordinate  $x_1$ . For characterization of surfaces where the surface profile function does not fulfill this property the reader is invited to consult Ref. [18].

In order for the surface profile function  $\zeta(x_1)$  to be planar on average, it must, with our choice for the coordinate system, have a vanishing mean, *i.e.* we must require that

$$\langle \zeta(x_1) \rangle = 0. \quad (23)$$

Here the angle brackets are used to denote a spatial average over a large spatial region. If, however, the surface is *ergodic* [13–17], as we will assume here, this spatial average is equal to an average over an ensemble of realizations of  $\zeta(x_1)$ . It is therefore, under the assumption of ergodicity, more convenient to think of  $\langle \cdot \rangle$  as an ensemble average.

Another notion that is important when characterizing rough surfaces, and studying light scattering from such, is the one of *stationarity* [6]. A surface is said to be stationary, or translation invariant, if its statistical properties are independent of which portion of the surface was used in their determination. That the surface roughness possess stationarity is crucial for the applicability of many of the theories used to study rough surface scattering. Rigorous numerical simulations (Sect. IIII), however, can still handle non-stationary surfaces.

### 1. Gaussian Random Surfaces

In theoretical studies of light scattering from rough surfaces, the random surfaces have in the overall majority of the studies been assumed to possess Gaussian height statistics. Such a statistics is rather appealing from a theoretical point of view since all moments can be related to the two first moments. such moments either vanish (odd moments), or they are related to the second moment (even moments) [6].

The zero-mean property, Eq. (23), does not specify how the different heights are located relative to one another along the surface. Such information is provided by the height-height correlation function. Under the assumption of  $\zeta(x_1)$  being stationary we can write

$$\langle \zeta(x_1)\zeta(x'_1) \rangle = \delta^2 W(|x_1 - x'_1|), \quad (24)$$

where  $\delta$  is the RMS-height of the surface profile function, and  $W(|x_1|)$  is the height auto-correlation function normalized so that  $W(0) = 1$ . In cases where  $W(|x_1|) = 1$  ( $W(|x_1|) = -1$ ) one speaks of perfect correlation (anti-correlation). Furthermore it can be shown that  $-1 \leq W(|x_1|) \leq 1$ . Notice, that since the heights-distribution is Gaussian, Eqs. (23) and (24) together determines uniquely the statistical properties of the surface since all higher order moments can (for a Gaussian surface) be related to the first two.

In many of the perturbation theories developed for rough surface scattering, the power spectrum of the surface randomness is a quantity that appear more-or-less naturally. It is defined as the Fourier transform of the (normalized) correlation function

$$g(|k|) = \int_{-\infty}^{\infty} dx_1 W(|x_1|) e^{-ikx_1}. \quad (25)$$

In order to get an intuitive picture of how the surface height varies along the surface, it is often useful to supply the mean slope,  $s$ , and the mean distance between consecutive peaks and valleys,  $\langle D \rangle$ , as measured along the (lateral)  $x_1$ -direction. For a stationary zero-mean, Gaussian random process, the RMS-slope,  $s$ , is related to the power spectrum by [19]

$$s = \langle (\zeta'(x_1))^2 \rangle^{1/2} = \delta \sqrt{\int_{-\infty}^{\infty} \frac{dk}{2\pi} k^2 g(|k|)}, \quad (26)$$

and a good estimator for  $\langle D \rangle$  has been shown to be [19]

$$\langle D \rangle \simeq \pi \sqrt{\frac{\int_{-\infty}^{\infty} dk k^2 g(|k|)}{\int_{-\infty}^{\infty} dk k^4 g(|k|)}}. \quad (27)$$

In the literature many different forms for the correlation function  $W(|x_1|)$  has been considered (see *e.g.* Ref. [6] and references therein). However, here we will only be dealing with two such forms. They are the Gaussian form given by

$$W(|x_1|) = \exp\left(-\frac{x_1^2}{a^2}\right), \quad (28a)$$

$$g(|k|) = \sqrt{\pi}a \exp\left(-\frac{a^2 k^2}{4}\right), \quad (28b)$$

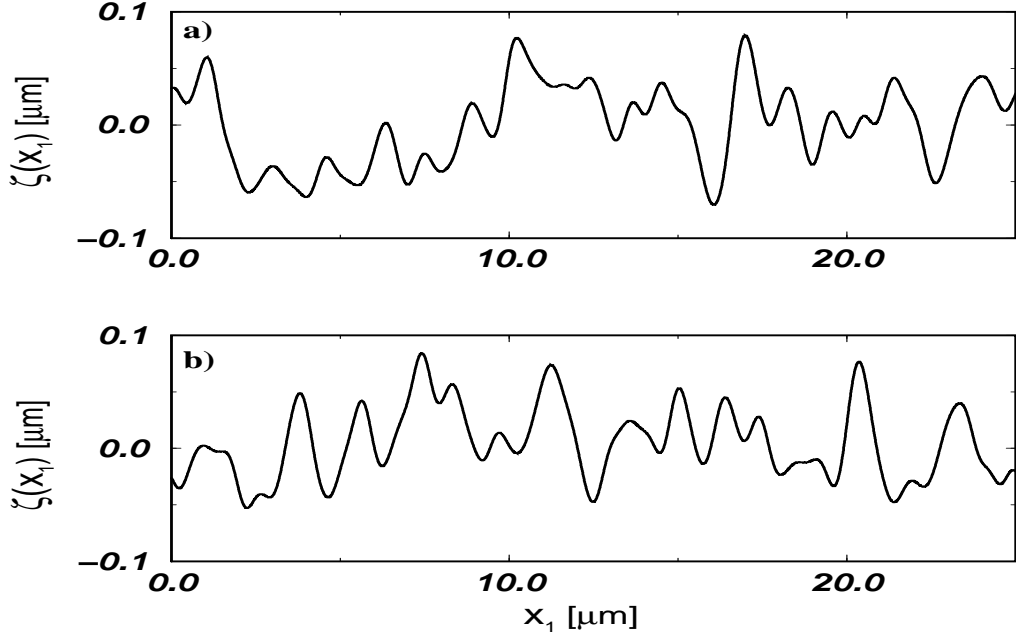


FIG. 4: Examples of two rough profiles both with Gaussian height distributions and with an RMS-value  $\delta = 30\text{nm}$ . The power spectrum is of the (a) Gaussian type, with  $a = 100\text{nm}$ , and the (b) West-O'Donnell type, with  $k_- = 0.82(\omega/c)$  and  $k_+ = 1.97(\omega/c)$ . Here the wavelength is  $\lambda = 632.8\text{nm}$ . With these parameters the RMS-slope and distance between consecutive peaks and valleys are respectively  $s = 0.424$  and  $\langle D \rangle = 128.3\text{nm}$  for the Gaussian power spectrum, and  $s = 0.427$  and  $\langle D \rangle = 201.1\text{nm}$  in case of the West-O'Donnell power spectrum. Note that there are different scales on the first and second axes, with the result that the profiles appear much rougher than they are in reality. The two surface profiles were generated from the same underlying uncorrelated random numbers.

where  $a$  is the transverse correlation length, and the so-called West-O'Donnell (or rectangular) form

$$W(|x_1|) = \frac{\sin k_+ x_1 - \sin k_- x_1}{(k_+ - k_-) x_1} \quad (29a)$$

$$g(|k|) = \frac{\pi}{k_+ - k_-} [\theta(k_+ - k) \theta(k - k_-) + \theta(k_- + k) \theta(-k - k_-)]. \quad (29b)$$

where  $\theta(\cdot)$  is the Heaviside unit step function. In Eqs. (29) the quantities  $k_{\pm}$ , with  $0 < k_- < k_+$ , denote the lower and upper momentum cut-off for the spectrum, and they will be given a more precise definition in later sections. The latter power spectrum was recently used by West and O'Donnell [20] in an experimental study of the enhanced backscattering phenomenon from weakly rough surfaces.

For the two above power spectra the mean slope,  $s$ , and the distance between consecutive peaks and valleys,  $\langle D \rangle$ , then become [19]

$$s = \begin{cases} \sqrt{2} \frac{\delta}{a}, & \text{Gaussian} \\ \frac{\delta}{\sqrt{3}} \sqrt{k_+^2 + k_+ k_- + k_-^2}, & \text{West-O'Donnell} \end{cases}, \quad (30)$$

and [19]

$$\langle D \rangle = \begin{cases} \frac{\pi}{\sqrt{6}} a, & \text{Gaussian} \\ \pi \sqrt{\frac{5}{3} \frac{k_+^3 - k_-^3}{k_+^5 - k_-^5}}, & \text{West-O'Donnell} \end{cases}. \quad (31)$$

Two surface profiles with the same (Gaussian) height distribution, but with a Gaussian and a West-O'Donnell power spectrum possessing nearly the same value of the RMS-slope,  $s$ , are plotted in Figs. 4.

It will later in explicate calculations prove useful to also have the Fourier representation of the surface profile function (and its inverse) at our disposal. They are defined as

$$\zeta(x_1) = \int_{-\infty}^{\infty} \frac{dk}{2\pi} \tilde{\zeta}(k) e^{ikx_1}, \quad (32a)$$

$$\tilde{\zeta}(k) = \int_{-\infty}^{\infty} dx_1 \zeta(x_1) e^{-ikx_1}. \quad (32b)$$

The Fourier transform,  $\tilde{\zeta}(k)$ , of the surface profile function also constitutes a zero-mean Gaussian random process with statistical properties

$$\langle \zeta(k) \rangle = 0, \quad (33a)$$

$$\langle \tilde{\zeta}(k) \tilde{\zeta}(k') \rangle = 2\pi \delta(k + k') \delta^2 g(|k|), \quad (33b)$$

where  $\delta(\cdot)$  denotes the Dirac delta function.

## 2. Non-Gaussian Random Surfaces

Naturally occurring surfaces have often more complicated height distributions than the Gaussian [6]. To fully characterize such surfaces are quite difficult and probably explains why they have gotten less attention in the literature than they probably deserve. The main problem is that in order to characterize them statistically, moments of infinite order have to be known. These moments are not, as for Gaussian surfaces, related to moments of lower order in a trivial way since the characteristic function is in general not known for non-Gaussian surfaces. We do not intend in this introduction to discuss non-Gaussian random surfaces in any detail, since we will not focus on them later. However, we would like to mention that as long as this kind of surfaces can be generated numerically, the scattering problem for non-Gaussian surfaces are not hard to handle by numerical simulations [21, 22]. On the other hand, small amplitude perturbation theory, say, can not be utilized in its standard form to non-Gaussian surfaces.

### G. Self-affine surfaces

It has been known for quite some time that self-affine surfaces are abundant in nature. They can be found in various areas of natural science such as surface growth [23–25], fractured surfaces [26], geological structures [27, 28], metallurgy [29], and biological systems [30] to mention a few.

A surface,  $\zeta(x_1)$ , is self-affine, according to its definition, between the scales  $\xi_-$  and  $\xi_+$ , if it remains (either exactly or statistically) invariant in this region under transformations of the form

$$x_1 \rightarrow \lambda x_1, \quad (34a)$$

$$\zeta \rightarrow \lambda^H \zeta, \quad (34b)$$

for all positive real numbers  $\lambda$ . Here  $H$  is the *roughness exponent*, also known as the *Hurst exponent*, and it characterizes this invariance. It is usually found in the range from zero to one. When  $H = 1/2$  the surface is an example of the famous random (Brownian) walk where the surface is uncorrected. However, if  $H \neq 1/2$  the profile shows correlations; for  $H > 1/2$  it is said to be *persistent* (correlated), and for  $H < 1/2$  it is *anti-persistent* (anti-correlated). The reason for this naming is that if the self-affine “walker” when moving from the previous to the present space step went up, say, it is more likely that it will go up (down) in the next one if  $H > 1/2$  ( $H < 1/2$ ).

The scaling relation (34) is often put in the more compact, but equivalent form

$$\zeta(x_1) \simeq \lambda^{-H} \zeta(\lambda x_1), \quad (35)$$

where  $\simeq$  is used to indicate statistical equality. This relation says that if we take the original profile  $\zeta(x_1)$ , enlarge (or contract) the lateral direction by rescaling  $x_1$  into  $\lambda x_1$ , and *simultaneously* scaling  $\zeta$  to  $\lambda^{-H} \zeta$ , the profile  $\zeta(x_1)$  and its rescaled version  $\lambda^{-H} \zeta(\lambda x_1)$  should be indistinguishable. Of course, this holds true in an exact sense only for deterministic surfaces. In the statistical case, however, it is the statistical properties of the profile and its rescaled version that are indistinguishable. In Figs. 5 we present some examples of self-affine surfaces of Hurst exponent  $H = 0.3$  (Fig. 5a),  $H = 0.5$  (Fig. 5b), and  $H = 0.7$  (Fig. 5c). As can be seen from these figures the landscapes become more “calm” the larger the Hurst exponent becomes.

The scaling relation Eq. (35) does not fully specify the self-affine surface. In particular no information is contained in Eq. (35) about the amplitude of the surface. Such information is provided by the length scale,  $\ell$ , known as the *topothesy*. This length scale is defined as the length,  $\ell$ , measured along the  $x_1$ -direction, for over which the root-mean-square of the height-difference between two points separated by  $\ell$  is just  $\ell$ . To make this even more clear, let us introduce

$$\sigma(\Delta x_1) = \left\langle \{ \zeta(x_1 + \Delta x_1) - \zeta(x_1) \}^2 \right\rangle_{x_1}^{\frac{1}{2}}, \quad (36)$$

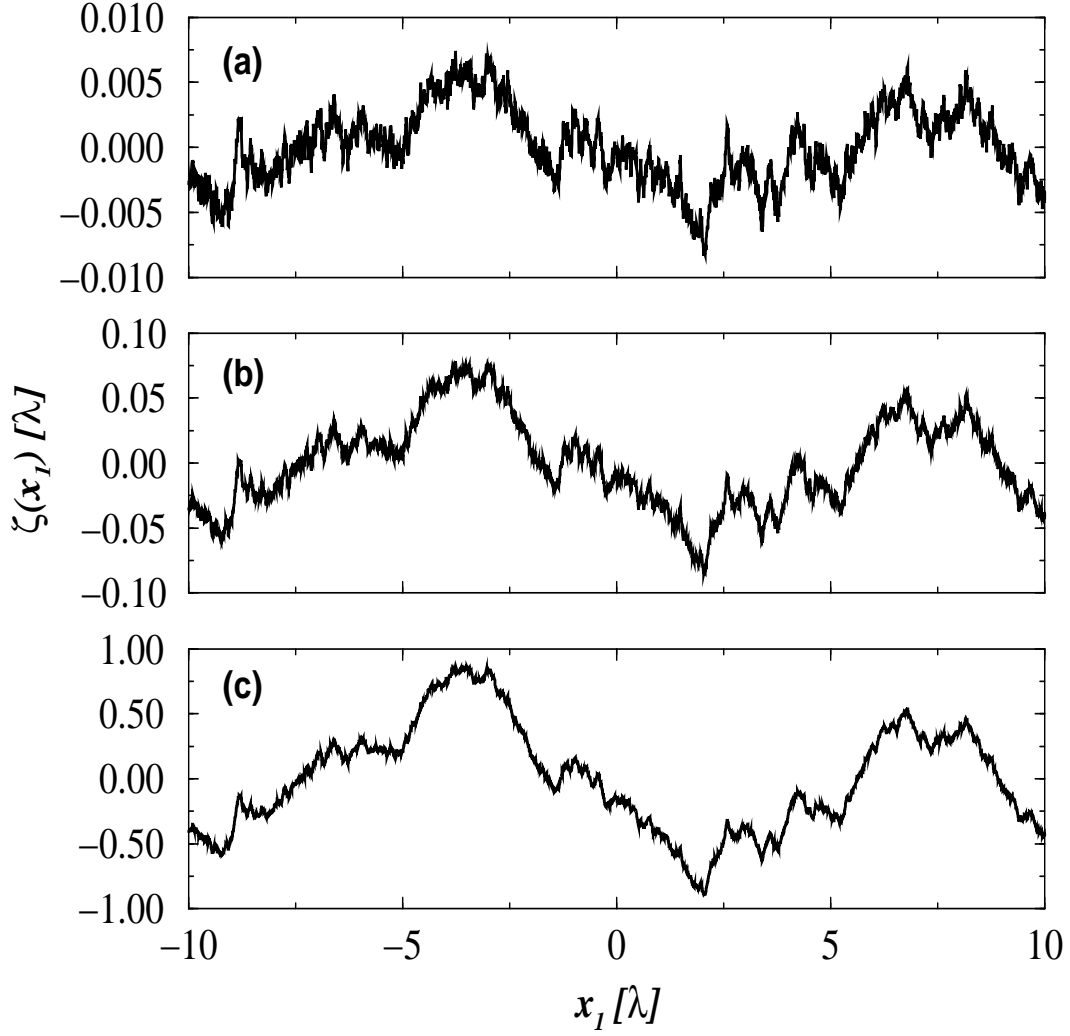


FIG. 5: Examples of self-affine profiles. The Hurst exponents were (a)  $H = 0.3$ , (b)  $H = 0.5$ , and (c)  $H = 0.7$ , and for all cases the topothesy where  $\ell = 10^{-3}\lambda$  where  $\lambda$  is an arbitrary length scale. The surfaces were generated by the Fourier filtering method from the same uncorrelated Gaussian distributed number. Notice how the RMS-height of the surface as measured over its total length increases as we increase the Hurst exponent. This is in agreement with Eq. (38).

as the RMS-value of the height-difference measured over a window of size  $\Delta x_1$ . With this definition the topothesy is defined as the length scale for which

$$\sigma(\ell) = \ell. \quad (37)$$

From Eq. (36) it follows immediately that  $\sigma(x_1) \sim x_1^H$ , so that with Eq. (37) we get

$$\sigma(\Delta x) = \ell^{1-H} \Delta x_1^H. \quad (38)$$

Notice that Eq. (37) allows for a geometrical interpretation of the topothesy as the length scale over which the profile has a mean slope of 45 degrees. The smaller  $\ell$ , the flatter the profile appears on a macroscopic scale. It should be stressed that in spite of the geometrical interpretation of  $\ell$ , there is nothing a priori that restricts the topothesy to length scales where the self-affinity can be found. However, for the surfaces usually considered in scattering problems, we rather expect that  $\ell \ll \xi_-$ . When  $\xi_- < \ell < \xi_+$ , the topothesy makes the transition between the scales, below  $\ell$ , for which a fractal dimension  $D = 2 - H$  can be measured using *e.g.* the box counting method [25, 31–33] and the scales, above  $\ell$ , for which this dimension is just unity. For length scales  $\xi_- < \Delta x_1 < \ell$  the fractal dimension is therefore nontrivial (read different from one) and we have an example of a self-affine fractal [25, 31–33]. It should

be noticed that the fractal property of the self-affine surface crucially depends on which length scale the surface is being observed. This essential point seems often to be overlooked in the literature where one too often treat self-affine surfaces as they were fractals [32, 33] at any length scale.

Even if the self-affine correlations of the profile is fully characterized by its Hurst exponent  $H$ , its topothesy parameter  $\ell$  and the bounds of the self-affine regime  $\xi_-$  and  $\xi_+$ , nothing is said about its height-distribution. It is therefore not uncommon to talk about for example a Gaussian self-affine surfaces meaning that the surface correlation is of the self-affine type, while the distribution of heights is Gaussian. Thus by specifying the self-affine parameters, *i.e.*  $H$ ,  $\ell$ , and  $\xi_{\pm}$ , in addition to the parameters needed in order to characterize the height-distribution, the surface is completely specified. Under the assumption that the surface has Gaussian height distribution it can be shown that the probability,  $p(\zeta; x_1)$  for finding height  $\zeta$  at position  $x_1$  given that  $\zeta(0) = 0$ , can be written as [25]

$$p(\zeta; x_1) = \frac{1}{\sqrt{2\pi}\ell^{1-H}x_1^H} \exp \left[ -\frac{1}{2} \left( \frac{\zeta}{\ell^{1-H}x_1^H} \right)^2 \right]. \quad (39)$$

However, independent of the height-distribute being Gaussian or not,  $p(\zeta; x_1)$  should satisfy the following scaling relation [25, 32]

$$p(\zeta; x_1) = \lambda^H p(\lambda^H \zeta; \lambda x_1), \quad (40)$$

which can be derived from the scaling relation Eq. (34).

In fact, the scaling relation (34), or the equivalent form given in Eq. (35), is extremely powerful and can be used to derive most, if not all, of the properties of a self-affine surface. To show an explicit example of this, we would like, before closing this section, to derive the scaling relation of the power spectrum of the surface. This scaling relation is the most popular one to use for both generating self-affine surfaces as well as to measure the Hurst exponent. For a surface,  $\zeta(x_1)$ , of length,  $L_1$ , the power spectrum is defined as

$$g(|k|) = \frac{1}{L_1} \int_{-\frac{L_1}{2}}^{\frac{L_1}{2}} dx_1 e^{ikx_1} \langle \zeta(y_1 + x_1) \zeta(y_1) \rangle_{y_1}. \quad (41)$$

where, as we recall,  $\langle \zeta(y_1 + x_1) \zeta(y_1) \rangle_{y_1}$  is the (two-point) correlation function. By now taking advantage of the scaling relations (34) and (35), one finds

$$g \left( \left| \frac{k}{\lambda} \right| \right) \simeq \frac{1}{\lambda L_1} \int_{-\frac{\lambda L_1}{2}}^{\frac{\lambda L_1}{2}} d(\lambda x_1) e^{ikx_1} \langle \lambda^H \zeta(y_1 + x_1) \lambda^H \zeta(y_1) \rangle_{y_1}. \quad (42)$$

Hence, one obtains from Eq. (42) that

$$g \left( \left| \frac{k}{\lambda} \right| \right) \simeq \lambda^{2H+1} g(|k|), \quad (43)$$

so that the power spectrum itself has to scale like

$$g(|k|) \sim k^{-2H-1}. \quad (44)$$

For more details about self-affine surfaces and their properties the reader is referred to the literature [25, 32, 33].

## H. Numerical Generation of Randomly Rough Surfaces

Earlier in the sections we have discussed how to statistically characterize randomly rough surfaces. In analytical work, this is all what we need. However in a numerical Monte Carlo simulation approaches to be presented in a later section, individual surface, called realizations, have to be generated so that they possess the right statistical properties. The question therefore is: How can we do this? We do not intend to give a detailed discussion here, but will instead sketch how it can be done.

As long as the power spectrum of the surface is known, an efficient way of generating the surface is by using the so-called Fourier filtering method [25, 32]. This method basically consists of two main steps. First, *uncorrelated* random numbers of the type wanted for the height distribution of the surface are generated in Fourier space. Second, these numbers are filtered by the square root of the power spectrum  $g(|k|)$ , and the result transform by an inverse Fourier transform to real space. It was in this way that the surfaces shown in Figs. 4 and 5 were generated. For more details the reader is advised to consult Refs. [21, 22, 25] and [32].



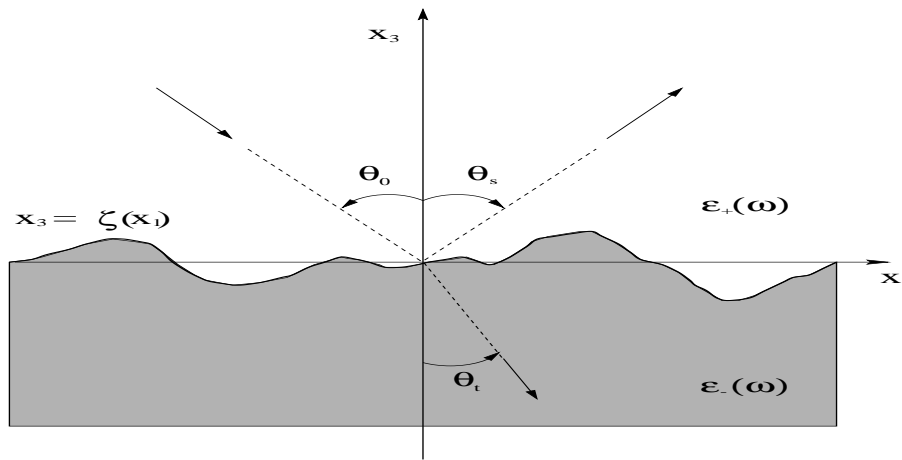


FIG. 6: The main scattering geometry used throughout this section for the wave scattering from a rough surface defined by  $x_3 = \zeta(x_1)$ . The region above the surface,  $x_3 > \zeta(x_1)$ , is assumed to be vacuum ( $\varepsilon_+(\omega) = 1$ ), while the one below is metal or a dielectric characterized by a frequency-dependent dielectric function  $\varepsilon_-(\omega) = \varepsilon(\omega)$ . Notice for which direction the incident ( $\theta_0$ ), scattering ( $\theta_s$ ), and transmission ( $\theta_t$ ) angles are defined positive. An angle of transmission is only well-defined if the lower medium is transparent, *i.e.* if  $\text{Re}\varepsilon(\omega) > 0$ .

### III. QUANTITIES AND TECHNIQUES USED IN ROUGH SURFACE SCATTERING STUDIES

The intention of the present section is to introduce some of the main quantities and techniques, both analytical and numerical, used in the field of wave scattering from randomly rough surfaces. The idea is to cover in some detail the most central techniques at the sacrifice of a wide coverage. The first part of this section is devoted to the discussion of some general properties of the scattering problem. This discussion is independent of the techniques used for its solution. In the second part, however, some of the central theoretical approaches towards the solution of the scattering problem are presented. Here the outlined theories will only sparsely be applied to a concrete problem. However, this is done in the next section where phenomena in rough surface scattering are discussed.

#### A. The Scattering Geometry

The scattering geometry that we will mainly concern ourselves with in this section is depicted in Fig. 6. It consists of vacuum ( $\varepsilon_+(\omega) = \varepsilon_0(\omega) = 1$ ) in the region  $x_3 > \zeta(x_1)$ , and a metal or dielectric characterized by an isotropic, frequency-dependent, dielectric function  $\varepsilon_-(\omega) = \varepsilon(\omega)$ , in the region  $x_3 < \zeta(x_1)$ . Here  $\zeta(x_1)$  denotes the surface profile function and it is assumed to be a single-valued function of  $x_1$  that is differentiable as many times as is necessary. Furthermore, it constitutes a zero mean, stationary, Gaussian random process which we from Sect. II F recall is defined by

$$\langle \zeta(x_1) \rangle = 0, \quad (45a)$$

$$\langle \zeta(x_1)\zeta(x'_1) \rangle = \delta^2 W(|x_1 - x'_1|). \quad (45b)$$

Here  $W(|x_1|)$  denotes the auto-correlation function and it will be specified later.

The incident wave is assumed to be either  $p$ - or  $s$ -polarized, as indicated by the index  $\nu$ , and the plane of incidence will be the  $x_1x_3$ -plane. Furthermore, the angle of incidence, reflection, and transmission,  $\theta_0$ ,  $\theta_s$ , and  $\theta_t$  respectively, are measured positive according to the convention indicated in Fig. 6.

#### B. The Scattered Field

From Sect. II we recall that in order to solve the scattering problem, we have to solve the Helmholtz equation and satisfy the boundary conditions, Eqs. (14), at the rough interface  $\zeta(x_1)$  as well as the boundary conditions at infinity. In the present section we will give the form of the far fields that automatically satisfy the Helmholtz equation and

the boundary conditions at infinity. We will discuss separately the case where the incident field is a plane wave and where it is a wave of finite width.

However, before we do so, we recall that for the scattering geometry depicted in Fig. 6, the Maxwell's equations are equivalent to the scalar Helmholtz equation for the field  $\Phi_\nu(x_1, x_3|\omega)$  defined by Eq. (11), *i.e.*

$$\Phi_\nu(x_1, x_3|\omega) = \begin{cases} H_2(x_1, x_3|\omega), & \nu = p, \\ E_2(x_1, x_3|\omega), & \nu = s, \end{cases}. \quad (46)$$

It is the asymptotic, far-field behavior of  $\Phi_\nu(x_1, x_3|\omega)$  that we are trying to determine.

### 1. Plane Incident Wave

Let us first consider the case where the incident field is (a either *p*- or *s*-polarized) plane wave of the form

$$\Phi_\nu^{inc}(x_1, x_3|\omega) = e^{ikx_1 - i\alpha_0(k, \omega)x_3}, \quad (47)$$

where<sup>6</sup>

$$\alpha_0(q, \omega) \equiv \alpha_+(q, \omega) = \begin{cases} \sqrt{\frac{\omega^2}{c^2} - q^2}, & |q| < \frac{\omega}{c}, \\ i\sqrt{q^2 - \frac{\omega^2}{c^2}}, & |q| > \frac{\omega}{c}. \end{cases}. \quad (48)$$

Then the form of the field in region  $x_3 > \max \zeta(x_1)$  that satisfied both the Helmholtz equation as well as the boundary conditions at infinity ( $x_3 = \infty$ ) can be written as

$$\Phi_\nu^+(x_1, x_3|\omega) = \Phi_\nu^{inc}(x_1, x_3|\omega) + \int_{-\infty}^{\infty} \frac{dq}{2\pi} R_\nu(q|k) e^{iqx_1 + i\alpha_0(q, \omega)x_3}. \quad (49a)$$

Similarly, a solution to the Helmholtz equation in the region  $x_3 < \min \zeta(x_1)$  that satisfy the boundary condition at  $x_3 = -\infty$  is

$$\Phi_\nu^-(x_1, x_3|\omega) = \int_{-\infty}^{\infty} \frac{dq}{2\pi} T_\nu(q|k) e^{iqx_1 - i\alpha_0(q, \omega)x_3}, \quad (49b)$$

where ( $\varepsilon_-(\omega) \equiv \varepsilon(\omega)$ )

$$\alpha_-(q, \omega) \equiv \alpha_-(q, \omega) = \sqrt{\varepsilon(\omega) \frac{\omega^2}{c^2} - q^2}, \quad Re \alpha, Im \alpha > 0. \quad (50)$$

In these equations  $R_\nu(q|k)$  and  $T_\nu(q|k)$  denote the scattering and transmission amplitudes respectively. Notice that these asymptotic expressions does not say anything about how the fields look like in the surface region  $\min \zeta(x_1) < x_3 < \max \zeta(x_1)$ . This and its consequence, will be discussed in more detail in Sect. III E when we derive the so-called reduced Rayleigh equation.

### 2. Finite Width Incident Wave

If the incident field is not a plane wave, but instead has a finite width, then the above expressions will have to be changed somewhat. In this case the incident field can be written as

$$\Phi_\nu^{inc}(x_1, x_3|\omega) = \int_{-\frac{\omega}{c}}^{\frac{\omega}{c}} \frac{dk}{2\pi} F(k) e^{ikx_1 - i\alpha_0(k, \omega)x_3}, \quad (51a)$$

---

<sup>6</sup> We will use the notation  $\alpha_0(q, \omega)$  instead of  $\alpha_+(q, \omega)$  in order follow the notation frequently used in the literature.

*i.e.* as a weighted sum of plane waves. Here  $F(k)$  is in principle an arbitrary function for which the integral exists. Due to the linearity of the Maxwell's equations, the scattered field becomes

$$\Phi_{\nu}^{sc}(x_1, x_3|\omega) = \int_{-\infty}^{\infty} \frac{dq}{2\pi} R_{\nu}(q, \omega) e^{iqx_1 + i\alpha_0(q, \omega)x_3}, \quad (51b)$$

where

$$R_{\nu}(q, \omega) = \int_{-\frac{\omega}{c}}^{\frac{\omega}{c}} \frac{dk}{2\pi} R_{\nu}(q|k) F(k). \quad (51c)$$

The total field in the region  $x_3 > \max \zeta(x_1)$  therefore is  $\Phi_{\nu}^{+}(x_1, x_3|\omega) = \Phi_{\nu}^{inc}(x_1, x_3|\omega) + \Phi_{\nu}^{sc}(x_1, x_3|\omega)$ .

In a similar way the field in the region  $x_3 < \min \zeta(x_1)$  can be written as

$$\Phi_{\nu}^{-}(x_1, x_3|\omega) = \int_{-\infty}^{\infty} \frac{dq}{2\pi} T_{\nu}(q, \omega) e^{iqx_1 - i\alpha_0(q, \omega)x_3}, \quad (52)$$

where  $T_{\nu}(q, \omega)$  is given by an expression similar to Eq. (51c).

In order to fully define the asymptotic forms of the field, the envelope  $F(k)$  has to be given. Here we will only consider so-called Gaussian finite beams. Such beams are obtained if  $F(k)$  has the Gaussian form. If the half-width of the incident beam is denoted by  $w$  the Gaussian envelope  $F(k)$  can be written as [21]

$$F(k) = \frac{w\omega}{2\sqrt{\pi}c} \frac{1}{\alpha_0(k, \omega)} \exp \left[ -\frac{w^2\omega^2}{4c^2} \left( \arcsin \frac{kc}{\omega} - \theta_0 \right)^2 \right]. \quad (53)$$

### C. The mean differential reflection coefficient

In the previous section, we obtained the asymptotic forms of the scattered and transmitted fields. These fields are known whenever the scattering and transmission amplitudes  $R_{\nu}(q|k)$  and  $T_{\nu}(q|k)$  are known. We will later in this section describe methods for how to determine these amplitudes.

However, these two amplitudes are not accessible in experiments. Since, of course, our ultimate goal is to compare the theoretical predictions to those of experimental measurements, one has to relate these amplitudes to measurable quantities. Such quantities are provided by the so-called mean differential reflection and transmission coefficients. These are not the only experimentally accessible quantities possible. However, other such quantities must necessarily be related to the reflection or transmission amplitudes, since they fully specify the scattering and transmission problem.

The mean differential reflection coefficient<sup>7</sup> is defined as the fraction of the total incident power scattered, by the randomly rough surface, into an angular interval of width  $d\theta_s$  about the scattering angle  $\theta_s$ . Thus, in order to obtain an expression for this quantity one has to find an expression for the power incident onto the rough surface and the power scattered from it. We recall that the total power contained in an electromagnetic wave of electric and magnetic field vectors  $\mathbf{E}$  and  $\mathbf{H}$  respectively is given by the real part of the complex Poynting vector  $\mathbf{S} = \mathbf{E} \times \mathbf{H}^*$ , where the asterisk denotes complex conjugate. More useful to us is in fact the time-averaged of this (complex) quantity. It is given by [10, 11, 34]

$$\langle \mathbf{S} \rangle_t = \frac{1}{2} \mathbf{E} \times \mathbf{H}^*, \quad (54)$$

where  $\langle \cdot \rangle_t$  indicates time average. Hence the time-averaged power incident onto the rough surface, and scattered from it, are given by the real part of the 3-component of  $\langle \mathbf{S} \rangle_t$ , evaluated for the fields involved. The corresponding time-averaged total energy flux therefore becomes<sup>8</sup>

$$P = \int dx_1 dx_2 \text{Re} \langle \mathbf{S} \rangle_t = L_2 \int dx_1 \text{Re} \langle \mathbf{S} \rangle_t. \quad (55)$$

<sup>7</sup> If the surface is two-dimensional, which we however will not discuss in great detail here, one has to consider scattering into solid angle  $d\Omega_s$  around the scattering direction  $(\theta_s, \phi_s)$  instead of into the angular interval  $d\theta_s$  around the scattering angle  $\theta_s$  as is the case if the surface is one-dimensional. Furthermore, one also has to take into account that depolarizations may occur in scattering from two-dimensional surfaces. Hence the mean differential reflection and transmission coefficients in the 2D-case have polarization indices referring to the polarization of the incident and scattered light respectively.

<sup>8</sup> Recall that the coordinate system is chosen so that the  $x_1x_2$ -plane coincide with the average (planar) surface, and that the incident plane is the  $x_1x_3$ -plane.

In writing the above equation we have taken advantage of the fact that for a one-dimensional rough surface with its generator along the  $x_1$ -direction (as we consider here), the  $x_2$ -integration becomes trivial and only contributes with a factor  $L_2$ , the length of the surface in the  $x_2$ -direction.

### 1. Plane incident wave

We recall that if the incident wave is a plane wave of the form given in Eq. (47), then the scattered field is given by the second term of Eq. (49a). The incident and scattered energy fluxes thus becomes

$$P_{inc} = \frac{L_1 L_2 c^2}{2} \frac{c^2}{\omega} \alpha_0(k, \omega), \quad (56a)$$

and

$$\begin{aligned} P_{sc} &= \frac{L_2 c^2}{2} \frac{c^2}{\omega} \int_{-\frac{\omega}{c}}^{\frac{\omega}{c}} \frac{dq}{2\pi} \alpha_0(q, \omega) |R_\nu(q|k)|^2, \\ &= \int_{-\frac{\pi}{2}}^{\frac{\pi}{2}} d\theta_s p_{sc}(\theta_s), \end{aligned} \quad (56b)$$

where

$$p_{sc}(\theta_s) = \frac{L_2}{4\pi} \omega \cos^2 \theta_s |R_\nu(q|k)|^2. \quad (56c)$$

Hence, the differential reflection coefficient, according to its definition, is given by the following expression

$$\frac{\partial R_\nu}{\partial \theta_s} = \frac{p_{sc}(\theta_s)}{P_{inc}} = \frac{1}{L_1} \frac{\omega}{2\pi c} \frac{\cos^2 \theta_s}{\cos \theta_0} |R_\nu(q|k)|.$$

In the above expression it is understood that the momenta  $k$  and  $q$  are related to the angles  $\theta_0$  and  $\theta_s$  according to

$$k = \frac{\omega}{c} \sin \theta_0, \quad (57a)$$

$$q = \frac{\omega}{c} \sin \theta_s. \quad (57b)$$

Notice that  $\partial R_\nu / \partial \theta_s$  includes the contribution from only one single realization of the rough surface. However, we are more interested in the mean of this quantity obtained by making an average over an ensemble of realizations of the rough surface profile. In consequence we obtain the following expression for the *mean differential reflection coefficient* (DRC)

$$\left\langle \frac{\partial R_\nu}{\partial \theta_s} \right\rangle = \frac{1}{L_1} \frac{\omega}{2\pi c} \frac{\cos^2 \theta_s}{\cos \theta_0} \left\langle |R_\nu(q|k)|^2 \right\rangle. \quad (58)$$

When light is scattered from a randomly rough surface both coherent (specular) and incoherent (diffuse) scattering processes will normally occur. The scattered power due to both these processes are contained in Eq. (58). In theoretical studies of wave scattering from rough surfaces it has proven useful to separate these two contributions even though such a separation is not possible under experimental conditions. The separation is done by noticing that  $\left\langle |R_\nu(q|k)|^2 \right\rangle$  can trivially be written as

$$\left\langle |R_\nu(q|k)|^2 \right\rangle = \left\langle |R_\nu(q|k)|^2 \right\rangle - |\langle R_\nu(q|k) \rangle|^2 + |\langle R_\nu(q|k) \rangle|^2. \quad (59)$$

Here the last term (on the right hand side) corresponds to the coherently scattered light, while the first two terms are related to the light scattered incoherently. By using this result we find that the mean DRC can be subdivided into a coherent and an incoherent part, and they are respectively given by

$$\left\langle \frac{\partial R_\nu}{\partial \theta_s} \right\rangle_{\text{coh}} = \frac{1}{L_1} \frac{\omega}{2\pi c} \frac{\cos^2 \theta_s}{\cos \theta_0} |\langle R_\nu(q|k) \rangle|^2, \quad (60a)$$

and

$$\left\langle \frac{\partial R_\nu}{\partial \theta_s} \right\rangle_{\text{incoh}} = \frac{1}{L_1} \frac{\omega}{2\pi c} \frac{\cos^2 \theta_s}{\cos \theta_0} \left[ \left\langle |R_\nu(q|k)|^2 \right\rangle - |\langle R_\nu(q|k) \rangle|^2 \right]. \quad (60b)$$

Expressions for the *mean differential transmission coefficient*,  $\langle \partial T_\nu / \partial \theta_s \rangle = \langle p_{tr}(\theta_t) / P_{inc} \rangle$ , can be obtained in an analogous way by calculating  $p_{tr}(\theta_t)$ , the equivalent of  $p_{sc}(\theta_s)$  in transmission. The results of such a calculation is that the expressions for  $\langle \partial T_\nu / \partial \theta_s \rangle$  can be obtained from those of  $\langle \partial R_\nu / \partial \theta_s \rangle$  by substituting the transmission amplitude  $T_\nu(q|k)$  for the reflection amplitude,  $R_\nu(q|k)$  and multiplying the final expression with a factor of  $\sqrt{\varepsilon(\omega)}$ .

## 2. Finite width incident beam

In the previous subsection we considered a plane incident wave. Such waves can never be achieved under experimental conditions, and it is therefore desirable in some cases to work with a incident beam of finite width.

Such a beam has already been defined in Subsection. III B 2 and with these expressions one gets for the incident and scattered energy fluxes

$$P_{inc} = L_2 \frac{wc}{2\sqrt{2}\pi} \left[ \text{erf} \left( \frac{w}{\sqrt{2}} \frac{\omega}{c} \left( \frac{\pi}{2} - \theta_0 \right) \right) + \text{erf} \left( \frac{w}{\sqrt{2}} \frac{\omega}{c} \left( \frac{\pi}{2} + \theta_0 \right) \right) \right], \quad (61a)$$

where  $\text{erf}(x)$  is the error-function [39], and

$$p_{sc}(\theta_s) = L_2 \frac{\omega}{2\pi^2} \cos^2 \theta_s |R_\nu(q|k)|^2. \quad (61b)$$

Hence, the differential reflection coefficient, according to its definition, is given by the expression

$$\left\langle \frac{\partial R_\nu}{\partial \theta_s} \right\rangle = \frac{2}{(2\pi)^{\frac{3}{2}}} \frac{\omega}{cw} \cos^2 \theta_s \frac{\left\langle |R_\nu(q, \omega)|^2 \right\rangle}{\frac{1}{2} \left[ \text{erf} \left( \frac{w\omega}{\sqrt{2}c} \left( \frac{\pi}{2} + \theta_0 \right) \right) + \text{erf} \left( \frac{w\omega}{\sqrt{2}c} \left( \frac{\pi}{2} - \theta_0 \right) \right) \right]}. \quad (62)$$

Also here  $q$  is understood to be related to the scattering angle by Eq. (57b). The coherent and incoherent part of the mean differential reflection coefficient are obtained in the same way as for the case of a plane incident wave. These expressions will not be explicitly included here since they follow from Eq. (62) by a simple substitution for of Eq. (59).

## D. General Properties of the Scattering Problem

In order to solve the scattering problem, we have to calculate the scattering and transmission amplitudes,  $R_\nu(q|k)$  and  $T_\nu(q|k)$ . However, before we start discussing various methods for obtaining this goal, we will introduce some general features that the scattering problem should fulfill. These properties are, among others, *reciprocity* and *unitarity*.

### 1. Reciprocity

A general property of the scattering problem is the one of reciprocity. It involves the scattering matrix,  $S_\nu(q|k)$ , defined via the scattering amplitude according to

$$S_\nu(q|k) = \frac{\sqrt{\alpha_0(q, \omega)}}{\sqrt{\alpha_0(k, \omega)}} R_\nu(q|k). \quad (63)$$

The reciprocity theorem states that this scattering matrix, or just S-matrix for short, should satisfy the following relation

$$S_\nu(q|k) = S_\nu(-k|-q). \quad (64)$$

This relation for the surface scattering problem can under rather general assumptions be derived rigorously from Lorentz's reciprocity theorem [8]. However, we will not present such an interesting, but lengthy derivation here. We would, however, like to point out that such a derivation does not assume anything about the dielectric functions involved. Furthermore, there is no restriction on how strongly rough the surface is, neither how it is correlated. Hence, the reciprocity theorem is generally valid. It should also be pointed out that there seems to be no equivalent theorem to Eq. (64) that involves the transmission amplitude  $T_\nu(q|k)$ . Reciprocity is therefore a property of the scattering amplitude.

## 2. Unitarity

In cases where the scattering medium is a perfect reflector, *i.e.* if  $\text{Re } \varepsilon(\omega) < 0$  and  $\text{Im } \varepsilon(\omega) = 0$ , the scattering matrix,  $S_\nu(q|k)$ , possess an additional property call *unitarity*. Since there is no absorption ( $\text{Im } \varepsilon(\omega) = 0$ ) and no transmission in the system the energy incident on the rough, perfectly reflecting surface must be conserved. Without going into details, this has the consequence that the following relation has to be satisfied [8]

$$\int_{-\frac{\omega}{c}}^{\frac{\omega}{c}} \frac{dq}{2\pi} S_\nu(q|k) S_\nu^*(q|k') = 2\pi \delta(k - k'), \quad |k|, |k'| < \frac{\omega}{c}. \quad (65)$$

It can be derived by calculating the total energy flux scattered from the surface that, due to energy conservation, should equal the incident energy flux. Eq. (65) expresses the unitarity of the scattering matrix, and it is a consequence of the conservation of energy in the scattering process.

Even if Eq. (65) is derived under the assumption that energy conservation is satisfied, let us for a moment show how this indeed follows from the unitarity condition. Let us assume that the rough surface has length  $L_1$ . Then we know from the sampling theorem [40] that the smallest momentum variable that we can resolve is  $2\pi/L_1$ . By multiplying each side of Eq. (65) by  $dk'/(2\pi)$  and integrating the resulting expression over an interval of length  $2\pi/L_1$  that contains  $k' = k$  one finds

$$\frac{1}{L_1} \int_{-\frac{\omega}{c}}^{\frac{\omega}{c}} \frac{dq}{2\pi} |S_\nu(q|k)|^2 = 1. \quad (66)$$

By now using the definition of the scattering matrix, Eq. (63), together with Eq. (57b), one arrives at

$$\int_{-\pi/2}^{\pi/2} \left\langle \frac{\partial R_\nu}{\partial \theta_s} \right\rangle d\theta_s = 1, \quad (67)$$

where we have taken advantage of Eq. (58). From the definition of the mean differential reflection coefficient given in Sect. III C 1, we understand that Eq. (67) is just the conservation of energy for the scattering system considered.

## 3. Energy Conservation

If, however, the lower medium is *not* a perfect conductor, but still is a non-absorbing medium ( $\text{Im } \varepsilon(\omega) = 0$ ) the unitarity condition Eq. (65) will no longer hold true. However, we should still have conservation of energy. This means that all energy incident onto the rough surface should be either scattered from it or transmitted through it. This fact is expressed by the following equation

$$\mathcal{U}_\nu^{\text{sc}}(\theta_0, \omega) + \mathcal{U}_\nu^{\text{tr}}(\theta_0, \omega) = 1, \quad (68)$$

where  $\theta_0$  is the angle of incidence of the light, and

$$\mathcal{U}_\nu^{\text{sc}}(\theta_0, \omega) = \int_{-\pi/2}^{\pi/2} \left\langle \frac{\partial R_\nu}{\partial \theta_s} \right\rangle d\theta_s, \quad (69a)$$

$$\mathcal{U}_\nu^{\text{tr}}(\theta_0, \omega) = \int_{-\pi/2}^{\pi/2} \left\langle \frac{\partial T_\nu}{\partial \theta_t} \right\rangle d\theta_t. \quad (69b)$$

Physically  $\mathcal{U}_\nu^{\text{sc}}(\theta_0, \omega)$  expresses the fraction of the incident energy scattered from the surface, while in a similar way  $\mathcal{U}_\nu^{\text{tr}}(\theta_0, \omega)$  expresses the energy fraction transmitted through the system. Notice that the energy conservation condition

should hold true for all incident angles and polarizations as well as being independent of the width of the incident beam. The only restriction being that there should be no medium that absorbs energy. However, if absorption is present, Eq. (68) might be modified by adding an absorption term to the right hand side. Unfortunately, this absorption term is hard to calculate in a rigorous way.

For practical purposes, the conditions Eqs. (67) and (68) are most frequently used as a test of the quality of numerical simulations (see Sect. IIII). In such an approach these conditions are necessary, but not sufficient conditions for the correctness of the simulations.

### E. Derivation of the Reduced Rayleigh Equation

The reduced Rayleigh equation (RRE), under which name we know it today, was first derived by Toigo, Marvin and Celli [44] in the last half of the 1970's. This equation is the single integral equation satisfied by the reflection or transmission amplitudes. This equation, even if its precise region of validity is hard to quantify in detail, has served as the starting point for many, if not all, of the perturbative techniques developed in the field of wave scattering from rough surface. We would, however, already at this early stage like to stress that the reduced Rayleigh equation is not restricted to the same limitations as perturbation theory, and that its validity goes beyond that of such theories. It can in fact also be used in numerical simulations to obtain non-perturbative results.

We will below give the detailed derivation of the RRE for reflection. The scattering geometry that we consider is the one presented in Fig. 6. This geometry is illuminated from above by a plane incident wave of either  $p$ - or  $s$ -polarization, and the incident plane is the  $x_1x_3$ -plane.

#### 1. The Rayleigh Hypothesis

It should be clear that for the region above the maximum point of the surface the total field takes the form given by Eq. (49a) and similarly the total field below the minimum point of the surface can be expressed according to Eq. (49b). However, in order to solve the scattering problem, one has to take into account the boundary conditions to be satisfied at the randomly rough surface  $\zeta(x_1)$  separating the two media above and below it. The problem is that we don't know the form of the total field close to the surface, or to be more precise, in the region  $\min \zeta(x_1) < \zeta(x_1) < \max \zeta(x_1)$ . It should be obvious from a ray optical point of view, that at least for rather rough surfaces, expansions of the form (49) are not adequate to describe the total field in this region due to the lack of not allowing downward propagating scattered modes. However, as the surface becomes smoother and smoother, the asymptotic expansions of the field given earlier should represent a better and better approximation for the total field. This lead Lord Rayleigh [1, 2], when studying scattering from sinusoidal surfaces, to assume that the asymptotic expansions for the total field was not only valid in the region far away from the rough surface, but could also be used all the way down to the rough surface. Under this assumption, known today as the *Rayleigh hypothesis*, he could satisfy the boundary conditions on the rough surface and thereby derive equation which lead to the solution of his scattering problem.

#### The Validity of the Rayleigh Hypothesis

We will in the next subsection demonstrate this procedure when applied to the wave scattering from a randomly rough surface. However, before we do so, we will dwell a little upon the validity of the Rayleigh hypothesis. Theories based on this approximation do not properly include, as mentioned above, downward propagating scattered or upward propagating transmitted waves. From a naive geometrical optics argument, we realize that a scattering process producing incoming scattered or transmitted waves has to be a multiple scattering process. So, scattering geometries where the Rayleigh hypothesis is not valid, has thus to be dominated by multiple scattering, and has therefore to be rather rough. It should, however, be stressed that this do not imply that for any scattering geometry dominated by multiple scattering, the Rayleigh hypothesis is doomed to break down. One might very well have processes dominated by multiple scattering without receiving essential contributions from downward propagating scattered waves. Good examples of this are provided by the ability of perturbative and numerical studies based on the Rayleigh hypothesis to show multiple scattering phenomena like the enhanced backscattering and satellite peaks [21, 42, 121].

The Rayleigh hypothesis is hence a good approximation if the surface is not too rough. However, at what level of roughness must we say that this approximation no longer is valid? There has been many papers devoted to the study of the validity of the Rayleigh approximation. There seems today to be consensus on the criterion [43]

$$\frac{\delta}{a} \ll 1, \quad (70)$$

where  $\delta$  and  $a$  are the RMS-height and correlation length of the surface respectively. The reader is encouraged to consult the literature for more details [43].

## 2. The Rayleigh Equations

In this subsection we will derive a set of two inhomogeneous coupled integral equation for the scattering and transmission amplitudes,  $R_\nu(q|k)$  and  $T_\nu(q|k)$ . These equations are referred to as the Rayleigh equations, and we will now demonstrate how they are obtained.

From Sect. II C we recall that the boundary conditions to be satisfied by the field on the surface are the continuity of the field and its normal derivative, *i.e.*

$$\Phi_\nu^+(x_1, x_3|\omega)\Big|_{x_3=\zeta(x_1)} = \Phi_\nu^-(x_1, x_3|\omega)\Big|_{x_3=\zeta(x_1)}, \quad (71a)$$

$$\partial_n \Phi_\nu^+(x_1, x_3|\omega)\Big|_{x_3=\zeta(x_1)} = \frac{\partial_n \Phi_\nu^-(x_1, x_3|\omega)}{\kappa_\nu(\omega)}\Big|_{x_3=\zeta(x_1)}, \quad (71b)$$

where the normal derivative,  $\partial_n$ , and the symbol  $\kappa_\nu(\omega)$  have been defined earlier in Eqs. (14b) and (14d).

If now the Rayleigh hypothesis holds true, the asymptotic field expansions of Sect. IIIB, can be used in order to fulfill those boundary conditions. By substituting the asymptotic expansions, Eqs. (49), into the boundary condition for the field, Eq. (71a), one is lead to the following integral equation

$$e^{ikx_1 - i\alpha_0(k, \omega)\zeta(x_1)} + \int \frac{dq}{2\pi} R_\nu(q|k) e^{iqx_1 + i\alpha_0(q, \omega)\zeta(x_1)} = \int \frac{dq}{2\pi} T_\nu(q|k) e^{iqx_1 - i\alpha(q, \omega)\zeta(x_1)}.$$

If we now rewrite this equation, which will prove useful later on, by using the properties of the Dirac  $\delta$ -function we get

$$\int \frac{dq}{2\pi} e^{iqx_1} \left[ 2\pi\delta(q-k) e^{-i\alpha_0(q, \omega)\zeta(x_1)} + R_\nu(q|k) e^{i\alpha_0(q, \omega)\zeta(x_1)} \right] = \int \frac{dq}{2\pi} e^{iqx_1} T_\nu(q|k) e^{-i\alpha(q, \omega)\zeta(x_1)}. \quad (72a)$$

By doing the same for the boundary condition for the normal derivative, *i.e.* Eq.(71b), one arrives at

$$\begin{aligned} \int \frac{dq}{2\pi} e^{iqx_1} \left[ -2\pi\delta(q-k) \{ \zeta'(x_1)q + \alpha_0(q, \omega) \} e^{-i\alpha_0(q, \omega)\zeta(x_1)} + R_\nu(q|k) \{ -\zeta'(x_1)q + \alpha_0(q, \omega) \} e^{i\alpha_0(q, \omega)\zeta(x_1)} \right] \\ = -\frac{1}{\kappa_\nu(\omega)} \int \frac{dq}{2\pi} e^{iqx_1} T_\nu(q|k) \{ \zeta'(x_1)q + \alpha(q, \omega) \} e^{-i\alpha(q, \omega)\zeta(x_1)}. \end{aligned} \quad (72b)$$

Together Eqs. (72) constitute a set of coupled inhomogeneous integral equations announced earlier — the Rayleigh equations.

## 3. The Reduced Rayleigh Equations

We will now continue to derive the so-called reduced Rayleigh equation (RRE) for reflection [44] and transmission [45]. The RRE is a single integral equation satisfied by the reflection or transmission amplitude. They are derived from the Rayleigh equations by eliminating respectively the transmission and reflection amplitudes.

### The Reduced Rayleigh Equation for Reflection

In order to obtain the reduced Rayleigh equation for reflection, we have to eliminate the transmission amplitude,  $T_\nu(q|k)$  from the (coupled) Rayleigh equations given in the previous subsection. By multiply Eq.(72a) by

$$e^{-ipx_1 - i\alpha(p, \omega)\zeta(x_1)} [-\zeta'(x_1)p + \alpha(p, \omega)], \quad (73)$$

and Eq.(72b) by

$$\kappa_\nu(\omega) e^{-ipx_1 - i\alpha(p, \omega)\zeta(x_1)}, \quad (74)$$



adding the two resulting equations, and integrating the final result over  $x_1$ , one finds that the terms containing the transmission amplitude vanishes identically. In detail what one gets for terms proportional to  $T_\nu(q|k)$  are

$$\int dx_1 \frac{dq}{2\pi} T_\nu(q|k) [-\zeta'(x_1)(p+q) + \alpha(p, \omega) - \alpha(q, \omega)] e^{-i(p-q)x_1} e^{i(-\alpha(p, \omega) - \alpha(q, \omega))\zeta(x_1)}. \quad (75)$$

This expression is simplified by introducing an integral defined according to<sup>9</sup>

$$I(\gamma|q) = \int dx_1 e^{-i\gamma\zeta(x_1)} e^{-iqx_1}. \quad (76)$$

From this definition it follows that

$$\frac{qI(\gamma|q)}{\gamma} = \int dx_1 \zeta'(x_1) e^{-i\gamma\zeta(x_1)} e^{-iqx_1}. \quad (77)$$

With Eqs. (76) and (77), Eq. (75) can be written in the form

$$\int \frac{dq}{2\pi} T_\nu(q|k) \left[ \frac{(p-q)(p+q)}{\alpha(p, \omega) + \alpha(q, \omega)} + \alpha(p, \omega) - \alpha(q, \omega) \right] I(\alpha(p, \omega) + \alpha(q, \omega)|p-q).$$

By some simple algebra it can readily be shown that the expression in the square brackets is identically zero, and thus the transmission amplitude  $T_\nu(q|k)$  has been eliminated from the Rayleigh equations.

The reduced Rayleigh equation for reflection now follows from the remaining non-vanishing parts of the equation. It reads

$$\int \frac{dq}{2\pi} M_\nu^+(p|q) R_\nu(q|k) = M_\nu^-(p|q) \quad (78a)$$

where

$$M_\nu^\pm(p|q) = \pm \left[ \frac{(p + \kappa_\nu(\omega)q)(p - q)}{\alpha(p, \omega) \mp \alpha_0(q, \omega)} + \alpha(p, \omega) \pm \kappa_\nu(\omega)\alpha_0(q, \omega) \right] I(\alpha(p, \omega) \mp \alpha_0(q, \omega)|p - q). \quad (78b)$$

#### *P-polarization*

If we restrict ourselves to  $p$ -polarization, the reduced Rayleigh equation as presented in Eqs. (78) takes on a simpler form. By a straight forward calculation one finds<sup>10</sup>

$$\int \frac{dq}{2\pi} N_p^+(p|q) R_p(q|k) = N_p^-(p|q), \quad (79a)$$

where

$$N_p^\pm(p|q) = \pm \frac{pq \pm \alpha(p, \omega)\alpha_0(q, \omega)}{\alpha(p, \omega) \mp \alpha_0(q, \omega)} I(\alpha(p, \omega) \mp \alpha_0(q, \omega)|p - q). \quad (79b)$$

#### *S-polarization*

Similarly for  $s$ -polarization one finds<sup>11</sup>

$$\int \frac{dq}{2\pi} N_s^+(p|q) R_s(q|k) = N_s^-(p|q), \quad (80a)$$

where

$$N_s^\pm(p|q) = \pm \frac{1}{\alpha(p, \omega) \mp \alpha_0(q, \omega)} I(\alpha(p, \omega) \mp \alpha_0(q, \omega)|p - q). \quad (80b)$$

<sup>9</sup> Be aware that various sign conventions seems to appear in the literature for this quantity.

<sup>10</sup> Here the matrix elements  $M_p^\pm(p|q)$  and  $N_p^\pm(p|q)$  are related by  $M_p^\pm(p|q) = (\varepsilon(\omega) - 1)N_p^\pm(p|q)$ .

<sup>11</sup> Here is  $M_s^\pm(p|q) = (\varepsilon(\omega) - 1)(\omega/c)^2 N_s^\pm(p|q)$ .

#### 4. The Reduced Rayleigh Equation for Transmission

In the previous subsection it was shown that by eliminating the terms containing the transmission amplitude from the two coupled Rayleigh equations, the reduced Rayleigh equation for reflection was obtained. In a similar way, the scattering amplitude might be eliminated from the same equations, resulting in the reduced Rayleigh equation for transmission.

We will not go into details about how this is done, since the derivation mimics the one given in the previous subsection. Here we will only give the results that are [45]

$$\int_{-\infty}^{\infty} \frac{dq}{2\pi} \frac{I(\alpha(q, \omega) - \alpha_0(p, \omega)|p - q)}{\alpha(q, \omega) - \alpha_0(p, \omega)} [pq + \alpha_0(p, \omega)\alpha(q, \omega)] T_p(q|k) = 2\pi\delta(p - k) \frac{2\varepsilon(\omega)\alpha_0(k, \omega)}{\varepsilon(\omega) - 1}. \quad (81a)$$

for  $p$ -polarization, and [45]

$$\int_{-\infty}^{\infty} \frac{dq}{2\pi} \frac{I(\alpha(q, \omega) - \alpha_0(p, \omega)|p - q)}{\alpha(q, \omega) - \alpha_0(p, \omega)} T_s(q|k) = 2\pi\delta(p - k) \frac{2\alpha_0(k, \omega)}{\frac{\omega^2}{c^2}(\varepsilon(\omega) - 1)}. \quad (81b)$$

for  $s$ -polarization.

This concludes the section on the reduced Rayleigh equation.

### F. Small Amplitude Perturbation Theory

Among the oldest theories addressing rough surface scattering we find the small amplitude perturbation theory [4]. The starting point for this perturbation theory, like most of the perturbation theories developed for handling wave scattering from rough surface, is the reduced Rayleigh equation (78). If the rough surface is weakly rough, most of the light incident upon it is scattered into the specular direction. However, due to the surface roughness, a small fraction of the incident power is scattered away from the specular direction. Theoretically, this non-specular scattering is taken into account by assuming an expansion for the scattering amplitude in powers of the surface profile function of the form<sup>12</sup>

$$R_\nu(q|k) = \sum_{n=0}^{\infty} \frac{R_\nu^{(n)}(q|k)}{n!}. \quad (82)$$

Here  $R_\nu^{(n)}(q|k)$  is assumed to be of order  $\mathcal{O}(\zeta^n)$  in the surface profile function  $\zeta(x_1)$ . In order to solve the scattering problem in this way, we therefore have to determine the expansion coefficients  $\{R_\nu^{(n)}(q|k)\}$ . However, to determine all these coefficients is obviously not practically possible if  $\zeta(x_1)$  is a rough surface. Therefore, the expansion (82) is terminated at some upper value  $N$ , resulting in an  $N$ 'th order perturbation theory. In practical application one usually has  $N \leq 3-5$ . If the surface is weakly rough the sum of these  $N$  terms will provide a good approximation to the total scattering amplitude  $R_\nu(q|k)$ . However, as the surface roughness becomes stronger and stronger, a higher number of terms has to be included in the expansion, and the method becomes cumbersome and not very practical since  $R_\nu^{(n)}(q|k)$  for big values of  $n$  easily becomes complicated. Thus, the small amplitude perturbation theory is only of interest for weakly rough surfaces. Hence, it should therefore not represent any restriction to assume that the Rayleigh hypothesis is valid and therefore that  $R_\nu(q|k)$  should satisfy the reduced Rayleigh equation, Eq. (78).

Under this assumption, the various terms in the expansion for the scattering amplitude can in principle be obtained by substituting its expansion, Eq. (82), into the reduced Rayleigh equation, Eq. (78), and satisfy the resulting equation order-by-order in the surface profile function  $\zeta(x_1)$ . However, before this can be done,  $N_\nu^\pm(p|q)$ , or equivalently  $M_\nu^\pm(p|q)$ , that enter via the reduced Rayleigh equation, also have to be expanded in powers of the surface profile function. Since the matrix-elements,  $N_\nu^\pm(p|q)$ , only depend on  $\zeta(x_1)$  through the integrals  $I(\gamma|q)$ , defined in Eq. (76), one makes the following expansion

$$I(\gamma|q) \equiv \int dx_1 e^{-i\gamma\zeta(x_1)} e^{-iqx_1} = \sum_{n=0}^{\infty} \frac{(-i\gamma)^n}{n!} \tilde{\zeta}^{(n)}(q), \quad (83a)$$

---

<sup>12</sup> The prefactors in this expansion is included for later convenience.

where

$$\tilde{\zeta}^{(n)}(q) = \int_{-\infty}^{\infty} dx_1 \zeta^n(x_1) e^{-iqx_1}, \quad (83b)$$

is the (inverse) Fourier transform of the  $n$ th power of the surface profile function. From the above equations it should be apparent why we made the choice we did for the prefactors in the expansion for  $R_\nu(q|k)$ .

When the expansion (83) is substituted into the expressions for  $N_\nu^\pm(p|q)$ , Eqs. (79b) and (80b), one obtains

$$N_\nu^\pm(p|q) = \sum_{n=0}^{\infty} \frac{\mathcal{N}_\nu^{\pm(n)}(p|q)}{n!} \tilde{\zeta}^{(n)}(p-q), \quad (84a)$$

where for  $p$ -polarization

$$\mathcal{N}_p^{\pm(0)}(p|p) = \frac{\varepsilon(\omega)\alpha_0(p,\omega) \pm \alpha(p,\omega)}{\varepsilon(\omega) - 1}, \quad (84b)$$

and

$$\mathcal{N}_p^{\pm(n)}(p|q) = (-i)^n [\pm pq + \alpha(p,\omega)\alpha_0(q,\omega)] [\alpha(p,\omega) \mp \alpha_0(q,\omega)]^{n-1}, \quad (84c)$$

when  $n \geq 1$ , while for  $s$ -polarization we have

$$\mathcal{N}_s^{\pm(0)}(p|p) = \frac{\alpha_0(p,\omega) \pm \alpha(p,\omega)}{\frac{\omega^2}{c^2} (\varepsilon(\omega) - 1)}, \quad (84d)$$

and

$$\mathcal{N}_s^{\pm(n)}(p|q) = \pm(-i)^n [\alpha(p,\omega) \mp \alpha_0(q,\omega)]^{n-1}, \quad (84e)$$

when  $n \geq 1$ .

With these relations available, a recurrence relations for  $\{R_\nu^{(n)}(p|q)\}$ , is readily obtained by substituting Eqs. (82) and (84) into the reduced Rayleigh equation, Eqs. (79a) and (80a), and equating terms of the same order in  $\tilde{\zeta}(q)$ . The recurrence relation reads

$$\sum_{m=0}^{\infty} \binom{n}{m} \int_{-\infty}^{\infty} \frac{dp}{2\pi} \mathcal{N}_\nu^{+(n-m)}(q|p) \tilde{\zeta}^{(n-m)}(q-p) R_\nu^{(m)}(p|k) = \mathcal{N}_\nu^{-(n)}(q|k) \tilde{\zeta}^{(n)}(q-k). \quad (85)$$

Now the expansion coefficients for the scattering amplitude,  $R_\nu^{(n)}(p|q)$ , should be rather straight forward to obtain (at least in principle). The lowest order term,  $n = 0$ , is given by

$$R_\nu^{(0)}(q|k) = 2\pi \delta(p-k) R_\nu^{(0)}(k,\omega) \quad (86a)$$

where  $R_\nu^{(0)}(k,\omega)$  given by ( $\varepsilon = 1$ )

$$R_\nu^{(0)}(k,\omega) = \begin{cases} \frac{\varepsilon(\omega)\alpha_0(k,\omega) - \varepsilon_0(\omega)\alpha(k,\omega)}{\varepsilon(\omega)\alpha_0(k,\omega) + \varepsilon_0(\omega)\alpha(k,\omega)}, & \nu = p, \\ \frac{\alpha_0(k,\omega) - \alpha(k,\omega)}{\alpha_0(k,\omega) + \alpha(k,\omega)}, & \nu = s. \end{cases} \quad (86b)$$

In these expressions, the momentum variables  $k$  and  $q$  are understood to be related to the angles of incidence and scattering,  $\theta_0$  and  $\theta_s$  respectively, through

$$k = \frac{\omega}{c} \sin \theta_0, \quad (87a)$$

$$q = \frac{\omega}{c} \sin \theta_s. \quad (87b)$$

The above results are, as expected, the result that we would get for the scattering from a planar surface, and we note that  $R_\nu^{(0)}(k,\omega)$  is nothing else then the Fresnel reflection coefficients [10]. Notice that the  $\delta$ -function in Eq. (86a), coming from  $\tilde{\zeta}^{(0)}$ , guarantees that the scattering is only into the specular direction.

The results for the higher order terms ( $n \geq 1$ ) in the expansion of  $R_\nu(q|k)$ , describe the light scattered by the roughness into directions other than the specular. These terms can be calculated recursively from Eq. (85), but, unfortunately, such expressions easily become rather cumbersome for higher the order terms. However, the first few terms are manageable, and they are given by the following expressions [46]

$$R_\nu^{(1)}(q|k) = \chi_\nu^{(1)}(q|k) \tilde{\zeta}(q-k), \quad (88a)$$

$$R_\nu^{(2)}(q|k) = \frac{1}{2!} \int_{-\infty}^{\infty} \frac{dp}{2\pi} \chi_\nu^{(2)}(q|p|k) \tilde{\zeta}(q-p) \tilde{\zeta}(p-k), \quad (88b)$$

$$R_\nu^{(3)}(q|k) = \frac{1}{3!} \int_{-\infty}^{\infty} \frac{dp_1}{2\pi} \int_{-\infty}^{\infty} \frac{dp_2}{2\pi} \chi_\nu^{(3)}(q|p_1|p_2|k) \tilde{\zeta}(q-p_1) \tilde{\zeta}(p_1-p_2) \tilde{\zeta}(p_2-k), \quad (88c)$$

where, the functions  $\chi_\nu^{(1)}(q|k)$ ,  $\chi_\nu^{(2)}(q|p|k)$ , ... are somewhat lengthy functions of their arguments, and are therefore given separately in Appendix B.

As discussed earlier, the first few terms of the expansion (82) with Eqs. (88) substituted, should hence for a weakly rough surfaces represent a good (3rd order) approximation to  $R_\nu(q|k)$ . Experimental accessible quantities could therefore be calculated based on this approximation. For instance, the mean differential reflection coefficient from the incoherent component of the scattered field is then, according to Eq. (60b), through fourth order in the surface profile function, given by

$$\begin{aligned} \left\langle \frac{\partial R_\nu}{\partial \theta_s} \right\rangle_{\text{incoh}} &= \frac{1}{L_1} \frac{\omega}{2\pi c} \frac{\cos^2 \theta_s}{\cos \theta_0} \left[ \left\langle \left| R_\nu^{(1)}(q|k) \right|^2 \right\rangle + \frac{1}{4} \left\{ \left\langle \left| R_\nu^{(2)}(q|k) \right|^2 \right\rangle - \left| \left\langle R_\nu^{(2)}(q|k) \right\rangle \right|^2 \right\} \right. \\ &\quad \left. + \frac{1}{3} \text{Re} \left\langle R_\nu^{(3)}(q|k) R_\nu^{(1)*}(q|k) \right\rangle \right] + \mathcal{O}(\delta^6). \end{aligned} \quad (89a)$$

In arriving at Eq. (89a) it has been assumed that the surface profile function,  $\zeta(x_1)$ , constitutes a zero-mean, stationary, Gaussian random process. Due to the Gaussian character of the surface only terms that contain an even number of surface profile function survives the averaging process. The different averaged contained in Eq. (89a) can all be related to the set of functions  $\{\chi_\nu^{(n)}(q|k)\}$  according to

$$\left\langle \left| R_\nu^{(1)}(q|k) \right|^2 \right\rangle = L_1 \delta^2 g(|q-k|) \left| \chi_\nu^{(1)}(q|k) \right|^2, \quad (89b)$$

$$\begin{aligned} \left\langle \left| R_\nu^{(2)}(q|k) \right|^2 \right\rangle - \left| \left\langle R_\nu^{(2)}(q|k) \right\rangle \right|^2 &= L_1 \delta^4 \int_{-\infty}^{\infty} \frac{dp}{2\pi} g(|q-p|) g(|p-k|) \\ &\quad \times \left\{ \left| \chi_\nu^{(2)}(q|p|k) \right|^2 + \chi_\nu^{(2)}(q|p|k) \chi_\nu^{(2)*}(q|q+k-p|k) \right\}, \end{aligned} \quad (89c)$$

and

$$\begin{aligned} \left\langle R_\nu^{(3)}(q|k) R_\nu^{(1)*}(q|k) \right\rangle &= L_1 \delta^4 g(|q-k|) \chi_\nu^{(1)*}(q|k) \\ &\quad \times \int_{-\infty}^{\infty} \frac{dp}{2\pi} \left\{ \chi_\nu^{(3)}(q|p|q|k) g(|p-q|) + \chi_\nu^{(3)}(q|k|p|k) g(|p-k|) + \chi_\nu^{(3)}(q|p|p+k-q|k) g(|p-q|) \right\}. \end{aligned} \quad (89d)$$

Notice that the term (89b) represents single scattering, while the terms in Eq. (89c) give the contribution due to double scattering. Eq. (89d) represents a ‘‘mixed’’ contribution.

### *Accuracy of the Small Amplitude Perturbation Theory*

So what accuracy can we expect to achieve by using the small amplitude perturbation theory, and for what range of surface parameters is it valid? There have been many studies in the past, both theoretical, numerical, and experimental, regarding this issue. Probably the most relevant for this introduction is the one by E. I. Thorsos and D. R. Jackson [57] who for an acoustic scattering problem studied the validity of small amplitude perturbation theory for Gaussian surfaces by comparing its prediction to the one obtained by rigorous numerical simulations (see Sect. III I). They found that the small amplitude perturbation theory is good if  $k\delta \ll 1$  and  $ka \leq 1$ , where  $\delta$  and  $a$  respectively

are the RMS-height and the correlation length of the surface. For an electromagnetic scattering problem this translate into

$$\sqrt{|\varepsilon(\omega)|} \frac{\omega}{c} \delta \ll 1, \quad (90a)$$

and

$$\frac{\omega}{c} a \leq 1, \quad (90b)$$

The first condition (90a) comes from the fact that quantities containing the surface profile function should be expandable in a Taylor series about their mean surface. The second criterion stating that the correlation length of the surface can not be too big originates from the fact that if the correlation length of the surface is too large the Gaussian height distribution becomes close to a  $\delta$ -function with the result that the second order term in the perturbative expansion can be of the same order as the first order term even if Eq. (90a) is satisfied.

If the surface is non-Gaussian it is found that the above criteria can be relaxed somewhat [58]

### G. Unitary and Reciprocal Expansions

In the previous section we presented small-amplitude perturbation theory, which is based on the expansion of the scattering amplitude  $R_\nu(q|k)$  in powers of the surface profile function  $\zeta(x_1)$ . In Sect. III D 1 we claimed that a valid theory for rough surface scattering should satisfy reciprocity, *i.e.* the theory should satisfy the relation  $S_\nu(q|k) = S_\nu(-k|-q)$ , where  $S_\nu(q|k)$  is the scattering matrix as defined in Eq. (63). By inspecting the formulae obtained in the previous section for  $R_\nu(q|k)$ , it is at least not obvious that reciprocity is satisfied. Does this mean that small amplitude perturbation theory does not respect the principle of reciprocity, and therefore is an incorrect theory? The answer to this question is no, as you might have guest, and the small amplitude perturbation theory does in fact respect reciprocity. However, to see this is not straight forward since an extensive rewriting of the expressions are need for. Theories where reciprocity is not apparent at first glance is normally referred to by saying that the theory is not manifestly reciprocal.

Due to the lack of manifest reciprocity in the small amplitude perturbation theory as well as the desire to map the classical scattering problem onto the formalism of a quantum mechanical scattering problem [47], Brown *et al.* [48, 49], in the fist half of the 1980's, constructed a theory which was manifestly reciprocal. This theory goes today under the name of many-body perturbation theory, but is also known as self-energy perturbation theory. It is this kind of perturbation theory that we will concern ourselves with in this section.

#### 1. The Transition Matrix

The starting point for the many-body perturbation theory is to make the postulation that the scattering amplitude  $R_\nu(q|k)$  should satisfy the relation [49]

$$R_\nu(q|k) = 2\pi\delta(q-k)R_\nu^{(0)}(k,\omega) - 2iG_\nu^{(0)}(q,\omega)\mathcal{T}_\nu(q|k)G_\nu^{(0)}(k,\omega)\alpha_0(k,\omega). \quad (91)$$

Here  $R_\nu^{(0)}(k,\omega)$  is the Fresnel reflection coefficient and defined by Eq. (86b). The second term of this equation, containing the transition matrix  $\mathcal{T}_\nu(q|k)$ , also known as the T-matrix, represents the field scattered away from the specular direction. Furthermore,  $G_\nu^{(0)}(k,\omega)$  is the surface plasmon polariton Green's function for the planar vacuum-metal interface. This Green's function can be defined from the relation

$$2i\alpha_0(k,\omega)G_\nu^{(0)}(k,\omega) + R_\nu^{(0)}(k,\omega) = -1, \quad (92a)$$

That leads to the following expressions

$$G_\nu^{(0)}(k,\omega) = \begin{cases} \frac{i\varepsilon(\omega)}{\varepsilon(\omega)\alpha_0(k,\omega) + \alpha(k,\omega)}, & \nu = p, \\ \frac{i}{\alpha_0(k,\omega) + \alpha(k,\omega)}, & \nu = s. \end{cases} \quad (92b)$$

## 2. The Scattering Potential

The transition matrix is postulated to satisfy the following equation [49]

$$\mathcal{T}_\nu(p|k) = V_\nu(p|k) + \int_{-\infty}^{\infty} \frac{dq}{2\pi} V_\nu(p|q) G_\nu^{(0)}(q, \omega) \mathcal{T}_\nu(q|k), \quad (93a)$$

$$= V_\nu(p|k) + \int_{-\infty}^{\infty} \frac{dq}{2\pi} \mathcal{T}_\nu(p|q) G_\nu^{(0)}(q, \omega) V_\nu(q|k), \quad (93b)$$

where  $V(q|k)$  is known as the *scattering potential*. It is supposed to be a non-resonant function of its arguments, *i.e.* not containing the Green's function  $G_\nu^{(0)}$ . In arriving at Eq. (93b) we have used explicitly that both  $V_\nu(p|k)$  and  $\mathcal{T}_\nu(p|k)$  are reciprocal, *i.e.* that  $V_\nu(p|k) = V_\nu(-k|-p)$  with a similar expression for the transition amplitude<sup>13</sup>.

We now seek an (integral) equation satisfied by the T-matrix. This is done by substituting Eq. (91) into the reduced Rayleigh equation (78), and thereby obtain

$$\int \frac{dq}{2\pi} N_\nu^+(p|q) G_\nu^0(q, \omega) \mathcal{T}_\nu(q|k) = \frac{R_\nu^{(0)}(k, \omega) N_\nu^+(q|k) - N_\nu^-(p|k)}{2i\alpha_0(k, \omega) G_\nu^{(0)}(k, \omega)}. \quad (94)$$

Even though, the many-body perturbation theory could have proceeded from this equation, it has proven useful from a purely algebraic point of view, to instead of the T-matrix work in terms of the scattering potential  $V_\nu(q|k)$ . Thus we aim to obtain an integral equation for this quantity which our perturbation theory will be based directly upon. By substituting the right hand side of Eq. (93a) into Eq. (94), making a change of variable and using Eq. (93a) once more, one obtains the desired integral equation for the scattering potential. It reads

$$\int \frac{dq}{2\pi} A_\nu(p|q) V_\nu(q|k) = B_\nu(p|k), \quad (95a)$$

where the matrix elements are given by

$$A_\nu(p|q) = \frac{[2i\alpha_0(q, \omega) G_\nu^{(0)}(q, \omega) + R_\nu^{(0)}(q, \omega)] N_\nu^+(p|q) - N_\nu^-(p|q)}{2i\alpha_0(k, \omega)} = -\frac{N_\nu^+(p|q) + N_\nu^-(p|q)}{2i\alpha_0(q, \omega)}, \quad (95b)$$

and

$$B_\nu(p|k) = \frac{R_\nu^{(0)}(p, \omega) N_\nu^+(p|k) - N_\nu^-(p|k)}{2i\alpha_0(k, \omega) G_\nu^{(0)}(k, \omega)}. \quad (95c)$$

To obtain  $A_\nu(p|q)$  we have explicitly taken advantage of Eq. (92a). With the expression presented for the matrix elements for the reduced Rayleigh equation,  $N_\nu^\pm(q|k)$ , it is now straightforward to obtain closed form expressions for  $A_\nu(p|q)$  and  $B_\nu(p|k)$ , but we will not present such expressions here.

The integral equation (95) will be the starting point for our manifestly reciprocal many-body perturbation theory. The essence of the theory is to expanding the scattering potential in powers of the surface roughness  $\zeta(x_1)$  according to

$$V_\nu(q|k) = \sum_{n=0}^{\infty} \frac{(-i)^n}{n!} V_\nu^{(n)}(q|k). \quad (96)$$

with similar expansions for  $A_\nu(p|q)$  and  $B_\nu(p|q)$ . In these expressions the superscripts denotes, as earlier, the order of the corresponding terms in the surface profile function.

One of the advantages of this theory is that even a lower order approximation to the scattering potential corresponds to a resummation of an infinite number of terms in an expansion in powers of the surface profile function<sup>14</sup>

<sup>13</sup> That this is indeed the case might be confirmed from the expressions to be derived later for these quantities.

<sup>14</sup> This is also the case for the so-called self-energy perturbation theory to be presented in the next section.

We will not go into details here, but it can be shown that the results for the few first terms in the expansion of the scattering potential are [55]

$$V_\nu^{(1)}(q|k) = \begin{cases} i \frac{\varepsilon(\omega)-1}{\varepsilon^2(\omega)} [\varepsilon(\omega)qk - \alpha(q, \omega)\alpha(k, \omega)] \tilde{\zeta}^{(1)}(q-k), & \nu = p \\ i \frac{\omega^2}{c^2} (\varepsilon(\omega) - 1) \tilde{\zeta}^{(1)}(q-k), & \nu = s, \end{cases} \quad (97a)$$

for the 1st order term, and

$$V_p^{(2)}(q|k) = i \frac{\varepsilon(\omega)-1}{\varepsilon^2(\omega)} [\alpha(q, \omega) + \alpha(k, \omega)] [qk - \alpha(q, \omega)\alpha(k, \omega)] \tilde{\zeta}^{(2)}(q-k) \\ + 2i \frac{(\varepsilon(\omega)-1)^2}{\varepsilon^3(\omega)} \alpha(q, \omega) \int_{-\infty}^{\infty} \frac{dp}{2\pi} \tilde{\zeta}^{(1)}(q-p) \alpha(p, \omega) \tilde{\zeta}^{(1)}(p-k) \alpha(k, \omega), \quad (97b)$$

and

$$V_s^{(2)}(q|k) = i \frac{\omega^2}{c^2} (\varepsilon(\omega) - 1) [\alpha(q, \omega) + \alpha(k, \omega)] \tilde{\zeta}^{(2)}(q-k), \quad (97c)$$

for the second order terms. Higher order terms can be found in *e.g.* Ref. [51]. It should be mentioned that by definition the lowest non-vanishing order of the scattering potential is 1st order in the surface profile function. In other words  $V_\nu^{(0)}(p|q) = 0$  always.

As the reader easily may check, the above expressions are manifest reciprocal, *i.e.*

$$V_\nu^{(n)}(q|k) = V_\nu^{(n)}(-k|-q),$$

and this property should hold true to all orders in the surface profile function [49]. However, it should be emphasized that expressions of this form are not obtained directly from the solution of Eq. (95), but that some rewritings instead are needed for [55].

If the transmission matrix is expanded in the same way as in Eqs. (96), *i.e.*

$$\mathcal{T}_\nu(q|k) = \sum_{n=0}^{\infty} \frac{(-i)^n}{n!} \mathcal{T}_\nu^{(n)}(q|k), \quad (98)$$

a recurrence relation for  $\{\mathcal{T}_\nu^{(n)}(p|q)\}$  in terms of  $V_\nu^{(m)}(p|q)$  can be derived and thus  $T_\nu(q|k)$  to some order can be calculated.

Hence, through the calculation of the scattering potential the T-matrix is now known. The contribution to the mean differential reflection coefficient from the incoherent component of the scattered light is

$$\left\langle \frac{\partial R_\nu}{\partial \theta_s} \right\rangle_{\text{incoh}} = \frac{1}{L_1} \frac{2}{\pi} \left( \frac{\omega}{c} \right)^3 \cos^2 \theta_s \cos \theta_0 \left| G_\nu^{(0)}(q, \omega) \right|^2 \left[ \left\langle |\mathcal{T}_\nu(q|k)|^2 \right\rangle - |\langle \mathcal{T}_\nu(q|k) \rangle|^2 \right] \left| G_\nu^{(0)}(k, \omega) \right|^2. \quad (99)$$

This expression is obtained by substituting Eq. (91) into the defining expression for the incoherent component of the mean DRC (Eq. (60b)). The expression in the square brackets for the

## H. Many-Body Perturbation Theory

The Green's function  $G_0(q, \omega)$ , we recall, is the surface plasmon polariton Green's function at a planar interface. In addition to this Green's function it is also useful to define a rough surface Green's function,  $G_\nu(k, \omega)$ , or more formally the Green's function of a  $\nu$ -polarized electromagnetic field at the randomly rough interface. Some authors refer to this function as the *renormalized* Green's function. It is defined as the solution of the following equation [49]

$$G_\nu(q|k) = 2\pi\delta(q-k)G_\nu^{(0)}(k) + G_\nu^{(0)}(q) \int_{-\infty}^{\infty} \frac{dp}{2\pi} V_\nu(q|p)G_\nu(p|k). \quad (100a)$$

This equation is often in the literature referred to as the Lippmann-Schwinger equation for the renormalized Green's function  $G_\nu(q|k)$ . Notice that from Eqs. (91) and (100a) it follows that  $R(q|k) = -2\pi\delta(q-k) - 2iG(q|k)\alpha_0(k)$ . An alternative way of expressing the above equation is obtained by iterating on  $G_\nu(q|k)$ . The result can be written as

$$G_\nu(q|k) = 2\pi\delta(q-k)G_\nu^{(0)}(k) + G_\nu^{(0)}(q)\mathcal{T}_\nu(q|p)G_\nu^{(0)}(k), \quad (100b)$$

where we have used a Born series [47] expansion for the of the T-matrix in Eq. (93). This equation is often for simplicity expressed in operator form like  $G = G_0 + G_0 T G_0$ .

In terms of the renormalized Green's function the mean DRC takes on the form

$$\left\langle \frac{\partial R_\nu}{\partial \theta_s} \right\rangle_{\text{incohr}} = \frac{1}{L_1} \frac{2 \omega^3}{\pi c^3} \cos^2 \theta_s \cos \theta_0 \left[ \left\langle |G_\nu(q|k)|^2 \right\rangle - |\langle G_\nu(q|k) \rangle|^2 \right], \quad (101)$$

where the method of smoothing [50] has been applied to Eq. (91) as well as the reduced Rayleigh equation. In these expressions the mean of the renormalized Greens function satisfies the *Dyson equation*

$$\langle G_\nu(q|k) \rangle = 2\pi\delta(q-k)G_\nu^{(0)}(k) + G_\nu^{(0)}(q) \int_{-\infty}^{\infty} \frac{dp}{2\pi} \langle M_\nu(q|p) \rangle \langle G_\nu(p|k) \rangle, \quad (102a)$$

where the unaveraged *proper self-energy*  $M_\nu(q|k)$  is a solution of the equation

$$M_\nu(q|k) = V_\nu(q|k) + \int_{-\infty}^{\infty} \frac{dp}{2\pi} M_\nu(q|p) G_\nu^{(0)}(p) [V_\nu(p|k) - \langle V_\nu(p|k) \rangle]. \quad (102b)$$

Since the surface profile function is stationary, both the renormalized Green's function and the proper self-energy are diagonal in the momentum variables  $q$  and  $k$ , *i.e.*

$$\langle G_\nu(q|k) \rangle = 2\pi\delta(q-k)G_\nu(k), \quad (103)$$

with a similar expression for the proper self-energy. Under this assumption the renormalized Green's function can formally be written as

$$G_\nu(k) = \frac{1}{(G_\nu^{(0)}(k))^{-1} - M_\nu(k)}. \quad (104)$$

Hence the surface polariton poles in  $G_\nu(k)$  are shifted as compared to those of  $G_\nu^{(0)}$  due to the presence  $M_\nu(k)$ . The self-energy can be calculated perturbatively as an expansion in powers of the surface profile function. The resulting perturbation theory is known as self-energy perturbation theory [52].

The two-particle average Green's satisfies a *Bethe-Salpeter* equation [47] of the form<sup>15</sup>

$$\left\langle |G_\nu(q|k)|^2 \right\rangle = L_1 2\pi\delta(q-k) |G_\nu(q)|^2 + |G_\nu(q)|^2 \int_{-\infty}^{\infty} \frac{dp}{2\pi} U_\nu(q|p) \left\langle |G_\nu(p|k)|^2 \right\rangle, \quad (105)$$

where  $U_\nu(q|p)$  is the so-called irreducible vertex function. Formally, one may write the solution to Eq. (105) as

$$\left\langle |G_\nu(q|k)|^2 \right\rangle = L_1 2\pi\delta(q-k) |G_\nu(q)|^2 + L_1 |G_\nu(q)|^2 X_\nu(q|k) |G_\nu(k)|^2 \quad (106)$$

where  $X_\nu(q|k)$  is the reducible vertex function. With this equation the mean DRC takes on the form

$$\left\langle \frac{\partial R_\nu}{\partial \theta_s} \right\rangle_{\text{incohr}} = \frac{2 \omega^3}{\pi c^3} \cos^2 \theta_s \cos \theta_0 |G_\nu(q)|^2 X_\nu(q|k) |G_\nu(k)|^2. \quad (107)$$

The reducible vertex function can be shown to be related to  $U_\nu(Q|k)$  though the equation

$$X_\nu(q|k) = U_\nu(q|k) + \int_{-\infty}^{\infty} \frac{dp}{2\pi} U_\nu(q|p) |G_\nu(p)|^2 X_\nu(p|k). \quad (108)$$

Unfortunately we do not know, in general, how to solve the Bethe-salpeter equation (105). Hence some approximative methods have to be employed. The most frequently used methods are the Freilikher factorization [53], or a diagrammatic method [47, 54, 73]. In this latter approach  $X_\nu(q|k)$  is approximated by a subset of (an infinite number of)

---

<sup>15</sup> In arriving at this equation also here the method of smoothing [50] has been applied.



diagrams. Those usually are the ladder diagrams and the maximally-crossed diagrams, where the former describes wave diffusion in the random media, while the latter is related to wave localization.

With this approach it can be shown that the reducible vertex function for  $p$ -polarized light incident on a rough metal surface can be written as [54]

$$X_p(q|k) = \left[ U_p^{(0)}(q|k) + \frac{A(q|k)}{4\Delta^2} + \frac{A\left(\frac{q-k}{2}|\frac{k-q}{2}\right)}{(q+k)^2 + 4\Delta^2} \right], \quad (109)$$

which when substituted into Eq. (107) defines the mean DRC in this approximation. Here,  $A(q|k)$  is a smooth function of its arguments and  $\Delta = \Delta_\varepsilon + \Delta_{sp}$  is the (total) decay rate of surface plasmon polaritons due to Ohmic losses ( $\Delta_\varepsilon$ ) in the metal and conversion into other surface plasmon polaritons ( $\Delta_{sp} \simeq \text{Im}(M(k_{sp}))$ ). Their mathematical expressions, as well as the other quantities appearing in Eq. (109), can be found in Ref. [54]. The first term in Eq. (109) is due to single-scattering, the second arises from the ladder diagrams, while the last one is the contribution from the maximally-crossed diagrams. This last term is the one that is responsible for the enhanced backscattering phenomenon that we will discuss in the next section.

It should be mentioned that in arriving at Eq. (109) the *pole-approximation* for the renormalized Green's function has been utilized. This approximation amount to writing

$$G_p(k) \simeq \frac{C(\omega)}{k - k_{sp} - i\Delta} - \frac{C(\omega)}{k + k_{sp} + i\Delta}, \quad (110)$$

where  $k_{sp}$  is the wave vector of the surface plasmon polariton (See. Eq. (19)), and  $C(\omega)$  is a constant. The Green's function for  $s$ -polarization does not have poles, and the pole-approximation is thus not relevant in this case.

## I. Numerical Simulation Approach

In the previous sections various perturbation theories were discussed. Such theories catch the main physics of the scattering problem if the surface is not too rough. However, for interfaces that are strongly rough, none of the perturbative approaches can be used because too many terms in the expansion have to be included in order for the approach to be practical.

At the present time, there does not exist any analytic non-perturbative theory that is valid for an arbitrary roughness. The reason for the lack of such general analytic theory is that for strongly rough surfaces higher order scattering processes become important. In consequence the boundary conditions to be satisfied on the random interface become dominated by non-local effects. This means that the total field on the surface at some point depends on the total field in other locations on the surface. These non-local boundary conditions hamper the development of analytic theories for strongly rough surfaces.

The best one can do at the present for these strongly rough surfaces is to resort to a numerical simulation approach. This approach, as we will see below, is based on deriving a set of coupled integral equation for the source functions, the field and its normal derivative evaluated on the surface. With the knowledge of these sources, the total field, and therefore the solution to the scattering problem, can be obtained from the extinction theorem in any point above the surface. We will now outline how all this comes about.

### 1. The Extinction Theorem

We will now derive the so-called *Ewald-Oseen extinction theorem* first formulated by P. P. Ewald and C. W. Oseen in the beginning of this century. The numerical simulation approach to be presented later in this section will be based directly upon this theorem.

Let us start by recall from Sect. IIIB that the primary field,  $\Phi_\nu(\mathbf{r}|\omega)$ , satisfies the wave equation

$$\left( \partial_{\mathbf{r}}^2 + \varepsilon(\omega) \frac{\omega}{c} \right) \Phi_\nu(\mathbf{r}|\omega) = -J_\nu^{ext}(\mathbf{r}, \omega) \quad (111)$$

where  $\varepsilon(\omega)$  is the dielectric function of the medium where the field is evaluated,  $\partial_{\mathbf{r}} = \nabla$  is the nabla-operator in the number of spatial dimensions considered, while  $J_\nu^{ext}(\mathbf{r})$  is an external source term for the field. In order to solve the scattering problem in question, one may solve this equation in the regions of constant dielectric function and match these solutions by the boundary conditions that the field, and its normal derivative, should satisfy on any

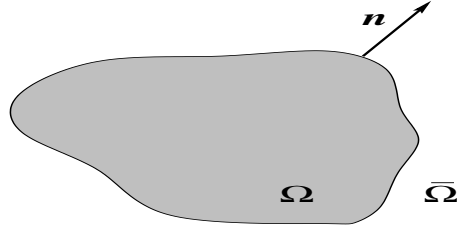


FIG. 7: The geometry considered in the extinction theorem.

interface (See Sect. II C). However, it is often more convenient to take advantage of certain integral theorems that is a consequence of the wave equation (111). The extinction theorem provides such an example.

The wave equation (111) is accompanied by the following equation for its Green's function [56]

$$\left(\partial_{\mathbf{r}}^2 + \varepsilon(\omega)\frac{\omega}{c}\right) G(\mathbf{r}|\mathbf{r}'; \omega) = -4\pi\delta(\mathbf{r} - \mathbf{r}'). \quad (112)$$

Furthermore, we are only interested in out-going solutions to this equation that fulfill the Sommerfeld's radiation condition (at infinity) [107]

$$\lim_{r \rightarrow \infty} r (\partial_r G - ikG) = 0, \quad (113)$$

where  $r = |\mathbf{r}|$ .

In two-dimensions, that we consider in the present introduction, an explicit representation of the out-going, free space Green's function is provided by [34, 56]

$$G(\mathbf{r}|\mathbf{r}'; \omega) = i\pi H_0^{(1)}\left(\varepsilon(\omega)\frac{\omega}{c}|\mathbf{r} - \mathbf{r}'|\right), \quad (114)$$

where,  $H_0^{(1)}(z)$ , is the Hankel-function of the first kind and zeroth-order [39, 56] and  $\mathbf{r} = (x_1, x_3)$ .

Let us start by considering a spatial region  $\Omega$  containing a homogeneous, isotropic dielectric medium. This region has a boundary  $\partial\Omega$  (See Fig. 7). The exterior of the region  $\Omega$  will be denoted by  $\bar{\Omega}$  where its boundary is  $\partial\bar{\Omega}$ . Notice that  $\partial\bar{\Omega}$  includes  $\partial\Omega$  in addition to the surface at infinity. We assume that an external source is present somewhere in the external region  $\bar{\Omega}$  and that no sources are present within  $\Omega$ .

If we multiply Eqs. (111) and (112) by respectively  $G(\mathbf{r}|\mathbf{r}'; \omega)$  and  $-\Phi_\nu(\mathbf{r}|\omega)$ , add the resulting equations, and finally integrate the result over the exterior region  $\bar{\Omega}$  we are left with<sup>16</sup> ( $\mathbf{r}' \in \bar{\Omega}$ )

$$\begin{aligned} & -\frac{1}{4\pi} \int_{\bar{\Omega}} d\mathbf{r}' [\Phi_\nu(\mathbf{r}'|\omega)\partial_{\mathbf{r}'}^2 G(\mathbf{r}'|\mathbf{r}; \omega) - \partial_{\mathbf{r}'}^2 \Phi_\nu(\mathbf{r}'|\omega)G(\mathbf{r}'|\mathbf{r}; \omega)] \\ & = -\frac{1}{4\pi} \int_{\bar{\Omega}} d\mathbf{r}' J_\nu^{ext}(\mathbf{r}', \omega)G(\mathbf{r}'|\mathbf{r}; \omega) + \begin{cases} \Phi_\nu(\mathbf{r}|\omega), & \mathbf{r} \in \bar{\Omega} \\ 0, & \mathbf{r} \notin \bar{\Omega} \end{cases}. \end{aligned} \quad (115)$$

Since  $G(\mathbf{r}'|\mathbf{r}; \omega)$  is the out-going free space Green's function the first term of the right hand side is just the incident field due to the source, *i.e.*

$$\frac{1}{4\pi} \int_{\bar{\Omega}} d\mathbf{r}' J_\nu^{ext}(\mathbf{r}', \omega)G(\mathbf{r}'|\mathbf{r}; \omega) = \Phi_\nu^{inc}(\mathbf{r}|\omega). \quad (116)$$

This relation holds true independent of  $\mathbf{r}$  is located in the exterior ( $\bar{\Omega}$ ) or interior ( $\Omega$ ) region.

Furthermore, by taking advantage of Green's second integral identity that for two well-behaved<sup>17</sup> functions  $u(\mathbf{r})$  and  $v(\mathbf{r})$  defined on a region  $V$ , reads [34, 56]

$$\int_V d\mathbf{r} [u(\mathbf{r})\partial_{\mathbf{r}}^2 v(\mathbf{r}) - v(\mathbf{r})\partial_{\mathbf{r}}^2 u(\mathbf{r})] = \int_{\partial V} dS [u(\mathbf{r})\partial_n v(\mathbf{r}) - v(\mathbf{r})\partial_n u(\mathbf{r})], \quad (117)$$

<sup>16</sup> We have here interchanged  $\mathbf{r}$  and  $\mathbf{r}'$  for later convenience.

<sup>17</sup> By well-behaved we here mean functions that at least are differential two times.

where  $\partial_n$  denotes the *outward* normal derivative to  $\partial V$ , Eq. (115) can be written as

$$\Phi_\nu^{inc}(\mathbf{r}|\omega) + \frac{1}{4\pi} \int_{\partial\Omega} dS' [\Phi_\nu(\mathbf{r}'|\omega)\partial_{n'}G(\mathbf{r}|\mathbf{r}';\omega) - \partial_{n'}\Phi_\nu(\mathbf{r}'|\omega)G(\mathbf{r}|\mathbf{r}';\omega)] = \begin{cases} \Phi_\nu(\mathbf{r}|\omega), & \mathbf{r} \in \bar{\Omega} \\ 0, & \mathbf{r} \notin \bar{\Omega} \end{cases} \quad (118)$$

where  $dS'$  is a surface element. In writing this equation we have explicitly used the fact that the portion of the surface integral over  $\partial\bar{\Omega}$ , that corresponds to the surface at infinity vanishes due to Sommerfeld's radiation condition satisfied by  $G(\mathbf{r}|\mathbf{r}';\omega)$ . Hence the only surface left in the surface integral is  $\partial\Omega$  as indicated in the above equation. In addition we have also utilized the relation  $\partial_n = -\partial_{\bar{n}}$  for the *outward* normal derivative to the region  $\Omega$ , while  $\partial_{\bar{n}}$  is the outward normal derivative for the same surface, but for region  $\bar{\Omega}$ . Notice that the incident field term is present due to the fact that the volume  $\bar{\Omega}$  contains a source. If this region is source-less this term is missing.

Eq. (118) with the right-hand-side set to zero is the extinction theorem. It is so named because the incident field is extinguished in region  $\Omega$  by the induced field as represented by the second term of the left-hand-side of this equation. Furthermore, Eq. (118) with  $\mathbf{r} \in \Omega$  expresses the fact that the field at any point outside  $\Omega$  can be found by performing a surface integral over  $\partial\Omega$ . In order to do so, however, the total field and its normal derivative on the surface  $\partial\Omega$  has to be known. Hence the scattering problem is equivalent to finding the field and the normal derivative on the surface.

### The Scattered and Transmitted fields

From the above discussion, we learned that the essential quantities to look for is the field and its normal derivative evaluated on the surface. We will now see how these two quantities can be calculated by taking advantage of the extinction theorem. This is done by applying Eq. (118) in turn to the different regions naturally defined by the scattering geometry as the regions of constant dielectric properties. For the scattering system depict in Fig. 6 this means to apply Eq. (118) separately to the regions  $x_3 > \zeta_1(x_1)$  and  $x_3 < \zeta_2(x_1)$ . The result is<sup>18</sup>

$$\theta(x_3 - \zeta(x_1))\Phi_\nu^+(\mathbf{r}) = \Phi_\nu^{inc}(\mathbf{r}) + \frac{1}{4\pi} \int dx'_1 \gamma(x'_1) [\Phi_\nu^+(\mathbf{r}')\partial_{n'}G_+(\mathbf{r}|\mathbf{r}') - \partial_{n'}\Phi_\nu^+(\mathbf{r}')G_+(\mathbf{r}|\mathbf{r}')] \Big|_{x'_3=\zeta(x'_1)}, \quad (119a)$$

$$\theta(\zeta(x_1) - x_3)\Phi_\nu^-(\mathbf{r}) = -\frac{1}{4\pi} \int dx'_1 \gamma(x'_1) [\Phi_\nu^-(\mathbf{r}')\partial_{n'}G_-(\mathbf{r}|\mathbf{r}') - \partial_{n'}\Phi_\nu^-(\mathbf{r}')G_-(\mathbf{r}|\mathbf{r}')] \Big|_{x'_3=\zeta(x'_1)}. \quad (119b)$$

where the superscripts  $\pm$  indicate solutions to the wave equation (111) in regions of dielectric function  $\varepsilon_\pm(\omega)$ . Furthermore, we have defined

$$\partial_n = \frac{\partial_{x_3} - \zeta'(x_1)\partial_{x_1}}{\gamma(x_1)}, \quad (120a)$$

where

$$\gamma(x_1) = \sqrt{1 + \zeta'(x_1)^2}. \quad (120b)$$

In writing Eqs. (119) we have taken advantage of the assumption made earlier that the surface,  $\zeta(x_1)$ , is a single-valued function of  $x_1$  so that its surface element becomes

$$dS = \gamma(x_1)dx_1. \quad (121)$$

If this assumption does not hold true, the discussion becomes considerably more difficult. A treatment of such a case can be found in *e.g.* Ref. [18]. However, we will not here considered this possibility any further.

Notice that the integral equations (119) are uncoupled. However, by taking into account the boundary conditions to be satisfied on the rough surface  $x_3 = \zeta(x_1)$ , *i.e.*

$$\Phi_\nu^+(x_1, x_3; \omega) \Big|_{x_3=\zeta(x_1)} = \Phi_\nu^-(x_1, x_3; \omega) \Big|_{x_3=\zeta(x_1)}, \quad (122a)$$

$$\frac{\partial_n \Phi_\nu^+(x_1, x_3; \omega)}{\kappa_\nu^+(\omega)} \Big|_{x_3=\zeta(x_1)} = \frac{\partial_n \Phi_\nu^-(x_1, x_3; \omega)}{\kappa_\nu^-(\omega)} \Big|_{x_3=\zeta(x_1)}, \quad (122b)$$

<sup>18</sup> In these equations, and some to come, we have suppressed an explicit reference to the frequency of the incident light in order to make the formulae more compact.

the two integral equations will be coupled, and Eqs. (119) take on the form

$$\begin{aligned}\theta(x_3 - \zeta(x_1))\Phi_\nu^+(\mathbf{r}|\omega) &= \Phi_\nu^{inc}(\mathbf{r}|\omega) \int dx'_1 [A_+(\mathbf{r}|x'_1; \omega)\mathcal{F}_\nu(x'_1|\omega) - B_+(\mathbf{r}|x'_1; \omega)\mathcal{N}_\nu(x'_1|\omega)], \\ \theta(\zeta(x_1) - x_3)\Phi_\nu^-(\mathbf{r}|\omega) &= - \int dx'_1 \left[ A_-(\mathbf{r}|x'_1; \omega)\mathcal{F}_\nu(x'_1|\omega) - \frac{\kappa_\nu^-(\omega)}{\kappa_\nu^+(\omega)} B_-(\mathbf{r}|x'_1; \omega)\mathcal{N}_\nu(x'_1|\omega) \right],\end{aligned}$$

where the symbols  $\kappa_\nu^\pm(\omega)$  have been defined earlier in Eq. (14d). Here we have introduced the source functions<sup>19</sup>

$$\mathcal{F}_\nu(x_1|\omega) = \Phi_\nu^+(x_1, x_3|\omega)|_{x_3=\zeta(x_1)}, \quad (124a)$$

$$\mathcal{N}_\nu(x_1|\omega) = \gamma(x_1)\partial_n\Phi_\nu^+(x_1, x_3|\omega)|_{x_3=\zeta(x_1)}, \quad (124b)$$

as well as the kernels

$$A_\pm(\mathbf{r}|x'_1; \omega) = \frac{1}{4\pi} \gamma(x'_1) \partial_{n'} G_\pm(x_1, x_3|x'_1, x'_3) \Big|_{x'_3=\zeta(x'_1)}, \quad (125a)$$

$$B_\pm(\mathbf{r}|x'_1; \omega) = \frac{1}{4\pi} G_\pm(x_1, x_3|x'_1, x'_3) \Big|_{x'_3=\zeta(x'_1)}. \quad (125b)$$

Notice that the second term on the right-hand-side of Eq. (123a) represents the field scattered from the rough surface,  $\Phi_\nu^{sc}(\mathbf{r}|\omega)$ . By substituting the following Fourier representation for the Green's function [39]

$$G_+(\mathbf{r}|\mathbf{r}'; \omega) = \int_{-\infty}^{\infty} \frac{dq}{2\pi} \frac{2\pi i}{\alpha_+(q, \omega)} e^{iq(x_1-x'_1)+i\alpha_+(q, \omega)|x_3-x'_3|}, \quad (126)$$

into Eqs. (125), and the resulting expression into Eq. (123a), we find that the scattered field far above the surface,  $x_3 \gg \zeta(x_1)$ , can be written as

$$\Phi_\nu^{sc}(\mathbf{r}|\omega) = \int_{-\infty}^{\infty} \frac{dq}{2\pi} R_\nu(q, \omega) e^{iqx_1+i\alpha_+(q, \omega)x_3}, \quad (127a)$$

where the scattering amplitude is given by the following expression

$$R_\nu(q, \omega) = \frac{i}{2\alpha_+(q, \omega)} \int_{-\infty}^{\infty} dx_1 e^{-iqx_1-i\alpha_+(q, \omega)\zeta(x_1)} [i \{q\zeta'(x_1) - \alpha_+(q, \omega)\} \mathcal{F}_\nu(x_1) - \mathcal{N}_\nu(x_1)].$$

In these expressions  $\alpha_+(q, \omega)$ , and later to be used  $\alpha_-(q, \omega)$ , are defined as in Eqs. (48) and (50).

If the medium occupying the region  $x_3 < \zeta(x_1)$  is transparent, a transmitted field will also exist. It is given by the right-hand-side of Eq. (123a). Under this assumption, a Fourier representation for  $G_-(\mathbf{r}|\mathbf{r}'; \omega)$ , equivalent the one given in Eq. (126), will give a transmitted field in the region  $x_3 \ll \zeta(x_1)$  of the form

$$\Phi_\nu^{tr}(\mathbf{r}|\omega) = \int_{-\infty}^{\infty} \frac{dq}{2\pi} T_\nu(q, \omega) e^{iqx_1-i\alpha_-(q, \omega)x_3}, \quad (128a)$$

where the transmission amplitude is defined as

$$T_\nu(q, \omega) = -\frac{i}{2\alpha_-(q, \omega)} \int_{-\infty}^{\infty} dx_1 e^{-iqx_1+i\alpha_-(q, \omega)\zeta(x_1)} \left[ i \{q\zeta'(x_1) + \alpha_-(q, \omega)\} \mathcal{F}_\nu(x_1) - \frac{\kappa_\nu^-(\omega)}{\kappa_\nu^+(\omega)} \mathcal{N}_\nu(x_1) \right].$$

### The Equations for the Source Functions

<sup>19</sup> Notice that the operator  $\gamma(x_1)\partial_n$  appearing in  $\mathcal{N}_\nu(x_1|\omega)$  is nothing else then the *unnormalized* normal derivative.

In order to solve the scattering problem we see from Eq. (127b) that we need to know the source functions  $\mathcal{F}_\nu(x_1|\omega)$  and  $\mathcal{N}_\nu(x_1|\omega)$ . The question therefore is: How to calculate these source functions? A coupled set of equations for these sources are most easily obtained by setting  $x_3 = \zeta(x_1) + \eta$ , with  $\eta \rightarrow 0^+$ , in Eqs. (123). Doing so results in the following set of inhomogeneous, coupled integral equations for the sources

$$\mathcal{F}_\nu(x_1) = \mathcal{F}_\nu^{inc}(x_1) \int dx'_1 [\mathcal{A}_+(x_1|x'_1)\mathcal{F}_\nu(x'_1) - \mathcal{B}_+(x_1|x'_1)\mathcal{N}_\nu(x'_1)], \quad (129a)$$

$$0 = \int dx'_1 \left[ \mathcal{A}_-(x_1|x'_1)\mathcal{F}_\nu(x'_1) - \frac{\kappa_\nu^-}{\kappa_\nu^+} \mathcal{B}_-(x_1|x'_1)\mathcal{N}_\nu(x'_1) \right], \quad (129b)$$

where the kernels are defined as

$$\mathcal{A}_\pm(x_1|x'_1) = \lim_{\eta \rightarrow 0^+} A_\pm(\mathbf{r}|x'_1)|_{x_3=\zeta(x_3)+\eta}, \quad (130a)$$

$$\mathcal{B}_\pm(x_1|x'_1) = \lim_{\eta \rightarrow 0^+} B_\pm(\mathbf{r}|x'_1)|_{x_3=\zeta(x_3)+\eta}. \quad (130b)$$

In order to solve Eqs. (129), the integral equations are converted into matrix equations by discretizing the spatial variables  $x_1$  and  $x'_1$  and using some kind of quadrature scheme for approximating the integrals that they contain. First of all, the infinitely long surface is restricted to a finite length  $L_1$ , so that the spatial integration range from  $-L_1/2$  to  $L_1/2$ . Second, a grid defined according to

$$\xi_n = [x_1]_n = -\frac{L_1}{2} + \left(n - \frac{1}{2}\right) \Delta\xi, \quad n = 1, 2, 3, \dots, N, \quad (131)$$

with  $\Delta\xi = L_1/N$  is introduced for  $x'_1$ . If we assume that the source functions are slowly varying functions over a grid cell (of size  $\Delta\xi$ ), they can be considered as constant over this distance and therefore put outside the integral. The integral equations (129) are thus converted into the following coupled matrix equations by putting  $x_1 = \xi_m$

$$\mathcal{F}_\nu(\xi_m) = \mathcal{F}_\nu^{inc}(\xi_m) + \sum_{n=1}^N [\mathcal{A}_{mn}^+ \mathcal{F}_\nu(\xi'_n) - \mathcal{B}_{mn}^+ \mathcal{N}_\nu(\xi'_n)], \quad (132a)$$

$$0 = \sum_{n=1}^N \left[ \mathcal{A}_{mn}^- \mathcal{F}_\nu(\xi'_n) - \frac{\kappa_\nu^-}{\kappa_\nu^+} \mathcal{B}_{mn}^- \mathcal{N}_\nu(\xi'_n) \right], \quad (132b)$$

where  $\mathcal{F}_\nu^{inc}(\xi_m)$  is defined from Eq. (124a) by using  $\Phi_\nu^{inc}(x_1, x_3|\omega)$  for the field  $\Phi_\nu^+(x_1, x_3|\omega)$ . Moreover, the matrix elements  $\mathcal{A}_{mn}^\pm$  and  $\mathcal{B}_{mn}^\pm$  are defined as

$$\mathcal{A}_{mn}^\pm = \int_{\xi_n - \Delta\xi/2}^{\xi_n + \Delta\xi/2} dx'_1 \mathcal{A}_\pm(\xi_m|x'_1), \quad (133a)$$

$$\mathcal{B}_{mn}^\pm = \int_{\xi_n - \Delta\xi/2}^{\xi_n + \Delta\xi/2} dx'_1 \mathcal{B}_\pm(\xi_m|x'_1). \quad (133b)$$

It should be kept in mind that these matrix elements are related to the Hankel function,  $H_0^{(1)}(z)$ , and its derivative, through the (two-dimensional) Green's function that enters via Eqs. (125) and (130). Care has to be taken when evaluating these matrix elements since the Hankel functions are singular when their arguments vanish. Hence the kernels,  $\mathcal{A}_\pm(x_1|x'_1)$  and  $\mathcal{B}_\pm(x_1|x'_1)$ , are also singular when  $x_1 = x'_1$ . Fortunately these singularities are integrable so that the matrix elements,  $\mathcal{A}_{mn}^\pm$  and  $\mathcal{B}_{mn}^\pm$ , in contrast to the kernels, are well define everywhere. The somewhat technical procedure for showing this is presented in Appendix A, from where we obtain that (see Eqs. (A11) and (A12))

$$\mathcal{A}_{mn}^\pm = \begin{cases} \Delta\xi A_\pm(\xi_m|\xi_n), & m \neq n, \\ \frac{1}{2} + \Delta\xi \frac{\zeta''(x_m)}{4\pi\gamma^2(\xi_m)}, & m = n, \end{cases} \quad (134a)$$

and

$$\mathcal{B}_{mn}^\pm = \begin{cases} \Delta\xi B_\pm(\xi_m|\xi_n), & m \neq n \\ -\frac{i}{4}\Delta\xi H_0^{(1)}\left(\sqrt{\varepsilon_\pm}\frac{\omega}{c}\frac{\gamma(\xi_m)\Delta\xi}{2e}\right), & m = n. \end{cases} \quad (134b)$$

The matrix equations (132), together with the expressions for the matrix elements Eqs. (134), can readily be put onto the computer and solved by standard techniques from linear algebra [40, 41] in order to obtain the source functions. With these source functions available, the scattering amplitude, and, if defined, the transmission amplitude, can be obtained from respectively Eqs. (127b) and (128b). These amplitudes are again related to physical observable quantities, like the mean differential reflection or transmission coefficients, as discussed earlier. Hence the scattering problem is in principle solved!

It should also be mentioned that the approach presented here can be generalized to more complicated scattering geometries like film systems etc. [22, 68, 122]. However, in such cases the higher demand is put on computational resources.

## 2. A Remark on the Accuracy of the Numerical Simulation Approach

The numerical approach described above is formally exact since *no* approximations have been introduced. It is therefore in principle applicable to scattering from surfaces of any roughness. It has proven useful in many situations, and serve today as a standard, and invaluable, tool for rough surface scattering studies. This is in particular true for scattering from strongly rough surfaces where it represents the only rigorous available method at present.

Even if this approach is formally exact, it has some practical limitations. Imagine a weakly rough metal surface that is illuminated by  $p$ -polarized light. In this case the incident light can excite surface plasmon polaritons that will travel along the rough surface. The mean free path of these surface plasmon polaritons will in the present case be quite large.

In computer simulations we are, of course, not able to represent infinitely long surfaces. Instead we are limited to surface of finite length. To avoid essential contributions to the simulation results from artificial scattering processes *e.g.* where surface plasmon polaritons are being scattered from the edges of our (finite length) surface, its length needs to be long. In order not to compromise the spatial resolution used in the simulations, big demands on computer memory and CPU-time is a consequence. This sets a practical limit for the use of rigorous numerical simulations for weakly rough surfaces. However, for such kind of roughness, perturbation theory, where we by construction are using surfaces of infinite length, are adequate and accurate as discussed earlier. The present limitation of the rigorous numerical simulation approach should therefore not represent a too severe restriction from a practical point of view.

We should also mention that there exists another numerical technique that for the same amount of memory used in the rigorous approach can handle much longer surfaces (and therefore reduce edge effects). This technique is based on a numerical solution of the reduced Rayleigh equation, that was introduced in Eq. (78) of Sect. III E, and is the single integral equation satisfied by the scattering amplitude. The interested reader should consult Refs. [42] and [121] for details regarding this numerical technique. This approach is obviously restricted to surfaces for which the Rayleigh hypothesis is valid. It can therefore not be applied to surfaces of arbitrary roughness, but it is valid for surfaces that practically can not be treated within perturbation theory. A direct numerical solution of the reduced Rayleigh (integral) equation can therefore be looked upon as a bridge between perturbation theory and the rigorous numerical simulation approach.

## IV. PHYSICAL PHENOMENA IN ELECTROMAGNETIC ROUGH SURFACE SCATTERING

Wave scattering from randomly rough surfaces has a long history in science [1–4]. In the overall majority of theoretical studies conducted up to the early 1980's, single-scattering approaches were used [5–8]. However, around this time people started getting interested in the effects and consequences of incorporating multiple-scattering events into the theories. It created a lot of excitement in the field when new and interesting multiple scattering phenomena were either predicted theoretically and/or observed in experiments. During the period of time that has passed since the early 1980's, multiple scattering effects from randomly rough surfaces have attracted much attention from theorists and experimentalists alike, and today the research in this field is concentrated around different kinds of multiple scattering effects [22].

It ought to be mentioned that many of the effects to be discussed here are not exclusive to surface scattering. Quite a few of them have in fact their analogies in light scattering from volume disordered systems. For discussion of light scattering from volume disordered systems the interested reader is referred to the literature [59, 60].

In this section we aim at discussing some of the new multiple scattering effects that might take place when electromagnetic waves are scattered from a randomly rough surface. The technical details on which the present section rely were mainly presented in the previous section. We have therefore tried to keep the discussion at a phenomenological, and hopefully pedagogical, level. Unnecessary technical details have been avoided whenever possible. As a service to the more technical oriented reader, an extensive reference to the original literature has been made.

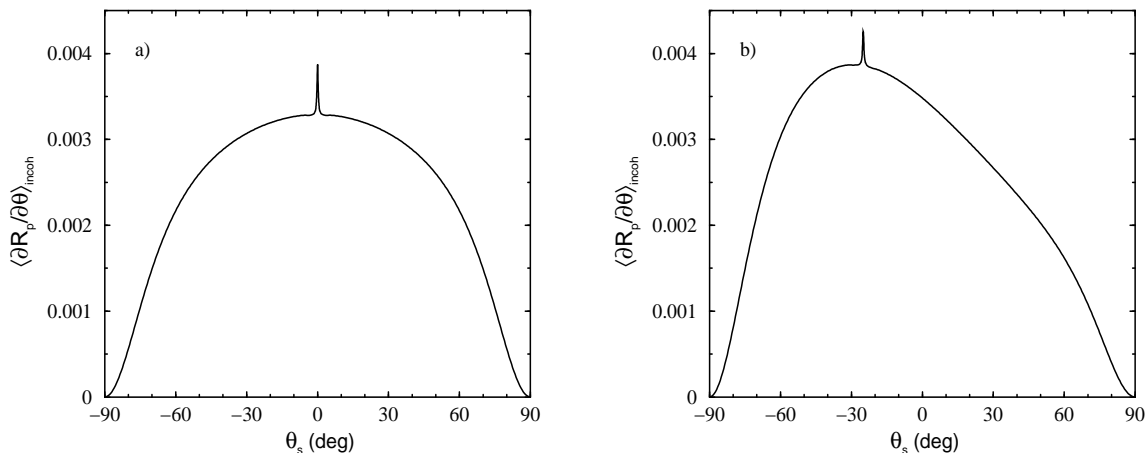


FIG. 8: Perturbative calculations for the mean differential reflection coefficient for the incoherent component of the light scattered from a randomly rough silver surface. The incident angles of the light of wavelength  $\lambda = 632.8\text{nm}$  were (a)  $\theta_0 = 0^\circ$  and (b)  $\theta_0 = 25^\circ$ . The dielectric constant of silver at this wavelength is  $\epsilon(\omega) = -7.5 + i0.24$ . The surface was characterized by a Gaussian height distribution of RMS-height  $\delta = 5\text{nm}$  and a Gaussian height-height correlation function of correlation length  $a = 100\text{nm}$ .

### A. Coherent Effects in Multiple-Scattered Fields: Weak Localization of Light on a Randomly Rough Surface

In 1985 McGurn, Maradudin, and Celli [54] predicted theoretically the existence of what later has been known as the *enhanced backscattering phenomenon* in surface scattering. This phenomenon express itself as a well-defined peak in the retroreflection direction of the angular dependence of the light scattered incoherently from a rough surface. The work in Ref. [54] was the first to report on an effect that was shown to be caused by multiple scattering processes taking place at the rough surface. The enhanced backscattering phenomenon is an example of what is known as a *coherent effect* in the multiple scattered field. Later on, other coherent phenomena, like the enhanced transmission [61], satellite peaks [65, 66] and enhancements due to the excitations of magnetoplasmons [67, 68] were predicted.

#### 1. Enhanced backscattering

In this subsection the backscattering enhancement phenomenon will be discussed. Since the mechanisms that give rise to it are different for weakly and strongly rough surfaces, they will be treated separately. The scattering system that will be considered is depicted in Fig. 6 and consists of a single rough vacuum-metal surface.

#### *Weakly Rough Surfaces*

It is familiar from every day life that if the surface is not too rough, the waves incident on it will mostly be scattered into the specular direction. That is, if the angle of incidence is  $\theta_0$ , then most of the energy will be scattered into the direction  $\theta_s = \theta_0$ , which defines the specular direction. For a weakly rough surfaces the intensity, or equivalently the mean differential reflection coefficient (DRC), will have a maximum — a specular peak — for the scattering angle  $\theta_s = \theta_0$ . Normally the specular peak is not of any interest to us, and it is therefore in theoretical studies usually subtracted of, leaving only the intensity that results from light scattered incoherently by the rough surface.

In 1985 McGurn, Maradudin, and Celli [54] predicted based on a perturbation theoretical study, that also in the retroreflection (anti-specular) direction of the angular dependence of the mean DRC there might be an enhancement. This effect, known today as enhanced backscattering, manifest itself as a well-defined peak in the retroreflection direction of the angular dependence of the intensity of the light that has been scattered incoherently from the random surface.

In the original paper by McGurn *et al.* [54], the calculation of the enhanced backscattering peak was carried out for *p*-polarized light scattered from a weakly rough silver surface. Their calculations, based on a many-body perturbation theory, took into account multiple scattering events in the calculation of the intensity scattered incoherently by the

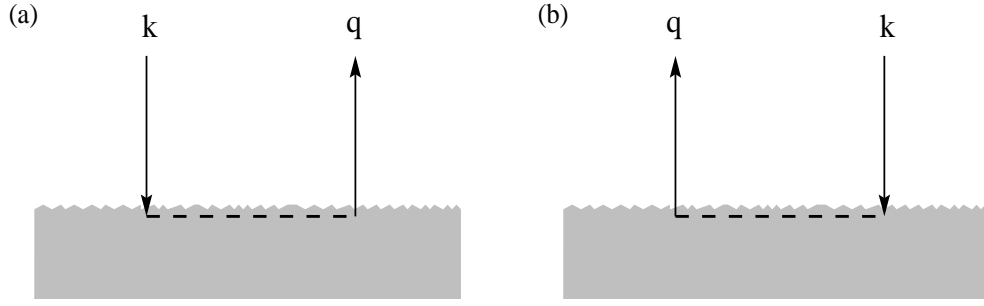


FIG. 9: Diagrams showing two of the scattering events that through interference give rise to the enhanced backscattering peak for weakly rough surfaces.

surface. In Figs. 8 we show the results of a small amplitude perturbative calculation, like the one given in Sect. III F, for the incoherent contribution to the mean differential reflection coefficient for  $p$ -polarized light incident at angles  $\theta_0 = 0^\circ$  (Fig. 8a) and  $\theta_0 = 25^\circ$  (Fig. 8b) on the rough silver surface. Terms to 4'th order in the surface profile function were included which is enough to include all double scattering processes. The wavelength of the incident light was  $\lambda = 632.8\text{nm}$ , and the dielectric constant of silver at this wavelength is  $\varepsilon(\omega) = -7.5 + i0.24$ . The surface was assumed to be characterized by a Gaussian height distribution and the height-height correlation function was also of the Gaussian type. The root-mean-square (RMS) height of the surface was  $\delta = 5\text{nm}$  while the correlation length was  $a = 100\text{nm}$ . From Fig. 8 we see well-pronounced peaks for the retroreflection directions. It should be stressed that it is the *incoherent* component of the mean DRC that is plotted in these figures, so that the peak seen at  $\theta_s = 0^\circ$  in Fig. 8a is no specular effect<sup>20</sup> since all contributions from specular scattering have been subtracted off. That this is the case should be obvious from the position of the enhanced backscattering peak seen in Fig. 8b corresponding to the incident angle  $\theta_0 = 25^\circ$ .

The natural question is now: What is the origin of the enhanced backscattering peak? It was realized that it had to be caused by multiple scattering since it had not been seen earlier when using single scattering theories. It turned

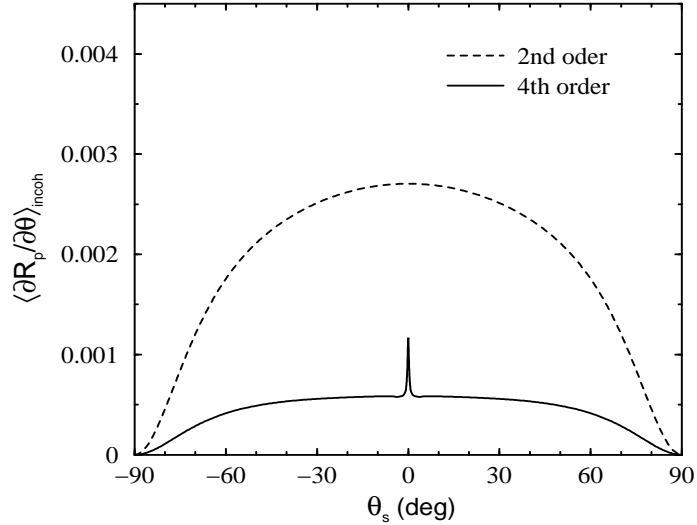


FIG. 10: The same as Fig. 8a, but now showing separately the 2nd and 4th order contribution in the surface profile function to the mean differential reflection coefficient. The sum of these terms gives the curve in Fig. 8a. Notice that the enhanced backscattering peak comes from the 4th order contribution, *i.e.* from the double scattering contribution.

<sup>20</sup> Recall that for normal incidence the specular and anti-specular directions coincide.



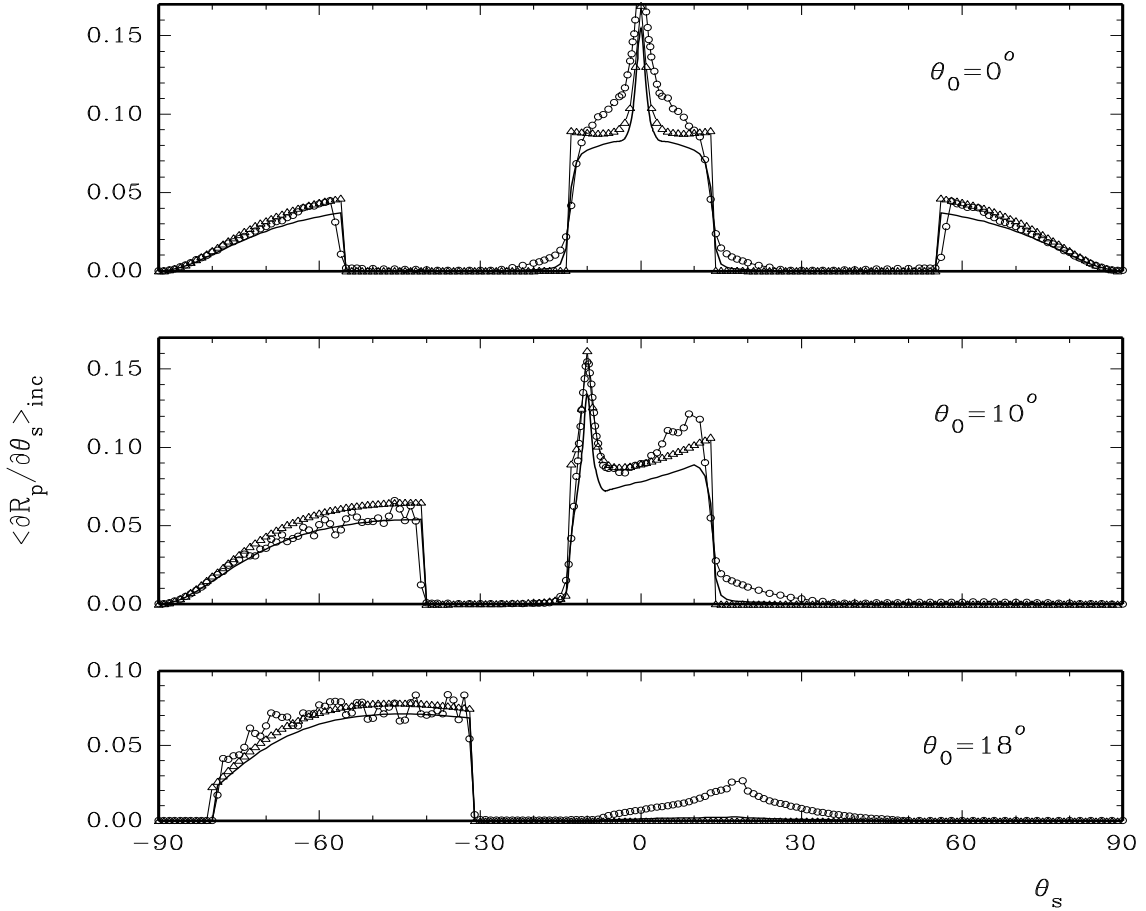


FIG. 11: Experimental results (open circles) for  $\langle \partial R_p / \partial \theta_s \rangle_{inc}$  as a function of the scattering angle  $\theta_s$  for three different incident angles when  $p$ -polarized light of wavelength  $\lambda = 612.7\text{nm}$  is incident on a one-dimensional random gold surface ( $\varepsilon(\omega) = -9.00 + i1.29$ ). For the random surface a West-O'Donnell power spectrum with  $k_- = 0.82(\omega/c)$  and  $k_+ = 1.29(\omega/c)$  was used. The RMS-height of the surface was  $\delta = 10.9\text{nm}$ . The solid lines and the open triangles are perturbation theoretical results based on respectively small amplitude and many-body perturbation theory. (After Ref. [20]).

out that the origin lies in the interference between a multiple scattered path with its reciprocal partner [20, 54]. To illustrate this, let us consider the double scattering path shown in Fig. 9a. Here an incident wave excites through the breakdown of infinitesimal translation invariance of the system, a surface plasmon polariton that propagates along the surface. At the next scattering event this surface polariton is converted back into a volume electromagnetic wave that propagating away from the surface. This path has a reciprocal partner (Fig. 9b) where the scattering takes place from the same scattering centers at the rough surface, but now in the opposite order. For the backscattering direction these two paths will have exactly the same amplitude and phase, *i.e.* they will be coherent, and hence they will interfere *constructively*. However, as we move away from the backscattering direction, the two paths fast become incoherent so that their intensities just add. Thus, due to the interference nature of the enhanced backscattering peak the amplitudes at the position of the peak would in the absence of single scattering be twice that of its background due to the cross-terms originating from the square modulus of the amplitudes needed in order to calculate the intensity. However, notice that it is not uncommon that single scattering gives considerable contribution to the mean differential reflection coefficient of the light scattered incoherently from the surface. In such cases, the height of the peak is not twice of its background.

To show that multiple scattering indeed is the origin of the enhanced backscattering phenomenon, we show in Fig. 10 the different contributions to the incoherent component of the mean DRC obtained from Eq. (89a). We recall that the first term of this equation is the single scattering contribution, *i.e.* it is of 2nd order in the surface profile function  $\zeta(x_1)$ . The next two terms are both double scattering contributions or, equivalently, 4th order contributions in the surface profile function. From Fig. 10 it is seen that the single scattering contribution (2nd order in  $\zeta(x_1)$ ) is a smooth function of the scattering angle. Furthermore, it is seen that the peak stems from the double scattering

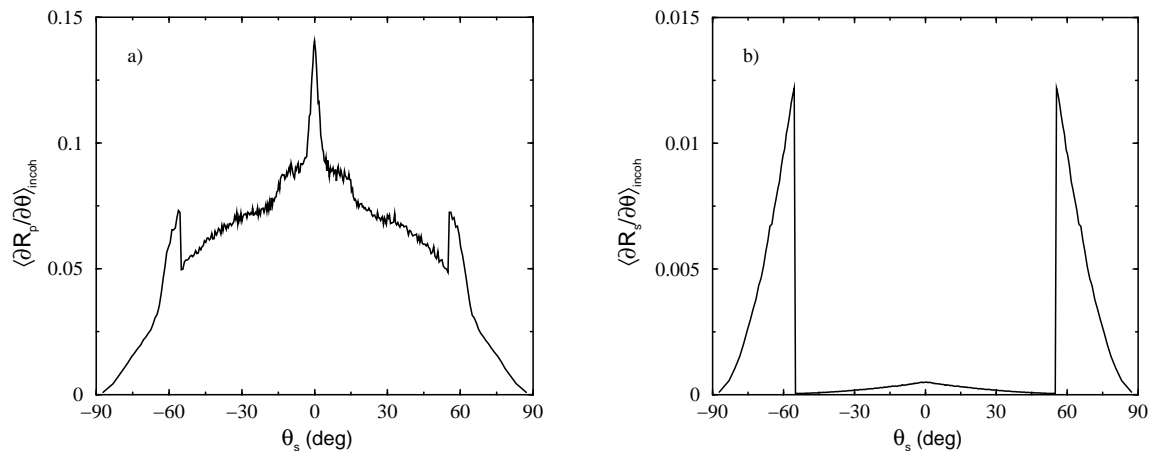


FIG. 12: Numerical Monte Carlo simulation results for the mean differential reflection coefficient,  $\langle \partial R_\nu / \partial \theta_s \rangle_{incoh}$ , for (a)  $p$ - and (b)  $s$ -polarized light scattered from a rough silver surface of RMS-height  $\delta = 15\text{nm}$ . The angle of incidence was  $\theta_0 = 0^\circ$  and the wavelength of the incident light was  $\lambda = 632.8\text{nm}$ . At this wavelength the dielectric constant of silver is  $\varepsilon(\omega) = -7.5 + i0.24$ . Furthermore, the surface was of the West-O'Donnell type characterized by the parameters  $k_- = 0.82(\omega/c)$  and  $k_+ = 1.92(\omega/c)$ . The simulations were performed by numerically solving the reduced Rayleigh equation that the scattering amplitude satisfies [42, 121]. The number of samples used in obtain these results was  $N_\zeta = 3000$ . Notice that in the case of  $s$ -polarization there is no enhanced backscattering peak in contrast to what is the case for  $p$ -polarization. This difference is caused by the fact that  $s$ -polarized incident light can not excite surface plasmon polaritons at a rough vacuum-metal interface.

contribution, *i.e.* it comes from the second and third terms of Eq. (89a). In a diagrammatic language this term comes from the maximally crossed diagrams. The interested reader should consult Ref. [54] for additional details.

It should be noted that even if we earlier only included fully the lowest order multiple scattering process (double scattering), higher order processes will not change the statement that the enhanced backscattering phenomenon is caused by multiple scattering through the constructive interference between a scattering path with its reciprocal partner.

The enhanced backscattering effect from weakly rough vacuum-metal surfaces was observed in experiments by West and O'Donnell [20] in 1995 in the scattering of  $p$ -polarization light from a rough gold surface of RMS-height  $\delta = 10.9\text{nm}$ . The power-spectrum used in these experiments was of the rectangular type also known as the West-O'Donnell power-spectrum. The remaining parameters used are defined in the caption of Figs. 11. We have in Figs. 11 reproduced their experimental results (open circles) together with some perturbation theoretically results (solid lines and open triangles). At least for the two smallest angles of incidence well-defined peaks around the retroreflection direction in the experimental results are seen.

For weakly rough surfaces we just argued that the origin of the enhanced backscattering effect involves surface plasmon polaritons. In  $s$ -polarization, a rough (one-dimensional) vacuum-metal interface does *not* support such surface waves. Hence, one does not expect to see any backscattering peak for this polarization for weakly rough surfaces. This is indeed seen from Figs. 12 showing numerical simulation results for  $p$ - and  $s$ -polarized incident light based on the solution of the reduced Rayleigh equation that the scattering amplitude satisfies. The power spectrum used for the surface was again of the West-O'Donnell type, and it was defined by the parameters  $k_- = 0.82(\omega/c)$  and  $k_+ = 1.92(\omega/c)$ . It is seen from Figs. 12 that only in  $p$ -polarization do we see an enhanced backscattering peak. From Eq. (89) we see that the single scattering contribution is proportional to the power spectrum,  $g(|k|)$ , of the surface roughness. Hence, if  $k_- > 0$  the incoherent component to the mean DRC,  $\langle \partial R_\nu / \partial \theta_s \rangle_{incoh}$  should not contain any contribution from single scattering events in the angular range  $-\theta_- < \theta_s < \theta_-$ , where  $\theta_- = \arcsin((k_-c)/\omega)$ . With the parameters used in obtaining Figs. 12 this gives  $\theta_- = 55.1^\circ$ . For scattering angles  $|\theta_s| > \theta_- = 55.1^\circ$  single scattering is allowed. This can be seen as a jump in Figs. 12 at this angle. Furthermore, around the backscattering peak, single scattering should be absent and indeed the enhanced backscattering peak is twice that of its background as predicted above. Notice also that the overall fraction of the light scatterer incoherently from the surface is at least one order of magnitude lower for  $s$ - than  $p$ -polarization.

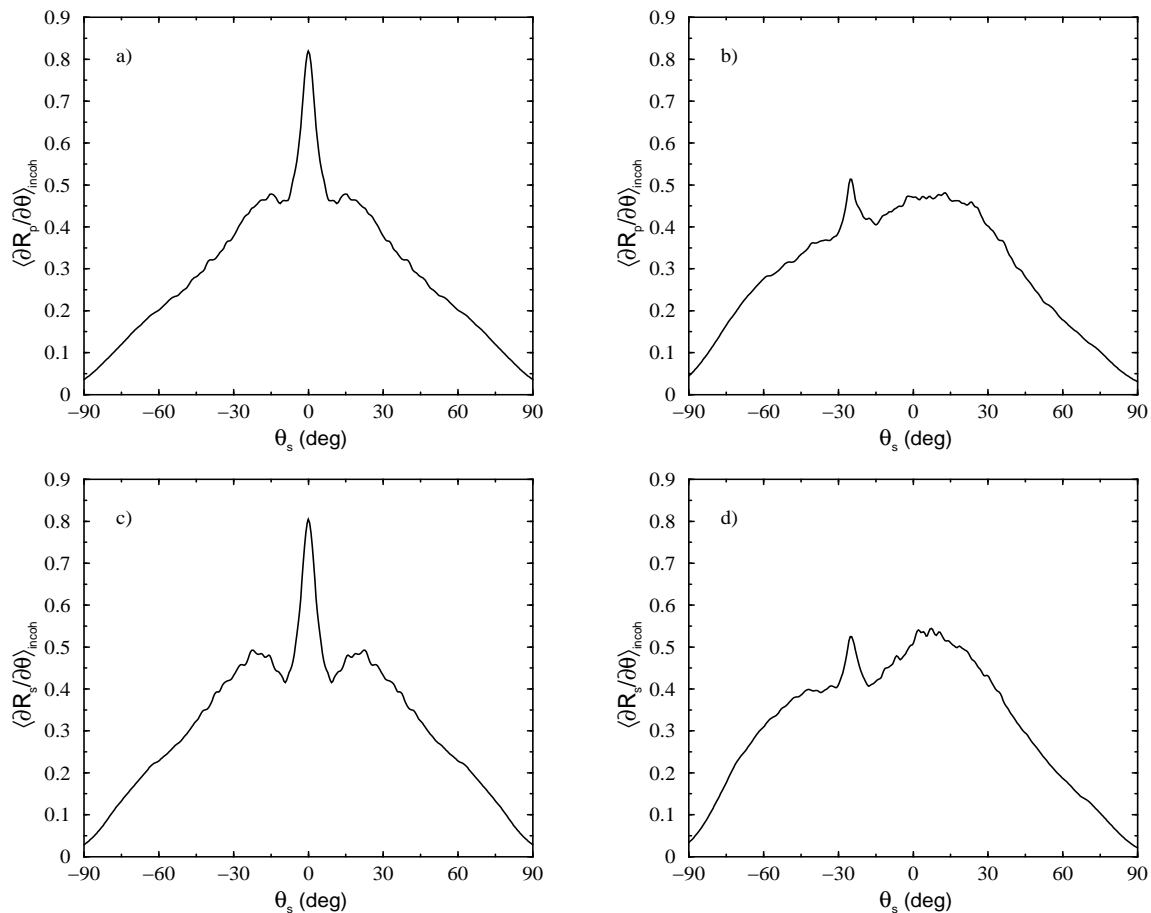


FIG. 13: Rigorous Monte Carlo simulation results for the angular dependence of the incoherent component of the mean differential reflection coefficient for the scattering of (a and b)  $p$ - and (c and d)  $s$ -polarized incident light from a strongly rough silver surface. The wavelength of the incident light was  $\lambda = 612.7\text{nm}$  for which the dielectric constant of silver is  $\varepsilon(\omega) = -17.2 + i0.498$ . The incident angles of the light were (a and c)  $\theta_0 = 0^\circ$  and (b and d)  $\theta_0 = 25^\circ$ . The strongly rough surface was characterized by Gaussian height distribution of RMS-height  $\delta = 1.2\mu\text{m}$  and the transverse correlation length for the Gaussian correlated surface was  $a = 2\mu\text{m}$ . The length of the surface was  $L = 25.6\mu\text{m}$  and a finite sized beam of width  $g = 6.4\mu\text{m}$  was used in the simulations. The number of discretization points was  $N = 500$ . The numerical results were all based on an ensemble average over  $N_\zeta = 3000$  realizations of the randomly rough surface.

We will now consider strongly rough surfaces. In order to study the backscattering phenomenon for such surfaces we have to resort to numerical simulations like *e.g.* the approach outlined in Sect. III. In Figs. 13 we present the results of such simulations for the angular dependence of the incoherent component of the mean DRC for (a and b)  $p$ - and (c and d)  $s$ -polarized light incident on a rough vacuum-metal surface of RMS-height  $\delta = 1.2\mu\text{m}$ . The correlation length for the Gaussian correlated surface was  $a = 2\mu\text{m}$ . The main difference between these results and those for the weakly rough surfaces presented earlier (Fig. 12) is that we now also observe an enhanced backscattering peak in the case of  $s$ -polarization. So what is the reason for this difference between weakly and strongly rough surfaces when it comes to the backscattering phenomenon? The explanation lies in the mechanism causing the backscattering peak for strongly rough surfaces [21, 62–64]. Since the excitation of surface plasmon polaritons is weak for strongly rough surface, it is unlikely that the reason for the backscattering peak is caused by this type of surface waves. Such a mechanism could not in any case explain the presence of the backscattering peak observed for  $s$ -polarization. Instead the backscattering peak for strongly rough surfaces arises due to the constructive interference between multiple scattered volume paths like *e.g.* those shown in Figs. 14. In this case no surface waves are excited, but instead the multiple scattering takes place within the valleys of the now strongly rough surface. The incident wave, that after its first encounter with the rough surface, is scattered at least one more time before leaving the surface for good. Also in this case for the backscattering direction this path has a reciprocal partner that is phase coherent with the first one and with which the latter path can interfere constructively. Since this mechanism does not involve any surface plasmon polaritons,

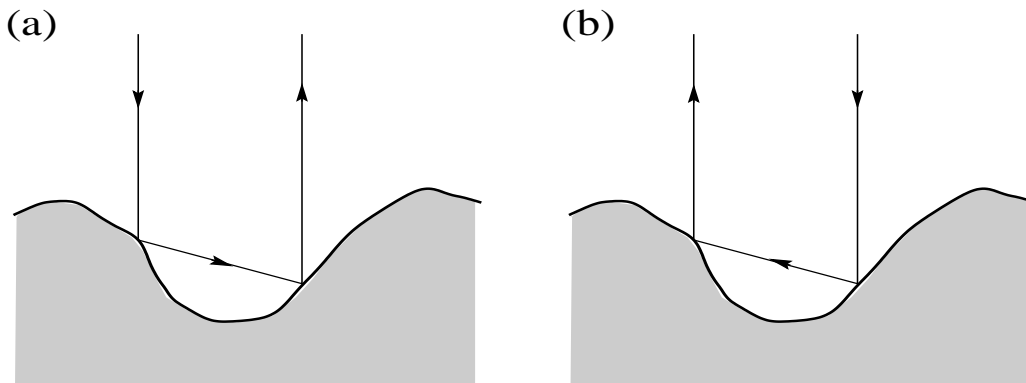


FIG. 14: Diagrams showing two double scattering paths that for strongly rough surfaces through interference represent the main contributors to the enhanced backscattering peak phenomenon.

there is no reason why the backscattering phenomenon should not show up also in  $s$ -polarization from strongly rough surfaces. In fact as can be seen from Fig. 13c and d, the backscattering peak in  $s$ -polarization is as pronounced as for  $p$ -polarization. Observe also that the energy scattered incoherently, which for strongly rough surfaces is close to the total scattered energy, is of roughly the same order for both polarizations. This is in contrast to the situation found for weakly rough surfaces.

The enhanced backscattering phenomenon from strongly rough surfaces was experimental confirmed as early as 1987 by Méndez and O'Donnell [62]. This was just two years after its theoretical prediction by McGurn *et al.* [54] for weakly rough surfaces. In fact these experiments provided the first experimental evidence what-so-ever for the enhanced backscattering phenomenon from rough surfaces.

## 2. Satellite Peaks

The backscattering phenomenon discussed in the previous subsection is not the only coherent effect that might exist when light is scattered from a randomly rough surface. Another such effect is the existence of so-called *satellite peaks* predicted by Freilikher, Pustilnik, and Yurkevich [65] in 1994. Satellite peaks are enhancements in the angular distribution of light scattered incoherently from scattering systems that supports more than one surface [65–68] or guided waves [42, 69–71, 109, 121]. As will be shown in detail in Subsect. IV A 3, they are not caused by interference between reciprocal paths as was the case for the backscattering phenomenon, but instead by interference of *nonreciprocal* paths. These enhancements should occur for scattering angles that are located symmetrically with respect to the position of the enhanced backscattering peaks that the scattering system also gives rise to.

To illustrate this, let us study the film scattering system shown in Fig. 15. Here the lower interface is rough and the upper one is planar. Furthermore, the lower semi-infinite medium is assumed to be a perfect conductor, while the incident medium is assumed to be vacuum. In Figs. 16 we show the results of numerical simulations for the mean differential reflection coefficient in the case of  $s$ - (Fig. 16a) and  $p$ -polarized (Fig. 16b) incident light. The remaining surface parameters are given in the caption of Figs. 16. In the case of  $s$ -polarization, the scattering system of mean thickness  $d = 500\text{nm}$  supports two satellite peaks, while in the case of  $p$ -polarization it can at most support six such peaks [121]. The positions of these peaks are indicated by dashed vertical lines in Figs. 16. From Fig. 16a the two satellite peaks that the scattering system supports in this case are easily distinguished from the background. However, from Fig. 16b one sees that only four out of the six possible peaks can be observed. There are two reasons why some of these satellite peaks may not be observable: First, some of them may lie in the non-radiative part of the spectrum, and are therefore not even in principle observable. Second, their strength might be too low to be observable [42, 121], *i.e.* one (or both) of the channels involved in the interference process that gives rise to the satellite peaks might have too low intensity [42, 121] (see Subsect. IV A 3).

It can be shown (result not shown) that by reducing the thickness of the film, and thus reducing the number of guided waves that the system supports say to one, all the satellite peaks vanish while the enhanced backscattering peak is still present [71]. In an analogous way, if the film thickness is increased, more than two satellite peaks might be seen [71].

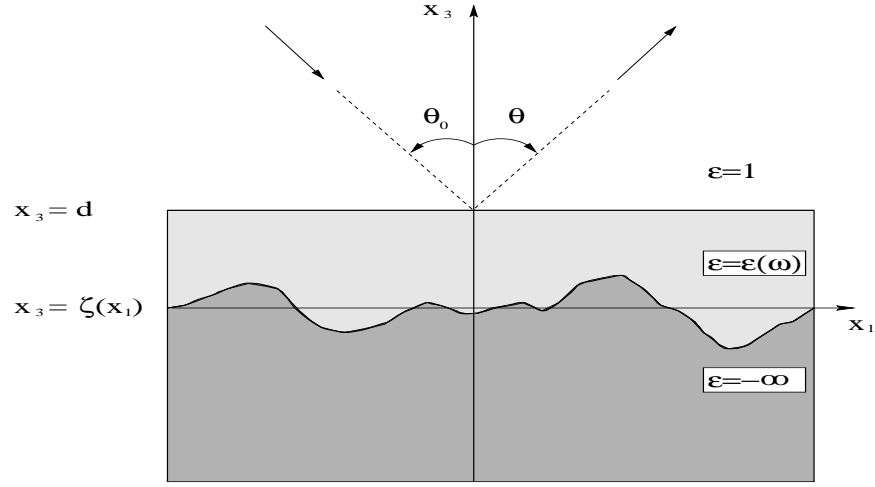


FIG. 15: A sketch of a film scattering geometry that supports guided waves and that may give rise to satellite peaks in the angular dependence of the scattered light.

### 3. A Formal Approach to Enhanced Backscattering and Satellite Peaks

In the previous two subsections the enhanced backscattering and satellite peaks phenomena were discussed. In the present subsection a more detailed analysis and formal approach towards these two phenomena will be presented. In particular we will determine at which positions the satellite peaks are to be expected.

Let us consider a general film scattering system, where at least one of the interfaces are rough. Fig. 15 provides one example of such a system. Depending on the thickness of the film, the scattering system supports  $N > 0$  guided waves at the frequency  $\omega$  of the incident light. The wavenumbers of these modes, or “channels” as some authors prefer to

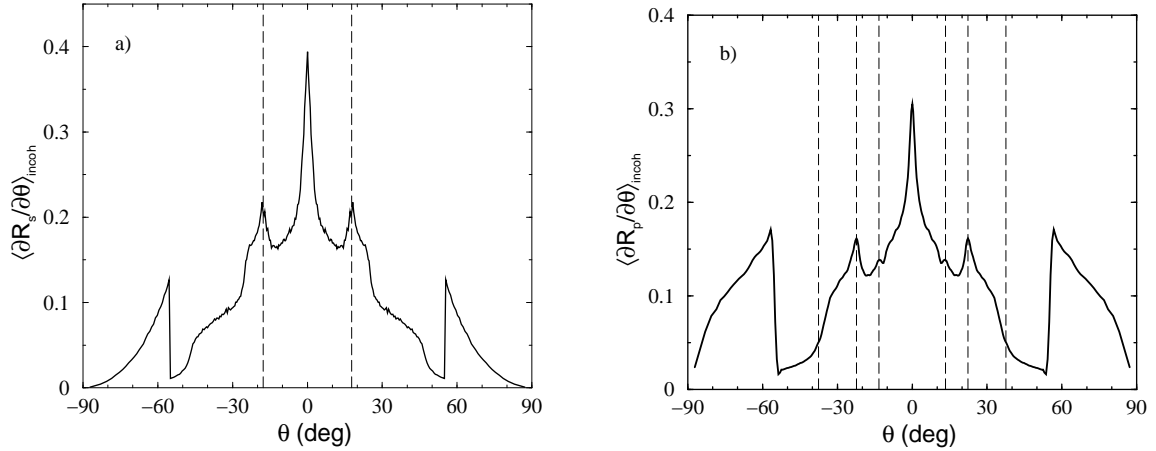


FIG. 16: The contribution to the mean differential reflection coefficient from the incoherent component of the scattered light  $\langle \partial R_\nu / \partial \theta \rangle_{incoh}$  as a function of the scattering angle  $\theta_s$  when an  $s$ - (Fig. 16a) or  $p$ -polarized (Fig. 16b) plane wave of wavelength  $\lambda = 633\text{nm}$  is incident normally ( $\theta_0 = 0^\circ$ ) on the film scattering geometry shown in Fig. 15. The dielectric constant of the film at the wavelength of the incident light is  $\varepsilon(\omega) = 2.6896 + i0.01$ , and the film's mean thickness was  $d = 500\text{nm}$ . The semi-infinite medium which the film is ruled on was a perfect conductor. The surface profile function  $\zeta(x_1)$  of the film-conductor interface was characterized by a Gaussian surface height distribution of RMS-height  $\delta = 30\text{nm}$  and a West-O'Donnell power spectrum defined by the parameters  $k_- = 0.82(\omega/c)$  and  $k_+ = 1.97(\omega/c)$ . The length of the surface used in the simulations was  $L = 160\lambda$ . The dashed vertical lines indicate the estimated positions of the satellite peaks (see Ref. [121] for details). The results were obtained by numerical simulations based on the reduced Rayleigh equation. The data in Fig. 16b have been smoothed to make the positions of the satellite peaks more apparent. (After Ref. [121].)

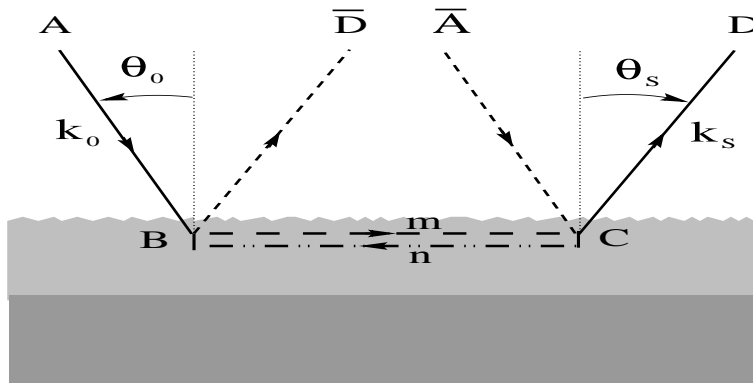


FIG. 17: Illustration of two double scattering sequences occurring in the scattering of electromagnetic waves from a bounded systems that supports more the one guided (or surface) wave.

call them, will be denote by  $q_n(\omega)$  where  $n = 1, \dots, N$ . Through the surface roughness the incident light may couple to these guided waves.

In Fig. 17 we show two general double scattering paths<sup>21</sup> where the scattering takes place at the same scattering centers, but in the reverse order. Such paths will in general be phase incoherent due to the randomness of the rough surface. However, we will now looking into if there are particular angles of incidence and scattering for which these two paths are phase coherent. Let us start by assume that path  $ABCD$  goes through channel  $m$  and path  $\bar{A}CB\bar{D}$  through the  $n$ -channel. The phase difference between these two paths can then be expressed as

$$\Delta\phi_{nm} = \mathbf{r}_{BC} \cdot (\mathbf{k}_0 + \mathbf{k}_s) + |\mathbf{r}_{BC}| [q_n(\omega) - q_m(\omega)]. \quad (135)$$

Here  $\mathbf{k}_0$  and  $\mathbf{k}_s$  are the wave vectors of the incident and scattered waves, respectively, while  $\mathbf{r}_{BC}$  is the distance (vector) from point  $B$  to  $C$ . According to its definition, we will have phase coherence when this phase-difference is zero, *i.e.* when  $\Delta\phi_{nm} = 0$ . Now let us consider separately two cases: (i)  $n = m$  and (ii)  $n \neq m$ . In the first case the last term in Eq. (135) is zero with the consequence that one has phase coherence if  $\mathbf{k}_s = -\mathbf{k}_0$ . This coherence is obviously what gives rise to the enhanced backscattering phenomenon. In the second case when  $m \neq n$ , the last part of Eq. (135) does not vanish. The condition for phase coherence then becomes

$$\sin \theta_s = -\sin \theta_0 \pm \frac{1}{\sqrt{\varepsilon_0(\omega)}} \frac{c}{\omega} |q_n(\omega) - q_m(\omega)|. \quad (136)$$

In this equation we have also allowed for the case  $m = n$  since it naturally includes the position of the backscattering peaks. Hence, Eq. (136) defines the angles for which peaks due to coherent effects are expected in the angular dependence of the light scattered incoherently from the randomly rough surface. The angle obtained for  $m = n$  is the position of the backscattering peak, while the angles obtained for  $m \neq n$  correspond to satellite peaks. The reader should check that the angles obtained from Eq. (136) fit the position of the satellite peaks shown in Fig. 16. The values for  $q_n(\omega)$  can be found in Refs. [42] and [121].

This concludes our discussion of coherent effects in the scattered field. Even though we have focused on the reflected light, it should be pointed out that there also exist similar effects in the transmitted light [61]. For a discussion of this case the reader is referred to the literature for details [22, 61].

## B. Localization

The notion of localization was introduced into physics by P.W. Anderson in his famous 1958 paper [72], a work that he was awarded the Nobel Prize for. Anderson studied the transport properties of electrons in materials with bulk disorder. This study led him to what today is known as the Anderson localization phenomenon, sometimes also

<sup>21</sup> We here consider double scattering for simplicity. Higher order scattering processes can be treated the same way, but doing so will not change the main conclusions.

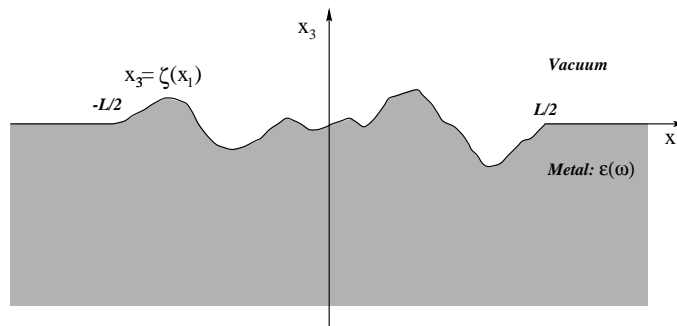


FIG. 18: The scattering system considered in the study of Anderson localization of surface plasmon polaritons on a rough surface.

called strong localization. The phenomenon expresses itself by a disorder-induced phase transition in the transport behavior of the electrons. As the disorder is increased in a three dimensional system, the scattering evolves from a diffusion regime, for which the well-known Ohm's law holds, to a localized regime in which the material behaves as an insulator and all states are localized in space. These two phases are separated by the mobility edge. Anderson suggested [72] that the localization regime was caused by strong interference that resulted in an exponential decay of the wave function of the electrons in all directions and a subsequent vanishment of the diffusion constant. Hence localization is a multiple scattering phenomenon. In contrast to what is the case for three dimensional systems, all states are expected to be localized for systems that are one- and two-dimensional [73]. However, in this latter case it might happen that the localization length is large, and even exceeds the sample size. For a more detailed introduction to localization the reader is directed to Refs. [73] and [74].

It was realized shortly after Anderson published his pioneering work [72], that a similar phenomenon should also be expected for multiple-scattering of electromagnetic waves. At room temperature, photons can be treated as non-interacting. They are therefore not hampered by the troublesome self-interaction that electrons have and that are known to represent another, but different mechanism towards an insulator regime [75]. This fact makes photon disordered systems ideal for studying Anderson localization [76]. However, it should still take several decades before localization of electromagnetic waves was confirmed experimentally. Finally in 1997 Wiersma, Bartolini, Lagendijk, and Righini were able to obtain direct experimental evidence that confirmed the localization hypothesis for electromagnetic waves in disordered media [77]. These experiments were performed on a system containing very strongly scattering semiconductor powders. Thus, the scattering system involved was of the bulk disordered type.

It is still, however, an open question if Anderson localization of electromagnetic waves can be observed experimentally for systems containing only surface disorder, even though it should exist in principle due to the system being two-dimensional (and in some cases effectively one-dimensional). Since there is only disorder on the surface, localization can only exist for electromagnetic waves that happen to "live" on or close to the surface. Such waves are called surface waves, and we will here focus on surface plasmon polaritons (SPP) that might exist on *e.g.* a vacuum-metal interface. SPP localization should be characterized by the exponential decay of the transmitted intensity as a function of distance traveled by the SPP along the rough surface.

However, the problem of observing SPP localization for surface disordered systems is that Anderson localization might be masked by more dominating effects giving rise to the same type of signature as localization itself — the decay  $\exp(-L/\ell_T(\omega))$  with system size  $L$  of the transmittance where  $\ell_T(\omega)$  is a decay length. The competing effects are in addition to the Anderson localization: (i) ohmic losses in the metal due to  $\text{Im} \varepsilon(\omega) \neq 0$ , and (ii) roughness-induced conversion of surface plasmon polaritons into volume waves above the surface — so-called *leakage*. Hence the decay length,  $\ell_T(\omega)$ , of the transmission coefficient (that we will define below), should be related to the decay length due to ohmic losses,  $\ell_\varepsilon(\omega)$ , the one due to leakage,  $\ell_{rad}(\omega)$ , and the Anderson localization length  $\ell(\omega)$ , according to the formulae

$$\frac{1}{\ell_T(\omega)} = \frac{1}{\ell(\omega)} + \frac{1}{\ell_{rad}(\omega)} + \frac{1}{\ell_\varepsilon(\omega)}. \quad (137)$$

In order to determine the Anderson localization length one has to sort out the contribution from each of these competing effects. In other words, we have to identify the lengths  $\ell_\varepsilon(\omega)$  and  $\ell_{rad}(\omega)$  in order to be able to estimate  $\ell(\omega)$ .

The decay rate due to ohmic losses is easily determined and doesn't represent any serious problem (see discussion below). However, a much more severe problem is how to separate the contribution from leakage and localization.

Leakage is expected to be a rather strong effect with the consequence that  $\ell_{rad}(\omega)$  is small compared to the other lengths appearing on the right-hand-side of Eq. (137). If this is the case, a measurement of the transmission coefficient for the SPP will result in  $\ell_T(\omega) \simeq \ell_{rad}(\omega)$ . It is therefore important, if we are trying to estimate  $\ell(\omega)$ , to be able to separate the localization length from the one of leakage, or to be able to suppress leakage. The approach we will follow here is the latter one — the suppression of leakage. This can be done by specially designing surfaces that suppress leakage. How this can be done will be presented briefly below (see Ref. [118] for more details).

### 1. The Scattering System

The scattering system that will be considered in this section is depicted in Fig. 18. We study the scattering of a p-polarized surface plasmon polariton of frequency  $\omega$  propagating in the positive  $x_1$ -direction and is incident onto a segment of a one-dimensional randomly rough surface defined by the equation  $x_3 = \zeta(x_1)$ . The surface profile function  $\zeta(x_1)$  is assumed to be a single-valued function of  $x_1$  that is nonzero only in the interval  $-L/2 < x_1 < L/2$ . The region  $x_3 > \zeta(x_1)$  is vacuum; the region  $x_3 < \zeta(x_1)$  is a metal characterized by an isotropic, frequency-dependent, complex dielectric function  $\varepsilon(\omega) = \varepsilon_1(\omega) + i\varepsilon_2(\omega)$ . We are interested in the frequency range in which  $\varepsilon_1(\omega) < -1, \varepsilon_2(\omega) > 0$ , within which surface plasmon polaritons exist. Furthermore, the rough portion of the surface is assumed to constitute a Gaussian random process and with the other “standard” properties described in Sect. II F.

### 2. Surfaces that Suppress Leakage

The first step towards the estimation of the Anderson localization length for this scattering system is to construct surfaces that suppress leakage. We recall that the incident surface plasmon polariton has a wave vector given by

$$k_{sp}(\omega) = \frac{\omega}{c} \left[ \frac{\varepsilon(\omega)}{\varepsilon(\omega) + 1} \right]^{\frac{1}{2}} = k_1(\omega) + ik_2(\omega), \quad (138)$$

where  $k_1(\omega)$  and  $k_2(\omega)$  are the real and imaginary part of the (complex) SPP wave vector and defined explicitly in Ref. [118].

By interaction with the surface roughness, the incident SPP picks up momenta available in the power-spectrum of the roughness, and due to scattering, changes its wave vector into  $q$ . If this momenta satisfies  $|q| \leq \omega/c$ , leakage has occurred. To prevent this, or at least reduce this effect, we might use an intelligently choice for the power-spectrum. Such a choice is provided by a (rectangular) West-O'Donnell power-spectrum of width  $2\Delta k$  located around  $\pm k_1(\omega)$  (see

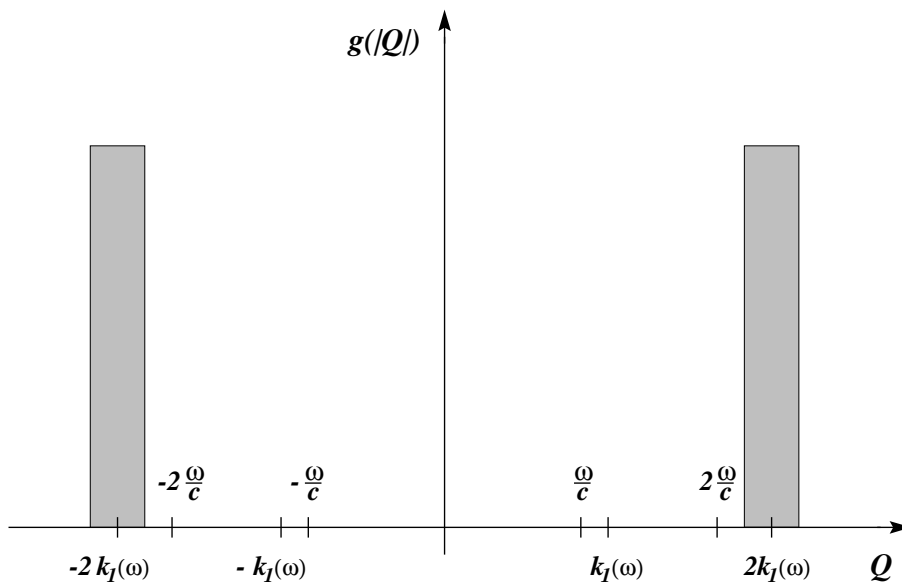


FIG. 19: A sketch of the power-spectrum used in order to suppress leakage. See text for details



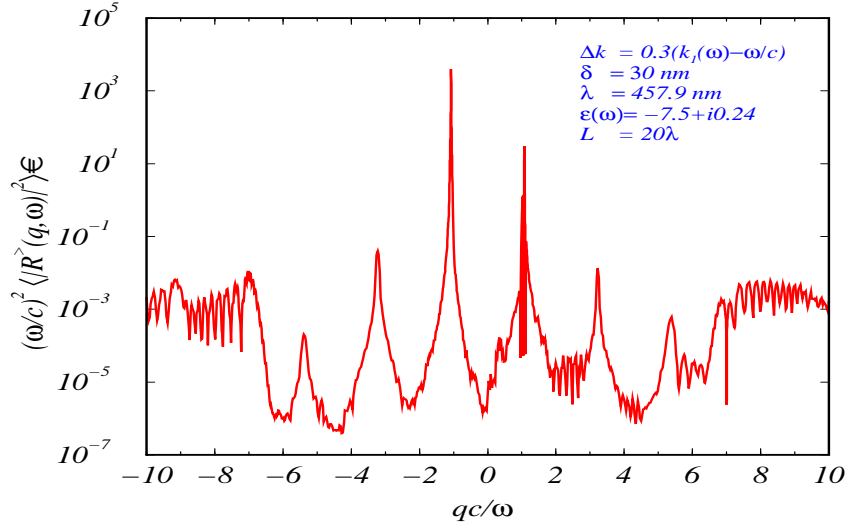


FIG. 20: Numerical calculations for  $(\omega/c)^2 \langle |R^>(q, \omega)|^2 \rangle$  as a function of  $qc/\omega$  for a rough silver surface characterized by the parameters  $\Delta k = 0.3(k_1(\omega) - (\omega/c))$  and  $\delta = 30\text{nm}$ . The rough portion of the surface had length  $L = 20\lambda$ . The frequency of the surface plasmon polariton,  $k(\omega) = k_1(\omega) + ik_2(\omega) = (1.0741 + i0.0026)\omega/c$ , corresponds to a vacuum wavelength of  $\lambda = 457.9\text{nm}$ , and the dielectric constant of silver at this frequency was  $\epsilon(\omega) = -7.5 + i0.24$ . The results for 50 realizations of the surface profile function were averaged to obtain the results plotted in this figure.

Fig. 19), *i.e.* a power-spectrum of the form

$$g(|Q|) = \frac{\pi}{2\Delta k} [\theta(Q - k_-)\theta(k_+ - Q) + \theta(-Q - k_-)\theta(k_+ + Q)], \quad (139)$$

where  $k_{\pm} = 2k_1(\omega) \pm \Delta k$  and  $\Delta k$  must satisfy the inequality  $\Delta k < k_1(\omega) - \frac{\omega}{c}$ .

That a surface characterized by the power spectrum (139) suppresses leakage can be seen from the following argument: The incident surface plasmon polariton has a wave number whose real part is  $k_1(\omega)$ . After its first interaction with the surface roughness the real part of its wave number will lie in the two intervals  $(3k_1(\omega) - \Delta k, 3k_1(\omega) + \Delta k)$  and  $(-k_1(\omega) - \Delta k, -k_1(\omega) + \Delta k)$ . For the same reason, after its second interaction with the surface roughness the real part of the wave number of the surface plasmon polariton will lie in the three intervals  $(5k_1(\omega) - 2\Delta k, 5k_1(\omega) + 2\Delta k)$ ,  $(k_1(\omega) - 2\Delta k, k_1(\omega) + 2\Delta k)$ , and  $(-3k_1(\omega) - 2\Delta k, -3k_1(\omega) + 2\Delta k)$ . After three interactions with the surface roughness the real part of its wave number will lie in the four intervals  $(7k_1(\omega) - 3\Delta k, 7k_1(\omega) + 3\Delta k)$ ,  $(3k_1(\omega) - 3\Delta k, 3k_1(\omega) + 3\Delta k)$ ,  $(-k_1(\omega) - 3\Delta k, -k_1(\omega) + 3\Delta k)$ , and  $(-5k_1(\omega) - 3\Delta k, -5k_1(\omega) + 3\Delta k)$ , and so on. Thus, for example, if  $-k_1(\omega) + 3\Delta k < -(\omega/c)$ , so that  $\Delta k < \frac{1}{3}(k_1(\omega) - (\omega/c))$ , after three scattering processes the surface plasmon polariton will not have been converted into volume electromagnetic waves. In general, if we wish the surface plasmon polariton to be scattered  $n$  times from the surface roughness without being converted into volume electromagnetic waves, we must require that

$$\Delta k < \frac{1}{n}(k_1(\omega) - (\omega/c)). \quad (140)$$

To illustrate that the above procedure really works, we present in Fig. 20 numerical simulation results for the scattering amplitude above the surface,  $(\omega/c)^2 \langle |R^>(q, \omega)|^2 \rangle$  as a function of  $qc/\omega$  for a silver surface characterized by the parameters  $\Delta k = 0.3(k_1(\omega) - (\omega/c))$  and  $\delta = 30\text{nm}$ . This surface should thus suppress leakage up to and including third order scattering processes. We see from Fig. 20 that  $\langle |R^>(q, \omega)|^2 \rangle$  indeed becomes heavily suppressed in the range  $-(\omega/c) < q < (\omega/c)$ . Notice that the six peaks seen in Fig. 20 correspond to the real parts of the wavenumbers of the scattered surface plasmon polaritons resulting from the scattering of an incident surface plasmon polariton of wave vector  $k(\omega) = k_1(\omega) + ik_2(\omega) = (1.0741 + i0.0026)\omega/c$ .

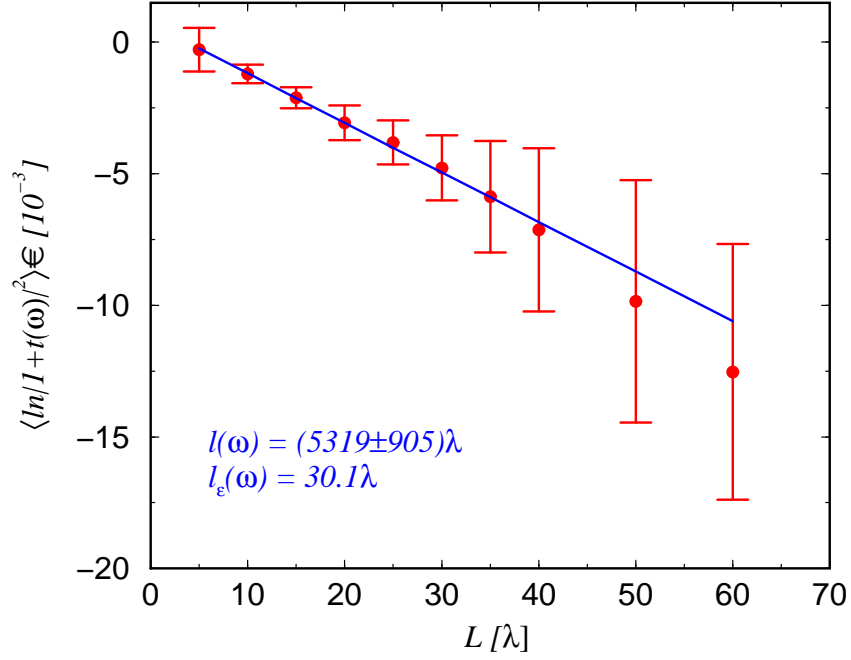


FIG. 21: Numerical simulation results for  $\langle \ln |1 + t(\omega)|^2 \rangle$  vs. the length of the rough portion of the surface  $L$ . The remaining surface parameters were the same used in Fig. 20. The number of realizations used for the rough surface in calculating the ensemble average was for each system size of the order of  $10^2$ . The error-bars indicate the spread in  $|1 + t(\omega)|^2$  that was part of this average. The solid line, which slope is related to the Anderson localization length,  $\ell(\omega)$ , is a  $\chi^2$ -fit to the numerical data corresponding to a localization length of  $\ell(\omega) = (5319 \pm 905)\lambda$ . The length due to ohmic losses in the metal is  $\ell_\varepsilon(\omega) = 30.1\lambda$ .

### 3. The Anderson Localization Length for Surface Plasmon Polaritons Localized on a Randomly Rough Surface

The transmission coefficient for surface plasmon polariton,  $T(L)$ , is defined as the fraction of the energy flux entering the random segment of the metal surface at  $x_1 = -L/2$  and that leaves it at  $x_1 = L/2$ , *i.e.*

$$T(L) = \frac{P_{\text{tr}}\left(\frac{L}{2}\right)}{P_{\text{inc}}\left(-\frac{L}{2}\right)}, \quad (141)$$

where  $P_{\text{inc}}(x_1)$  and  $P_{\text{tr}}(x_1)$  denote the incident and transmitted flux at position  $x_1$ .

Above the surface the field can be written as [118]

$$\begin{aligned} H_2^>(x_1, x_3|\omega) &= \int_{-\infty}^{\infty} \frac{dq}{2\pi} G_0(q, \omega) T(q, \omega) e^{iqx_1 + i\alpha_0(q, \omega)x_3} \\ &\sim t(\omega) e^{ik_{sp}(\omega)x_1 - \beta_0(\omega)x_3}, \quad x_1 \gg L/2, \end{aligned} \quad (142a)$$

with  $\beta_0(\omega) = i\alpha_0(k_{sp}(\omega), \omega)$  and

$$t(\omega) = i \frac{(-\varepsilon(\omega))^{3/2}}{\varepsilon^2(\omega) - 1} T(k_{sp}(\omega), \omega). \quad (142b)$$

Thus the transmission coefficient can alternatively be written as [118]

$$T(L) = |1 + t(\omega)|^2 \exp\left(-\frac{L}{\ell_\varepsilon(\omega)}\right) \quad (143)$$

where  $\ell_\varepsilon(\omega) = 1/(2k_2(\omega))$  is the SPP mean free path due to ohmic losses. Notice that Eq. (143) separates the contribution due to ohmic losses from the one of Anderson localization (and leakage).

The quantity that we will be interested in when studying the localization phenomenon is not the transmission coefficient itself, but instead  $\ln T(L)$  or more precisely its (ensemble) average given by

$$\langle \ln T(L) \rangle = \left\langle \ln |1 + t(\omega)|^2 \right\rangle - \frac{L}{\ell_\epsilon(\omega)}. \quad (144)$$

If the effect of leakage can be neglected, the first term on the right-hand-side of the above equation will *only* incorporate contributions from (Anderson) localization. One therefore writes

$$\left\langle \ln |1 + t(\omega)|^2 \right\rangle = \text{const.} - \frac{L}{\ell(\omega)}. \quad (145)$$

Hence, under the assumption that leakage can be neglected the localization length,  $\ell(\omega)$ , can be obtained from a straight line fit to  $\left\langle \ln |1 + t(\omega)|^2 \right\rangle$  vs. system size  $L$ .

In Fig. 21 we present such a plot resulting from numerical simulations using the same surface parameters that lead to the results shown in Fig. 20 except that now the length of the rough portion of the surface was different. These simulations were performed on the basis of the reduced Rayleigh equation that  $T(q, \omega)$  satisfies [118],

$$T(p, \omega) = V(p|k_{sp}(\omega)) + \int_{-\infty}^{\infty} \frac{dq}{2\pi} V(p|q) G_0(q, \omega) T(q, \omega), \quad (146)$$

where  $V(p|k_{sp}(\omega))$  is the scattering potential defined in Ref. [118], and from which  $t(\omega)$  can be calculated according to Eq. (142b). Notice that to perform such a calculation of  $t(\omega)$  is not at all straight forward. The reason being that the reduced Rayleigh equation, through the Green's function  $G_0(q, \omega)$ , has poles at  $q = \pm k_{sp}(\omega)$ . Details on the numerical method used for such calculations can be found in Ref. [118] and will therefore not be given here.

As can be see from Fig. 21,  $\left\langle \ln |1 + t(\omega)|^2 \right\rangle$  is consistent, within the error bars, with a linear dependence on  $L$ . The solid line in this figure is a  $\chi^2$ -fit to the numerical data. The slope of this curve is according to Eq. (144) related to the Anderson localization length,  $\ell(\omega)$ , as  $1/\ell(\omega)$ . Numerically the Anderson localization length for our system is found to be

$$\ell(\omega) = (5319 \pm 905) \lambda. \quad (147)$$

This length should be compared to the one due to ohmic losses, which for our set of parameters is  $\ell_\epsilon(\omega) = 30.1 \lambda$ .

We have thus shown theoretically that by using specially designed surfaces, there might be hopes of observing the localization of surface plasmon polaritons at a randomly rough metal surface.

### C. Angular Intensity Correlations for the Scattered Light from Randomly Rough Surfaces

It has been known for quite some time that when electromagnetic waves, all of the same frequency, are scattered from a random system, speckle patterns might be observed [78]. Such patterns are results of interference between waves scattered from different locations in the random medium. From studies off volume disordered systems, such patterns are known to contain a rather rich structure [78, 79]. In particular, it was predicted theoretically [79] for such scattering systems that there should exist three types of correlations — short-range correlations, long-range correlations, and infinitely-range correlations. These correlations were termed the  $C^{(1)}$ ,  $C^{(2)}$ , and  $C^{(3)}$ -correlations, respectively, and they have all been observed experimentally [80–82].

In this section we will discuss speckle correlations, not for light scattered from volume disordered systems, but instead for light scattered from randomly rough surfaces. Examples of such speckle patterns obtained when an electromagnetic wave is scattered from a randomly rough surface are shown in Fig. 22.

Let us start by considering a planar surface separating two different materials. Since the surface is planar, the scattering is completely understood as expressed through the celebrated Fresnel's formulae [10, 11]. Imagine an experiment where light is incident at an angle  $\theta_0$  onto the interface. Since the surface is planar, all the light is scattered into the specular direction  $\theta_s = \theta_0$ , and its intensity is given by Fresnel formula. If we in a second experiment incident the light at an angle  $\theta'_0 = -\theta_0$ , *i.e.* at an angle that was the specular direction in the first experiment, all the light will be scattered into  $\theta'_s = \theta'_0 = -\theta_0$  and its intensity is again given by Fresnel's formula. The scattered intensities in these two experiments are in fact equal. This is easily realized from the Fresnel formulae (86b) by noting that the  $\alpha$ -factors that they contain are unaffected by a change of sign in the momentum variables. Thus, if we know the result of the first experiment, say, we also know the outcome of the second one. In other words, these two intensities are

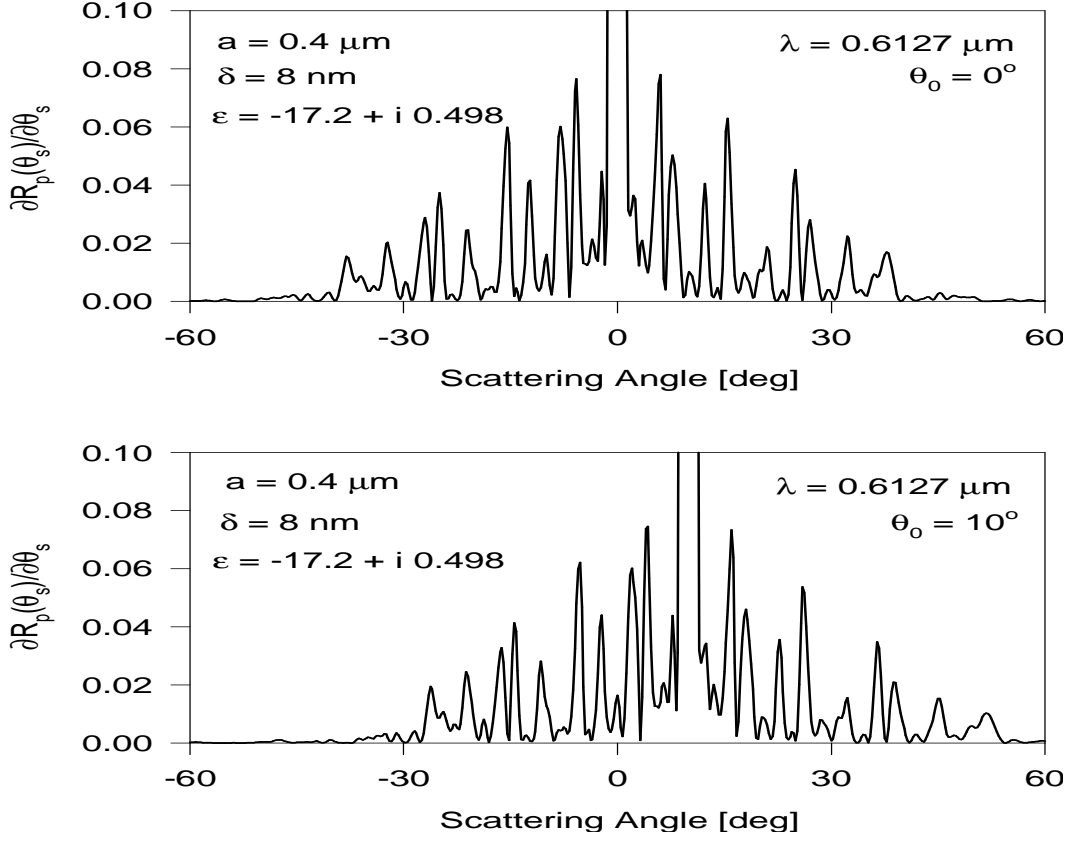


FIG. 22: Speckle patterns that result from the scattering of light of wavelength  $\lambda = 612.7\text{nm}$  incident on a rough silver surface at angles (a)  $\theta_0 = 0^\circ$  and (b)  $\theta_0 = 10^\circ$ . The Gaussian height-distributed surface was characterized by an RMS-height  $\delta = 10\text{nm}$  and a (Gaussian) correlation length  $a = 0.4\mu\text{m}$ . The length of the surface was  $L = 100\mu\text{m}$  and the dielectric constant of silver at the wavelength of the incident light is  $\varepsilon(\omega) = -17.2 + i0.498$ .

perfectly correlated. We now introduce the momentum variables  $q$  and  $k$  related in the usual way to the scattering and incident angles respectively (see *e.g.* Eq. (149) below). Let the notation  $(q, k)$  denotes a corresponding pair of momenta variables where  $q$  is the scattered momentum and  $k$  the incident one. For our planar surface geometry we will thus have perfect correlation between the two scattering processes  $(q, k)$  and  $(q', k')$  if  $(q, k) = (-k', -q')$ . Furthermore, since any process, of course, is correlated with itself, we in addition will expect perfect correlation when  $(q, k) = (q', k')$ .

The above example is rather trivial and well-known example of correlations in the scattered intensity from a planar surface. However, what happens to the intensity correlations if the surface is not planar, but instead randomly rough? This is an interesting and non-trivial question and we will address it in this section. In the discussion to be presented below we will be focusing on the angular correlations in the light scattered *incoherently* from a rough surface. Furthermore, we will mainly discuss the case where the surface is weakly rough. In particular we will try to answer the following question: When and under which conditions will the intensity scattered (incoherent) into the far field for different incident and scattering angles be related to one and other?

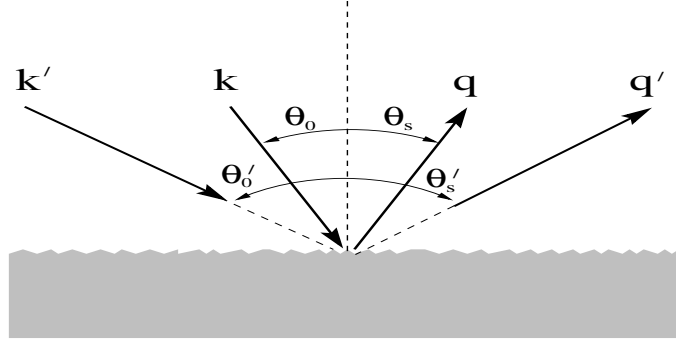


FIG. 23: The scattering system considered in the study of the angular correlation functions.

### 1. Definition of the Angular Intensity Correlation Functions

Let us start by introducing the *unnormalized* angular correlation function  $C(q, k|q', k')$ , which we will define as<sup>22</sup>

$$C(q, k|q', k') = \langle I(q|k)I(q'|k') \rangle - \langle I(q|k) \rangle \langle I(q'|k') \rangle, \quad (148)$$

where  $I(q|k)$  denotes the intensity of the light scattered from the surface, and the angle brackets denote an average taken over an ensemble of realizations of the surface profile function  $\zeta(x_1)$ . Furthermore, the (lateral) momentum variables,  $q$  and  $k$ , are both, in the radiative region ( $|q| \leq \sqrt{\varepsilon_0}\omega/c$ ), understood to be related to the scattering and incident angles  $\theta_s$  and  $\theta_0$  respectively according to

$$k = \sqrt{\varepsilon_0(\omega)} \frac{\omega}{c} \sin \theta_0, \quad q = \sqrt{\varepsilon_0(\omega)} \frac{\omega}{c} \sin \theta_s. \quad (149)$$

The primed momentum variables,  $q'$  and  $k'$ , are related in a similar way to the primed angles  $\theta'_s$  and  $\theta'_0$ . These angles, both primed and unprimed, are defined positive according to the convention indicated in Fig. 23. This figure also shows our scattering system consisting of a semi-infinite dielectric medium with a rough interface to vacuum.

Furthermore, the intensity  $I(q|k)$  can be defined through the scattering matrix  $S(q|k)$  according to the formula

$$I(q|k) = \frac{\sqrt{\varepsilon_0(\omega)}}{L_1} \left( \frac{\omega}{c} \right) |S(q|k)|^2, \quad (150)$$

where  $L_1$  is the length of the  $x_1$ -axis covered by the random surface.

In many cases it is convenient to work with a normalized correlation function,  $\Xi(q, k|q', k')$ , in contrast to the unnormalized one. The normalized angular intensity correlation function will we define by<sup>23</sup>

$$\Xi(q, k|q', k') = \frac{\langle I(q|k)I(q'|k') \rangle - \langle I(q|k) \rangle \langle I(q'|k') \rangle}{\langle I(q|k) \rangle \langle I(q'|k') \rangle}. \quad (151)$$

The lesson to be learned from the huge amount of research being conducted on correlation function in the field of random (bulk) disordered systems [79–81, 83, 84] is that there may exist correlations on many different length scales including *short* to *infinite* range correlations. Thus part of the challenge we are facing will be to separate these different contribution to  $C(q, k|q', k')$  (or equivalently to  $\Xi(q, k|q', k')$ ) from one another.

The first step towards such a separation is to rewrite the correlation function in terms of the S-matrix. This is done by substituting the expression for the intensity, Eq. (150), into the definition of the correlation function and thus obtaining

$$C(q, k|q', k') = \frac{\varepsilon_0 \omega^2}{L_1^2 c^2} \left[ \langle |S(q|k)|^2 |S(q'|k')|^2 \rangle - \langle |S(q|k)|^2 \rangle \langle |S(q'|k')|^2 \rangle \right]. \quad (152)$$

<sup>22</sup> We have here suppressed any explicit reference to the polarization (the  $\nu$ -index) since no confusion should result from doing so. All quantities in this section should be understood to be referring to one and the same polarization.

<sup>23</sup> It should be noticed that a somewhat different definition for the normalized angular intensity correlation function is used by some authors [89]. However, the advantage of the definition (151) is that it does not contain any  $\delta$ -functions in the denominator.

Due to the stationarity of the surface profile function, the average of the S-matrix should be diagonal in  $q$  and  $k$ ,

$$\langle S(q|k) \rangle = 2\pi\delta(q-k) S(k). \quad (153)$$

By now taking advantage of this relation in addition to the cumulant average [85, 86]

$$\{AB\} = \langle AB \rangle - \langle A \rangle \langle B \rangle, \quad (154)$$

the correlation function (152) can be written as

$$C(q, k|q', k') = \frac{\varepsilon_0 \omega^2}{L_1^2 c^2} \left[ |\langle \delta S(q|k) \delta S^*(q'|k') \rangle|^2 + |\langle \delta S(q|k) \delta S(q'|k') \rangle|^2 + \{\delta S(q|k) \delta S^*(q|k) \delta S(q'|k') \delta S^*(q'|k')\} \right] + s.t. \quad (155a)$$

where  $\delta S(q|k)$  denotes the incoherent component of the S-matrix defined as

$$\delta S(q|k) = S(q|k) - \langle S(q|k) \rangle. \quad (155b)$$

In Eq. (155a) the asterisks denote complex conjugate while *s.t.* means specular terms, *i.e.* terms that are proportional to  $\delta(q-k)$  and/or  $\delta(q'-k')$ . Such terms will not be focused on here since we will concentrate on the incoherent part of the scattered light. With Eq. (155a) we can now write<sup>24</sup>

$$C(q, k|q', k') = C^{(1)}(q, k|q', k') + C^{(10)}(q, k|q', k') + C^{(N)}(q, k|q', k'), \quad (156a)$$

where

$$C^{(1)}(q, k|q', k') = \frac{\varepsilon_0 \omega^2}{L_1^2 c^2} |\langle \delta S(q|k) \delta S^*(q'|k') \rangle|^2, \quad (156b)$$

$$C^{(10)}(q, k|q', k') = \frac{\varepsilon_0 \omega^2}{L_1^2 c^2} |\langle \delta S(q|k) \delta S(q'|k') \rangle|^2, \quad (156c)$$

and

$$C^{(N)}(q, k|q', k') = \frac{\varepsilon_0 \omega^2}{L_1^2 c^2} \{\delta S(q|k) \delta S^*(q|k) \delta S(q'|k') \delta S^*(q'|k')\}. \quad (156d)$$

Due to reasons which should be clear from the discussion below, the correlation functions in Eqs. (156b) and (156c) are termed *short-range* correlation functions, while the one in Eq. (156d) contains contribution from *long* and *infinite-range* correlations. They will now be discussed in turn.

## 2. Short Range Correlations for Weakly rough Surfaces

In this subsection the short-range correlation functions,  $C^{(1)}$  and  $C^{(10)}$ , for weakly rough surfaces will be discussed. These correlation functions are to leading order in the surface profile function a result of single scattering processes [91]. However, above leading order they will also receive contributions from multiple scattering. The long and infinite range correlations,  $C^{(N)}$ , contain at least one multiple scattering process as we will see [91]. Therefore the “optical paths” involved in the processes leading to  $C^{(1)}$  and  $C^{(10)}$  are typically shorter than those giving rise to  $C^{(N)}$ . This is one of the reasons why the  $C^{(1)}$  and  $C^{(10)}$  correlation functions are termed short-range correlation functions. Another reason stems from the fact that  $C^{(1)}$  and  $C^{(10)}$  are both independent of the length of the random surface. In the next subsection we will demonstrate explicitly that the  $C^{(N)}$ -correlation function is proportional to  $1/L_1$ . Hence, in the limit of a long surface the amplitude of the correlation function  $C^{(N)}$  is neglectable compared to  $C^{(1)}$  and  $C^{(10)}$ .

### The $C^{(1)}$ Correlations Function; The Memory- and Reciprocal Memory-Effect

---

<sup>24</sup> Notice that equivalent expressions can be derived for the normalized correlation functions based on Eq. (151).

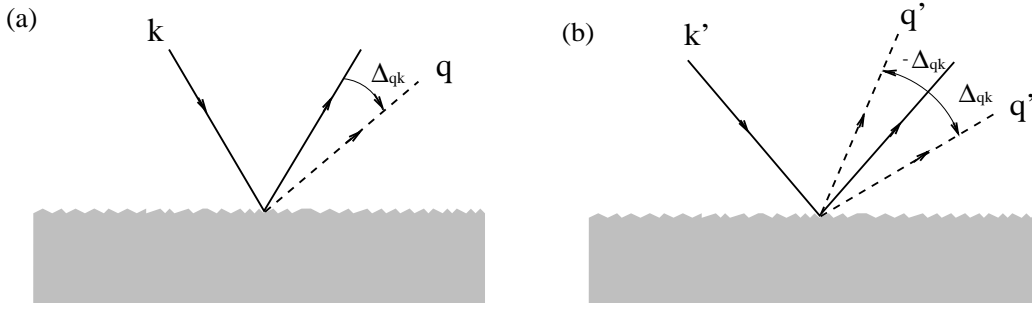


FIG. 24: Interpretation of the correlation condition for the short-range correlation functions  $C^{(1)}$  and  $C^{(10)}$ . The outgoing solid lines indicate the specular direction. The scattering process  $(q, k)$  that gives rise to the momentum transfer  $\Delta_{qk} = q - k$  might be correlated with the process  $(q', k')$  if  $\Delta_{qk} = \Delta_{q'k'}$  ( $C^{(1)}$ ) or if  $\Delta_{qk} = -\Delta_{q'k'}$  ( $C^{(10)}$ ).

At first sight, the expressions in Eqs. (156) might not seem too useful to us. However, they are as we now will try to explain. We will only be concerned about one-dimensional random surfaces,  $\zeta(x_1)$ , that are stationary and constitutes a Gaussian random process. Under this assumption the expression  $\langle \delta S(q|k) \delta S^*(q'|k') \rangle$ , contained in  $C^{(1)}$ , will be proportional to a  $\delta$ -function, *i.e.*

$$\langle \delta S(q|k) \delta S^*(q'|k') \rangle \propto 2\pi \delta(q - k - q' + k'). \quad (157)$$

This is so due to the stationarity of the surface profile function  $\zeta(x_1)$ . To motivate this we recalling from Sect. III, or Ref. [55], that to lowest order in the surface profile function the scattering amplitude that is proportional to the S-matrix, is proportional to  $\tilde{\zeta}(q - k)$ , where  $\tilde{\zeta}$  denotes the Fourier transform of the surface profile function. Since  $\langle \tilde{\zeta}(q) \tilde{\zeta}^*(k) \rangle = 2\pi \delta(q - k)$ , Eq. (157), to lowest order, follows immediately.

Thus, with Eq. (157) we find that the correlation function  $C^{(1)}$  can be written in the convenient form

$$C^{(1)}(q, k|q', k') = \frac{2\pi \delta(q - k - q' + k')}{L_1} C_0^{(1)}(q, k|q', q' - q + k). \quad (158)$$

Here  $C_0^{(1)}$  is known as the *envelope function* of  $C^{(1)}$  and it is *independent* of the length  $L_1$  of the surface. Notice that the  $C^{(1)}$ -correlation function can only be non-vanishing when the argument of the  $\delta$ -function vanishes. Therefore, since  $2\pi \delta(0) = L_1$ , the (full)  $C^{(1)}$ -correlation function is also independent of the length of the surface.

To see what the  $\delta$ -function condition of Eq. (158) means physically, it is convenient to introduce the momentum transfer that can be associated with the scattering process. If the incident light has momentum  $k$  and the scattered light is described by the momentum variable  $q$  the momentum transfer is

$$\Delta_{qk} = q - k. \quad (159)$$

Such a scattering event we recall was earlier denoted by  $(q, k)$ . Thus, what Eq. (158) says is that the two scattering processes  $(q, k)$  and  $(q', k')$  might have non-vanishing  $C^{(1)}$  correlations if and only if the two scattering events have the same momentum transfer, *i.e.* if and only if

$$\Delta_{qk} = \Delta_{q'k'}. \quad (160)$$

This condition is depicted in Fig. 24. From the condition (160) it follows that if the incident momentum is changed from say  $k$  to  $k' = k + \Delta k$ , the entire speckle pattern shifts in such a way that any feature initial at  $q$  moves to  $q' = q + \Delta q$ . In terms of the angles of incidence and scattering, we have that if  $\theta_0$  is changed to  $\theta'_0 = \theta_0 + \Delta\theta_0$ , any feature in the speckle pattern originally at  $\theta_s$  is shifted to  $\theta'_s = \theta_s + \Delta\theta_s$ , where  $\Delta\theta_s = \Delta\theta_0 (\cos \theta_0 / \cos \theta_s)$  to first order in  $\Delta\theta_0$ . This effect can indeed be seen from the speckle patterns presented in Figs. 22.

It should in particular be noticed that condition (160) is satisfied if (i)  $k = k'$  and  $q = q'$  as well as if (ii)  $k = -q'$  and  $q = -k'$ . These choices are the ones mentioned in the beginning of this section for the scattering from a planar surface. It is interesting to notice that these for a planar surface trivial correlations, also holds true for the scattering from randomly rough surfaces, even though as should be noticed, their physical origin is rather different. Case (i) is kind of trivial since any scattering process should be perfectly correlated with itself. This effect is known in the literature as the *memory-effect*. Situation (ii), that doesn't seem that obvious at first, is, in fact, a consequence of

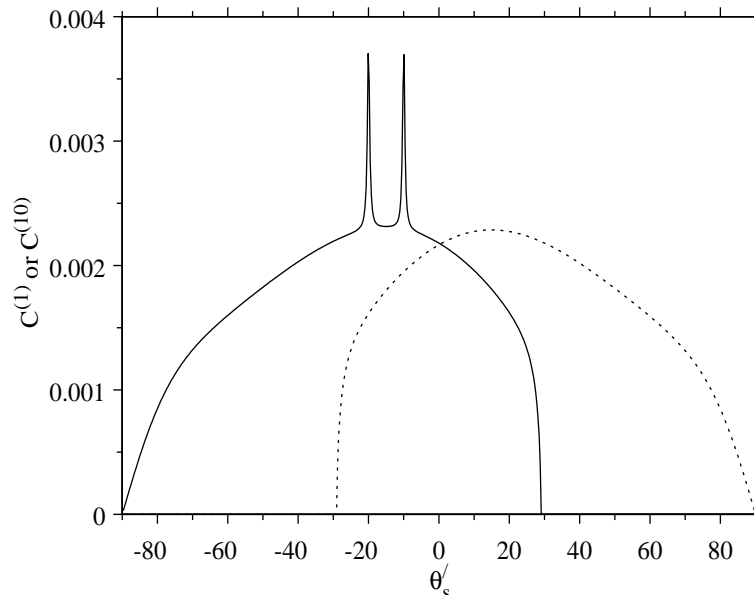


FIG. 25: The envelopes of the short-range correlation functions  $C^{(1)}(q, k|q', k')$  (solid line) and  $C^{(10)}(q, k|q', k')$  (dashed line) as a function of the scattering angle  $\theta'_s$  for  $\theta_s = -10^\circ$  and  $\theta_0 = 20^\circ$ . The angle  $\theta'_0$  is determined from the  $\delta$ -function constraint. The rough surface was a silver surface characterized by Gaussian height statistics of RMS-height  $\delta = 5\text{nm}$ . The correlation function was also Gaussian with a correlation length of  $a = 100\text{nm}$ . The wavelength of the incident light was  $\lambda = 457.9\text{nm}$ . At this wavelength the dielectric constant of silver is  $\varepsilon(\omega) = -7.5 + i0.24$ . (After Ref. [91].)

the reciprocity of the S-matrix;  $S(q|k) = S(-k|-q)$ . Hence, when  $k = -q'$  and  $q = -k'$  there should be perfect correlations, and the effect is known as the *reciprocal memory-effect*. If the scattering system does not possess any damping, the system also respects time-reversal symmetry. Due to this reason this latter effect is also known by some authors as the *time-reversed memory effect*.

In Fig. 25 (solid line) we present the result of perturbative calculations [91] for the envelope of the  $C^{(1)}$  correlation function as a function of the scattering angle  $\theta'_s$  for  $\theta_s = -10^\circ$  and  $\theta_0 = 20^\circ$ . The angle  $\theta'_0$  is determined from the  $\delta$ -function condition of Eq. (158). The incident wave was  $p$ -polarized, and the surface parameters are defined in the caption of this figure. Two well-pronounced peaks at scattering angles  $\theta_s = -20^\circ$  and  $\theta_s = -10^\circ$  are easily spotted in the envelope of  $C^{(1)}$ . They correspond respectively to the memory and reciprocal memory effect. It can in fact be shown that by instead considering the envelope of the normalized correlation function,  $\Xi^{(1)}$ , one will have perfect correlation at the maximum point of these two peaks (see *e.g.* Ref. [119]).

Before continuing, we would like to point out that the memory and reciprocal memory effect seen in Fig. 25 are due to multiple scattering processes that involves surface plasmon polaritons. Thus, for an  $s$ -polarized wave incident onto a weakly rough metal surface, such peaks are not expected to be seen since in this case the incident wave cannot excite surface plasmon polariton at the rough surface [119]. However, for scattering of an  $s$ -polarized wave at a dielectric-dielectric interface the  $C^{(1)}$  may show peaks [120] even though no surface plasmon polaritons are involved. These peaks originate from multiple scattering processes involving so-called lateral waves [88].

Recently both the memory and reciprocal memory effect have been observed experimentally by West and O'Donnell [89] in the scattering of  $p$ -polarized light from a weakly rough, one-dimensional, random gold surface. We have reproduced one of their graphs in Fig. 26.

### The $C^{(10)}$ Correlation functions

We now focus on the  $C^{(10)}$ -correlation function. This correlation function was originally overlooked in the early studies of correlation functions [87] due to the use of the factorization method [83]. By essentially duplicating the arguments used in arriving at Eq. (157), we find in an analogous way that

$$\langle \delta S(q|k) \delta S(q'|k') \rangle \propto 2\pi \delta(q - k + q' - k'), \quad (161)$$



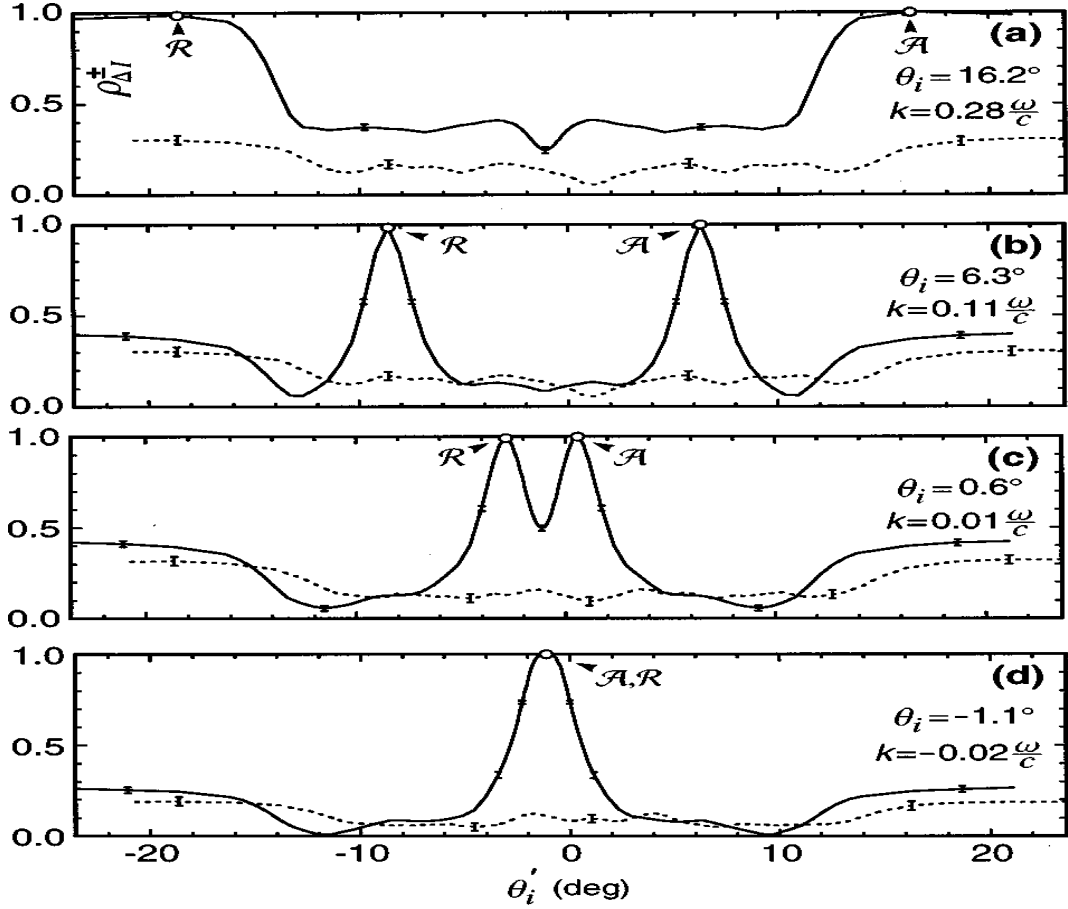


FIG. 26: Experimental measurements of the normalized correlation functions  $\rho_{\Delta I}^+(k, k', \Delta_{qk})$  (solid lines) and  $\rho_{\Delta I}^-(k, k', \Delta_{qk})$  (dashed lines) as defined by West and O'Donnell [89] as function of the angle of incidence  $\theta_i'$ . These correlation functions are these authors equivalent to our envelope functions  $\Xi_0^{(1)}(q, k|q', k')$  and  $\Xi_0^{(10)}(q, k|q', k')$  (see Ref. [89] for details). The incident light had wavelength  $\lambda = 6.12\text{nm}$  and the momentum transfer was  $\Delta_{qk} = 0.04(\omega/c)$ . The Gaussian height-distributed gold surface had RMS-height  $\delta \simeq 15.5\text{nm}$ . Its correlation was characterized by a West-O'Donnell (rectangular) power spectrum of parameters  $k_- = 0.83(\omega/c)$  and  $k_+ = 1.30(\omega/c)$ . These values satisfy  $k_- < k_{sp} < k_+$  where  $k_{sp} = 1.06(\omega/c)$  is the surface plasmon polariton wave vector, and hence an incident wave should couple strongly to such modes. The memory and the time-revised memory peaks are indicated in these figures by  $\mathcal{A}$  and  $\mathcal{R}$  respectively. At these two positions we see that there are perfect correlations. (After Ref. [89].)

with the consequence that we might write

$$C^{(10)}(q, k|q', k') \propto \frac{2\pi\delta(q - k + q' - k')}{L_1} C_0^{(10)}(q, k|q', q' + q + k). \quad (162)$$

Here  $C_0^{(10)}(q, k|q', q' + q + k)$  is an envelope function, and both  $C^{(10)}$  and its envelope  $C_0^{(10)}$  are independent of the length of the randomly rough surface.

The presence of the  $\delta$ -function on the right hand side of Eq. (162) is in terms of the momentum transfer equivalent to

$$\Delta_{qk} = -\Delta_{q'k'}. \quad (163)$$

What this condition implies for the speckle pattern is that if we change the angle of incidence in such a way that  $k$  goes into  $k' = k + \Delta k$ , a feature originally at  $q = k - \Delta q$  will be shifted to  $q' = k' + \Delta q$ , *i.e.* to a point as much to one side of the new specular direction as the original point was on the other side of the original specular direction. For one and the same incident beam the  $C^{(10)}$  correlation function therefore reflects the symmetry of the speckle pattern with respect to the specular direction (see Fig. 24).

The dashed line in Fig. 25 shows the angular dependence, obtained from perturbation theory [91], for the envelope of  $C^{(10)}$ . The parameters used to obtain these results were the same used to obtain the  $C^{(1)}$  correlation shown by the solid line in the same figure. It is seen that the  $C_0^{(10)}$  envelope is a smooth function of  $\theta'_s$ , and in particular does not show any peaks. Moreover, its amplitude is roughly of the same order of magnitude as the  $C^{(1)}$  correlation function. This behavior is the same as the one found by West and O'Donnell [89] in their experimental investigation of the  $C_0^{(10)}$  envelope (Fig. 26).

It should be pointed out that the  $C^{(10)}$  correlation function has no known analogy within scattering from volume disordered system. This new type of correlations in surface scattering was first predicted from perturbation theory by Malyshkin *et al.* in 1997 [90, 91].

### 3. Long- and Infinite-Range Correlations

We will now consider the last term of the right hand side of Eq. (156) that gives rise to  $C^{(N)}$ . Due to the stationarity of the surface

$$\{\delta S(q|k)\delta S^*(q|k)\delta S(q'|k')\delta S^*(q'|k')\} \propto 2\pi\delta(0) = L_1.$$

Hence, the correlation function itself, in light of Eq. (156d), should behave as

$$C^{(N)}(q, k|q', k') \propto \frac{1}{L_1}. \quad (164)$$

It should be noticed that the  $C^{(N)}$ -correlation function is not constrained in its momentum variables through  $\delta$ -functions as we saw earlier was the case for the short-range correlation functions.

Even though we will not address this point explicitly here it has recently been shown that  $C^{(N)}$  can be written as a sum of the three following terms [90, 91]

$$C^{(N)}(q, k|q', k') = C^{(1.5)}(q, k|q', k') + C^{(2)}(q, k|q', k') + C^{(3)}(q, k|q', k').$$

Here  $C^{(1.5)}$  denotes a correlation function of *intermediate-range*,  $C^{(2)}$  is a correlation function of *long-range*, while  $C^{(3)}$  is an *infinite-range* correlation function. For explicit expressions for these three correlation functions the interested reader is directed to Refs. [90, 91] and [92]. In scattering from bulk disordered systems  $C^{(2)}$  [79, 81, 84] and  $C^{(3)}$  [79, 80] have their analogies. However, the intermediate range correlation function,  $C^{(1.5)}$ , predicted theoretically by Malyshkin *et al.* in 1997 [90, 91], has no equivalent in scattering from volume disordered systems. It is unique to scattering from randomly rough surfaces that support surface plasmon polaritons at the frequency of the incident light. An explicit example of such a scattering system is provided by a randomly rough metal surface in *p*-polarization.

Based on a diagrammatic perturbation theoretical study, Malyshkin *et al.* [91] found that  $C^{(1.5)}$  shows a rather rich peak structure. Peaks in  $C^{(1.5)}$  are expected to occur for a number of cases in which a linear combination of three of the momenta  $q$ ,  $k$ ,  $q'$  and  $k'$  add up to  $\pm k_{sp}$ , where  $k_{sp}$ , is the wave vector of the surface plasmon polariton. These conditions are summarized in Table II. In an expansion of  $C^{(1.5)}$  in powers of the surface profile function the leading order is  $\mathcal{O}(\zeta^6)$ . The intermediate-range correlation function  $C^{(1.5)}$  is therefore for a weakly rough surface a result of correlations between a single scattering and a multiple scattering process that involves surface plasmon polaritons. In Fig. 27a we have plotted the intermediate-range correlation function  $C^{(1.5)}$  for the randomly rough silver surface that lead to the results shown earlier in Fig.25. In this graphs several peaks are easily seen. Their positions should be compared to the predictions that can be obtained from Table II.

So far there is no experimental measurements for any of the correlations contained in  $C^{(N)}$ . In fact such an experimental confirmation represents a real challenge to the experimentalists. The reason being that for long surface these correlations are rather small (due to Eq. (164)). In order to be able to observe them, one probably has to use a well-focused incident beam, or a short surface.

Malyshkin *et al.* [91] also showed perturbatively that the  $C^{(2)}$ -correlation function should have a peak structure, while the infinite range correlation function,  $C^{(3)}$ , should be a smooth function of its arguments. This is seen from the perturbative results plotted in Fig. 27b ( $C^{(2)}$ ) and Fig. 27c ( $C^{(3)}$ ). The correlations described by the  $C^{(2)}$ -correlations function are a result of correlation between two multiple scattering processes. For weakly rough metal surfaces this correlation function is dominated by double scattering processes. Its peaks are associated with surface plasmon polaritons, as was found to be the case also for  $C^{(1.5)}$ . The peak conditions for  $C^{(2)}$  are that two of the four momenta involved should add/subtract to zero. That is to say that for fixed  $k$ ,  $q$ , and  $k'$ , peaks are expected when  $q' = \pm k'$ ,  $q' = \pm k$  or  $q' = \pm q$  (see Table II). Also the infinite range correlations are due to multiple scattering events. What distinguish the long-range correlation,  $C^{(2)}$ , from the infinite-range,  $C^{(3)}$ , is that the latter involves at least one

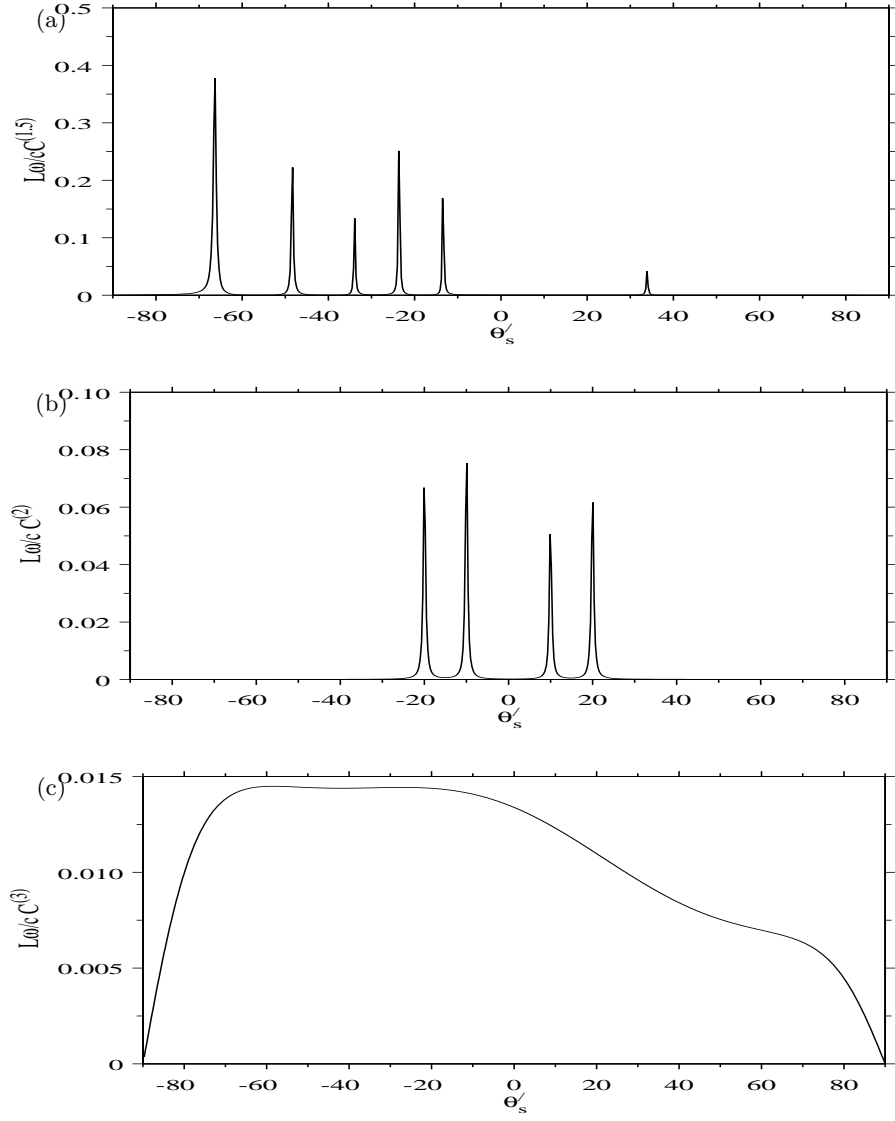


FIG. 27: Perturbative results for the angular dependence of the correlation functions (a)  $C^{(1.5)}(q, k|q', k')$ , (b)  $C^{(2)}(q, k|q', k')$  and (c)  $C^{(3)}(q, k|q', k')$  on the scattering angle  $\theta'_s$  for  $\theta_s = -10^\circ$ ,  $\theta_0 = 20^\circ$  and  $\theta'_0 = 30^\circ$ . The remaining parameters were the same used in Fig. 25. (After Ref. [91].)

triple scattering process<sup>25</sup>. For more details information about  $C^{(1.5)}$ ,  $C^{(2)}$ , and  $C^{(3)}$ , the reader is invited to consult Refs. [90, 91] and [92].

#### 4. Angular Intensity Correlation Functions for Strongly Rough Surfaces

Before closing this section, we would like to make a few remarks regarding strongly rough surfaces. Above we always assumed that the surface was a weakly rough metal surface. We saw that many of the interesting features of  $C(q, k|q', k')$  appeared due to excitations of surface plasmon polaritons. For strongly rough surfaces the excitation of surface plasmon polaritons, if any, is weak, and the dominating mechanism for multiple scattering from such surfaces

<sup>25</sup> The leading contribution to  $C^{(3)}$  is of order  $\zeta^{10}$  in the surface profile function  $\zeta(x_1)$  [91].

| Correlation function | Peak condition           |
|----------------------|--------------------------|
| $C^{(1.5)}$          | $-k' + k + q' = -k_{sp}$ |
| $C^{(1.5)}$          | $q - q' + k' = k_{sp}$   |
| $C^{(1.5)}$          | $q' + q - k' = -k_{sp}$  |
| $C^{(1.5)}$          | $q' - k' + q = -k_{sp}$  |
| $C^{(1.5)}$          | $k + k' - q' = k_{sp}$   |
| $C^{(1.5)}$          | $q' - q + k = k_{sp}$    |
| $C^{(2)}$            | $q' = -k$                |
| $C^{(2)}$            | $q' = q$                 |
| $C^{(2)}$            | $q' = -q$                |
| $C^{(2)}$            | $q' = k$                 |

TABLE II: The peak conditions for the intermediate range  $C^{(1.5)}$  and long range correlation function  $C^{(2)}$  for a metallic one-dimensional surface. See text for details.

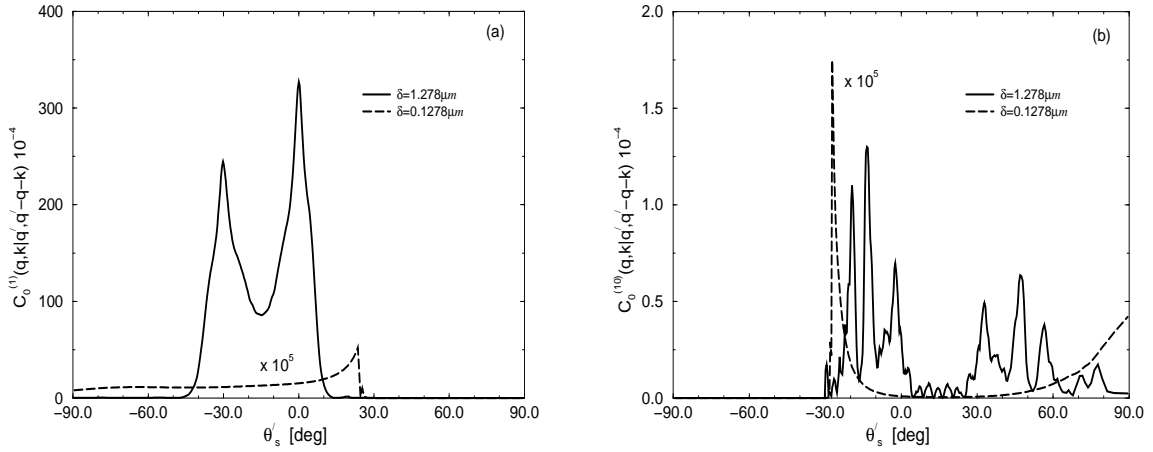


FIG. 28: Rigorous numerical simulation results for the (a)  $C_0^{(1)}$  and (b)  $C_0^{(10)}$  envelopes as functions of  $\theta'_s$  for  $\theta_0 = 30^\circ$  and  $\theta_s = 0^\circ$ . The angle  $\theta'_0$  was determined from the  $\delta$ -function constraint. The  $s$ -polarized incident light had wavelength  $\lambda = 632.8\text{nm}$ . The randomly rough silver surface characterized by a (Gaussian) correlation length  $a = 3.85\mu\text{m}$ . The RMS-height of the Gaussian height-distributed surface was  $\delta = 1.278\mu\text{m}$  (solid line)  $\delta = 0.1278\mu\text{m}$  (dashed line). As the RMS-height is increased one observes that the memory and reciprocal memory peaks start appearing in the envelope of  $C^{(1)}$ . (After Ref. [119].)

is multiple scattering of volume waves. As might have been guessed, multiple scattering of volume waves take over for strongly rough surfaces the role that surface plasmon polaritons had for weakly rough surfaces. These multiple scattered volume waves give rise to the memory and reciprocal memory effect for strongly rough surface. This is in fact the case for both  $p$ - and  $s$ -polarized incident light in contrast to what is the case for weakly rough surfaces. This is illustrated by the rigorous computer simulation results of Fig. 28a showing the  $C_0^{(1)}$  envelope for  $s$ -polarized incident light [119]. It is seen from this figure that as the RMS-height is increased from a value corresponding to a weakly rough surface the memory and reciprocal memory peaks start to emerge in the  $C_0^{(1)}$  envelope due to the increased contribution from multiple scattered volume waves.

It should also be noticed, as was realized recently [119], that a measurement of the angular intensity correlations can provide valuable information regarding the statistical properties of the amplitude of the scattered field. In particular, it was shown that the short-range correlation function  $C^{(10)}$  is in a sense a measure of the non-circularity of the complex Gaussian statistics of the scattering matrix. If the random surface is such that only the  $C^{(1)}$  and  $C^{(10)}$  correlation functions are observed, then  $S(q|k)$  obeys complex Gaussian statistics. If the random surface is such that only  $C^{(1)}$

is observed, then  $S(q|k)$  obeys circular complex Gaussian statistics<sup>26</sup>. This can indeed be seen from Fig. 28b, which shows that as the surface is made rougher, and therefore  $\delta S(q|k)$  approaches a circular complex Gaussian process, the  $C^{(10)}$ -correlation vanishes as compared to  $C^{(1)}$ . Finally, if the random surface is such that  $C^{(1.5)}$ ,  $C^{(2)}$  and  $C^{(3)}$  are observed in addition to both  $C^{(1)}$  and  $C^{(10)}$ , then  $\delta S(q|k)$  is not a Gaussian random process at all. However, which kind of statistics  $\delta S(q|k)$  satisfies in this case is not clear for the moment. These results fits the findings from standard speckle theory [78, 93, 94] which assumes that the disorder is strong and that  $\delta S(q|k)$  constitutes a circular complex Gaussian process.

#### D. Second Harmonic Generation of Scattered Light

So far in this section, we have discussed exclusively rough surface scattering phenomena that find their explanation within linear electromagnetic theory. There are still many exciting nonlinear [35] surface scattering effects that have to be addressed in the future. Such nonlinear studies are still at their early beginning. The studies that have been conducted so far on nonlinear surface scattering effects have mainly been related to the angular distribution of the scattered *second harmonic* generated light [10, 11]. In particular what have been studied are some new features in the backscattering directions of the second harmonic light. In this section we will discuss some of these results. The presentation given below follows closely the one given in Ref. [96].

It is well-known from solid state physics that an (infinite) homogeneous and isotropic metal has inversion symmetry [38, 116]. A consequence of this is that there is no nonlinear polarization in the bulk. If, however, the metal is semi-infinite with an interface to vacuum, say, the inversion symmetry is broken. Thus, a nonlinear polarization, different from zero, will exist close to the surface. As we move into the bulk of the metal, this effect will become smaller and smaller and finally vanish. Therefore, one might talk about a nonlinear surface layer which through nonlinear interactions will give rise to light that is scattered away from the rough surface at the second harmonic frequency.

The scattering system that we will be considering is the by now standard one depicted in Fig. 6. This geometry is illuminated from the vacuum side,  $x_3 > \zeta(x_1)$ , by a  $p$ -polarized planar wave of (fundamental) frequency  $\omega$ . Only the  $p$ -polarized component of the scattered second harmonic generated light will be considered here, even though there also will exit a weak  $s$ -polarized component due to the nonlinear interaction at the surface. However, the  $p$ -polarized component represents the main contribution to the scattered light at the second harmonic frequency  $2\omega$ , and will therefore be our main concern here. Moreover it will be assumed that the generation of the second harmonic light does not influence the field at the fundamental frequency in any significant way.

To motivate the study, we in Figs. 29 show some experimental results (open circles) due to K. A. O'Donnell and R. Torre [95] for the so-called normalized<sup>27</sup> intensity of the second harmonic light scattered incoherently from a strongly rough silver surface. The surface was characterized by Gaussian height statistics of RMS-height  $\delta = 1.81\mu\text{m}$  and a Gaussian correlation function. The transverse correlation length was  $a = 3.4\mu\text{m}$ . The wavelength of the incident light was  $\lambda = 2\pi c/\omega = 1.064\mu\text{m}$ , while the angles of incidence considered were  $\theta_0 = 0^\circ$ ,  $\theta_0 = 6^\circ$ , and  $\theta_0 = 15^\circ$  as indicated in Fig. 29.

The most noticeable feature of the experimental results (open circles) shown in Figs. 29 are, without question, the dips seen in the backscattering direction. It should be recalled that for the linear problem one gets at this scattering angle an enhanced backscattering *peak* (result not shown) similar to the one shown *e.g* in Fig. 13. So why do we have a dip for the second harmonic light at the backscattering direction, and not a peak?

##### 1. Strongly Rough Surfaces: A Numerical Simulation Approach to the Second Harmonic Generated Light

Below we will with the help of numerical simulations try to get a deeper understanding of what causes these dips. The nonlinear layer existing along the surface is of microscopic dimensions. Since we are working with the macroscopic Maxwell's equations it is natural to assume that this layer is infinitely thin. Under this assumption, the effect of the nonlinear boundary layer is accounted for in the boundary conditions to be satisfied by the field, and its normal

<sup>26</sup> Two complex random variables  $A = A_1 + iA_2$  and  $B = B_1 + iB_2$  are said to be *circular complex Gaussian* if [93, 94]  $\langle A_1 B_1 \rangle = \langle A_2 B_2 \rangle$  and  $\langle A_1 B_2 \rangle = -\langle A_2 B_1 \rangle$ .

<sup>27</sup> It can be shown that the total power scattered from a randomly rough surface at the second harmonic frequency is proportional to the square of the irradiance, the incident power per unit area, on the surface. One therefore defines the normalized intensity of the scattered second harmonic light so that it is independent of the incident power. The analytic expressions for this quantity can be found in Eq. (34) of Ref. [96].

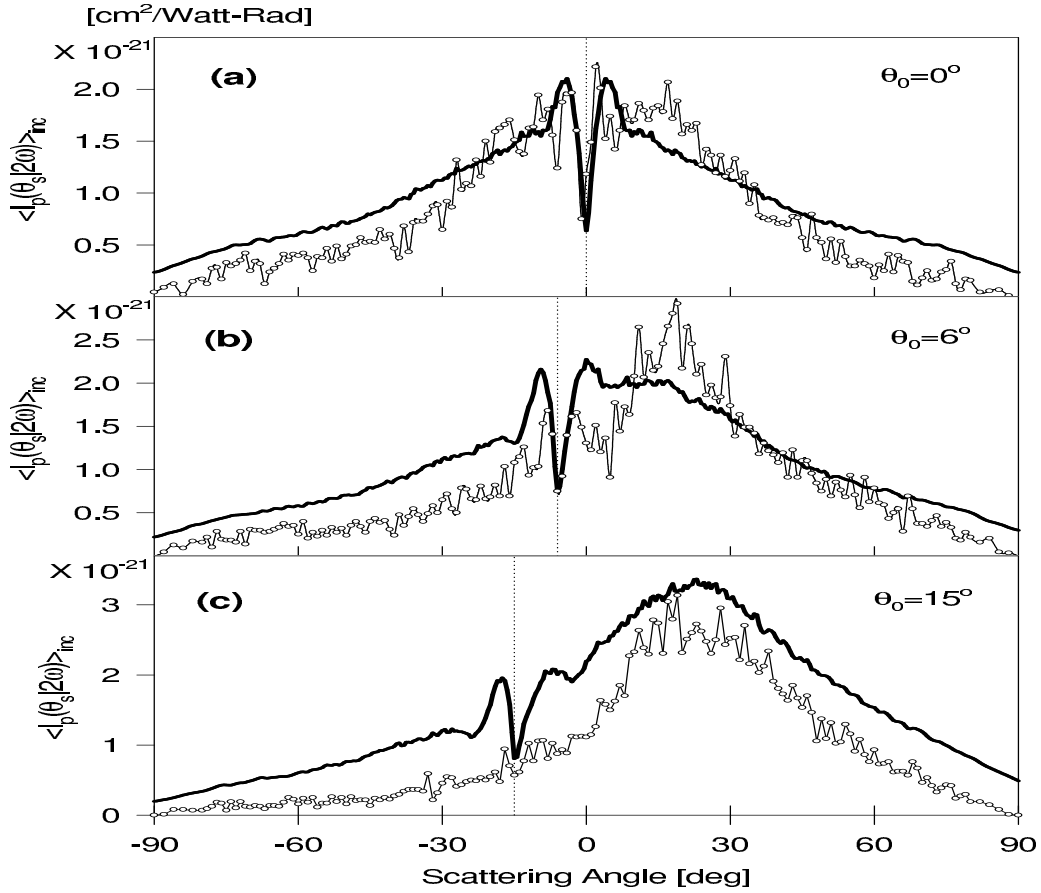


FIG. 29: The mean normalized second harmonic intensity as a function of the scattering angle  $\theta_s$  for the scattering of  $p$ -polarized light from a randomly rough silver surface. The surface was characterized by a Gaussian height distribution of RMS-height  $\delta = 1.81\mu\text{m}$ , as well as a Gaussian correlation function of correlation length  $a = 3.4\mu\text{m}$ . The dielectric constants were at the fundamental and second harmonic frequency  $\varepsilon(\omega) = -56.25 + i0.60$  and  $\varepsilon(2\omega) = -11.56 + 0.37$  respectively. The thick lines represent the results of numerical simulations and the open circles represent the experimental results of O'Donnell and Torre [95]. The incident plane wave had a wavelength  $\lambda = 1.064\mu\text{m}$ . In the numerical simulations the surface had length  $L = 40\lambda$  and it was sampled with an interval  $\Delta x_1 = \lambda/20$ . The numerical results were averaging over  $N_\zeta = 2000$  realizations of the surface, and the angles of incidence were (a)  $\theta_0 = 0^\circ$ , (b)  $\theta_0 = 6^\circ$ , and (c)  $\theta_0 = 15^\circ$ . (After Ref. [96].)

derivative, at the second harmonic frequency. These boundary conditions have jumps at the nonlinear interface, and their degree of discontinuity depends on the nonlinear polarization, or equivalently, on the parameters that describes this polarization. The form of the (nonlinear) boundary conditions at the second harmonic frequency  $2\omega$  can be shown to be [96]

$$\mathcal{F}_\nu^+(x_1|2\omega) - \mathcal{F}_\nu^-(x_1|2\omega) = \mathcal{A}(x_1), \quad (165a)$$

$$\mathcal{N}_\nu^+(x_1|2\omega) - \mathcal{N}_\nu^-(x_1|2\omega) = \mathcal{B}(x_1), \quad (165b)$$

where the sources  $\mathcal{F}_\nu$  and  $\mathcal{N}_\nu$  have been defined in Eqs. (124). As before, the superscripts  $\pm$  denote the sources evaluated just above (+) and below (-) the rough surface defined by  $x_3 = \zeta(x_1)$ . The functions  $\mathcal{A}(x_1)$  and  $\mathcal{B}(x_1)$  are related to the nonlinear polarization  $\mathbf{P}(x_1, x_3)$  through the integral of this quantity over the nonlinear boundary layer [96]. To fully specify the nonlinearity of the problem, the polarization  $\mathbf{P}(x_1, x_3)$  has to be specified. For instance for a free electron model, that we will consider here for simplicity, it takes on the form [97–99]

$$\mathbf{P}(x_1, x_3) = \gamma \nabla (\mathbf{E} \cdot \mathbf{E}) + \beta \mathbf{E} (\nabla \cdot \mathbf{E}). \quad (166a)$$

Here the constants  $\gamma$  and  $\beta$  are defined as

$$\gamma = \frac{e^3 n_0 (\mathbf{r}_\perp(x_1, x_3))}{8m^2 \omega^4}, \quad (166b)$$

$$\beta = \frac{e}{8\pi m \omega^2}, \quad (166c)$$

where  $n_0$  is the electron number density,  $\mathbf{r}_\perp(x_1, x_3)$  is a vector normal to the local surface at point  $(x_1, x_3)$ , and  $e$  and  $m$  are the charge and mass of the electron respectively. The explicit expressions, in this model, for  $\mathcal{A}(x_1)$  and  $\mathcal{B}(x_1)$  can be found in Ref. [96].

Since the surfaces used in the experiments leading to the results shown in Figs. 29 are strongly rough, perturbation theory does not apply, and one has in theoretical studies to resort to rigorous numerical calculations of the second harmonic scattered light. Such kind of simulations are conducted on the basis of the rigorous simulation approach presented in Sect. IIII. The calculations are now, however, made out of two main steps: First, one calculates the (linear) source functions  $\mathcal{F}_\nu(x_1|\omega)$  and  $\mathcal{N}_\nu(x_1|\omega)$ ; the field and its normal derivative evaluated on the surface at the fundamental frequency  $\omega$ . This is done exactly as described in Sect. IIII. From the knowledge of the linear sources functions at the fundamental frequency, the right-hand-side of the boundary conditions (165) can be calculated since they depend directly on these source functions as well as on the form of the nonlinear polarization  $\mathbf{P}(x_1, x_3)$  [96]. In all numerical results to be presented later in this section the form for the nonlinear polarization given by Eq. (166) will be used. With the functions  $\mathcal{A}(x_1)$  and  $\mathcal{B}(x_1)$  available, the nonlinear sources,  $\mathcal{F}_\nu^\pm(x_1|2\omega)$  and  $\mathcal{N}_\nu^\pm(x_1|2\omega)$ , are readily calculated from an approach similar to the one described in detail in Sect. IIII. The only main difference is that now the boundary conditions to be used when coupling the two integral equations are the nonlinear boundary conditions given in Eqs. (165). With the source functions both for the fundamental and second harmonic frequency available, all interesting quantities about the scattering process, both linear and nonlinear, are easily obtained. The full details of this approach can be found in Ref. [96].

Based on this numerical approach, we compare in Figs. 29 the numerical simulation results (solid lines) obtained by Leyva-Lucero *et al.* [96] to the experimental results obtained by O'Donnell and Torre (open circles) [95]. The dielectric constants used in the simulations were at the fundamental frequency  $\varepsilon(\omega) = -56.25 + i0.60$  and  $\varepsilon(2\omega) = -11.56 + i0.37$  at the second harmonic frequency. Indeed by comparing the experimental and theoretical results shown in Figs. 29, a nice correspondence is observed both qualitatively and quantitatively. Particular in light of the oversimplified model used in the simulations for the nonlinear interaction, the agreement is no less than remarkable.

From the experimental and theoretical results shown in Figs. 29a, a clear dip is seen in the incoherent component of the mean normalized second harmonic intensity for the backscattering direction  $\theta_s = 0^\circ$ . For the linear scattering problem, however, there is an enhancement at the same scattering angle. So what is the reason for the dip in the second harmonic light? O'Donnell and Torre [95], who conducted the experiments leading to the experimental results shown in Figs. 29, suggested that these dips were due to coherent effects. In particular they suggested that the dips originated from destructive interference between waves scattered multiple times in the valleys of the strongly rough surface. Since the numerical simulation approach seems to catch the main physics of the second harmonic generated light, it might therefore serve as a useful tool for testing the correctness of the suggestion made by O'Donnell and Torre [95].

This can be done by applying a single scattering approximation to the generation of the second harmonic light. As described above, the numerical approach leading to the theoretical results shown as solid lines in Figs. 29, consists mainly of a linear and nonlinear stage where each stage is basically solved by some variant of the approach given in Sect. IIII. By using a single scattering approach, like the Kirchhoff approximation [8, 106], to both stages of the calculation, a single scattering approximation for the full problem is obtained. The single scattering processes included in such a calculation is illustrated in Figs. 30. Notice that also unphysical scattering processes like the one shown in Fig. 30b, are included in this approximation.

In Fig. 31 we present the consequence for the angular dependence of the normalized intensity  $\langle I_p(\theta_s|2\omega) \rangle$  of only including single scattering processes in the second harmonic generation. From this figure it is easily seen that the intensity of the second harmonic generated light calculated in a single scattering approximation does *not* give rise to a dip (or peak) for the backscattering direction. In fact the overall angular dependence of  $\langle I_p(\theta_s|2\omega) \rangle$  in the single scattering approximation is quite different from the one obtained by the rigorous approach described above. Similar result holds for the other two angles incidence considered in Figs. 29. Hence, one may conclude that the dips present in the backscattering direction of the incoherent component for the mean second harmonic generated light is not due to single scattering. It therefore has to be a multiple scattering phenomenon.

To look more closely into this, the authors of Ref. [96] used an iterative approach for the linear part of the scattering problem which enabled them to calculate the scattered fields according to the order of the scattering process. Such a (Neumann-Liouville) iterative approach has been developed and used earlier in the literature [21, 100, 101]. For the nonlinear part of the calculation the rigorous simulation approach was used and thus all higher order scattering

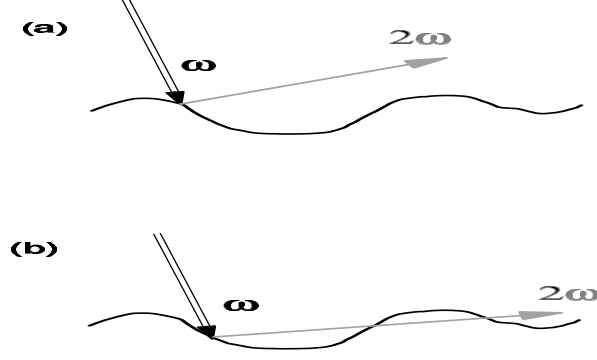


FIG. 30: Diagrams illustrating two of the single scattering processes that produce the second harmonic scattered light in a single scattering approach. The double line black arrows represent light of frequency  $\omega$ , while the thick gray arrows represent light of frequency  $2\omega$ . Notice that the process in Fig. 30b is unphysical.

processes were here taken into account. Some of the processes accounted for by this procedure and which give rise to the second harmonic light is depicted in Figs. 32.

We notice that the processes depicted in Figs. 32a and b represent single scattering in the linear part and are thus taken properly into account by using the standard Kirchhoff approximation [106] (for the linear part). However, for the paths shown in Figs. 32c and d, one needs to consider a pure double scattering approximation in order to include these processes properly. In Figs. 33 the simulation results for the second harmonic light  $\langle I_p(\theta_s|2\omega) \rangle$  are shown for the case where a single scattering (Fig. 33a) and a pure double scattering (Fig. 33b) approximation is used for the linear part of the scattering process. In both cases dips in the backscattering direction are observed. In order to obtain the solid curve of Fig. 33c *both* single and double scattering processes were taken into account for the linear part of the calculation. This result would therefore include any interference effect between paths like those show in Figs. 32a–e. The dashed line in Fig. 33c is just the sum of the curves shown in Figs. 33a and b. It does therefore not contain any interference effects between type I paths (Figs. 32a–b) and type II paths (Figs. 32c–d). That the two curves shown in Fig. 33c are so close to each other tells us that the interference between type I and type II paths are rather small (if any). Furthermore, paths of the type illustrated in Fig. 32e do not seem to be important, and they do not have coherent partners.

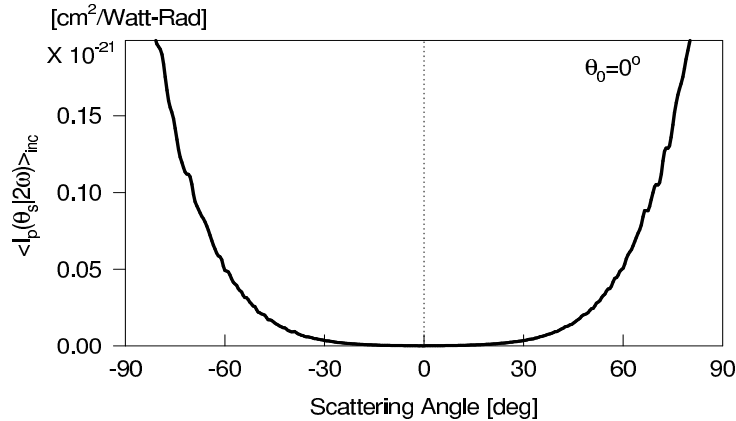


FIG. 31: The mean normalized second harmonic intensity  $\langle I_p(\theta_s|2\omega) \rangle_{inc}$  as a function of the scattering angle  $\theta_s$  calculated in a single scattering approximation. The remaining parameters of the simulation were the same as those used in obtaining the results shown in Figs. 29. The angle of incidence was  $\theta_0 = 0^\circ$ . (After Ref. [96].)



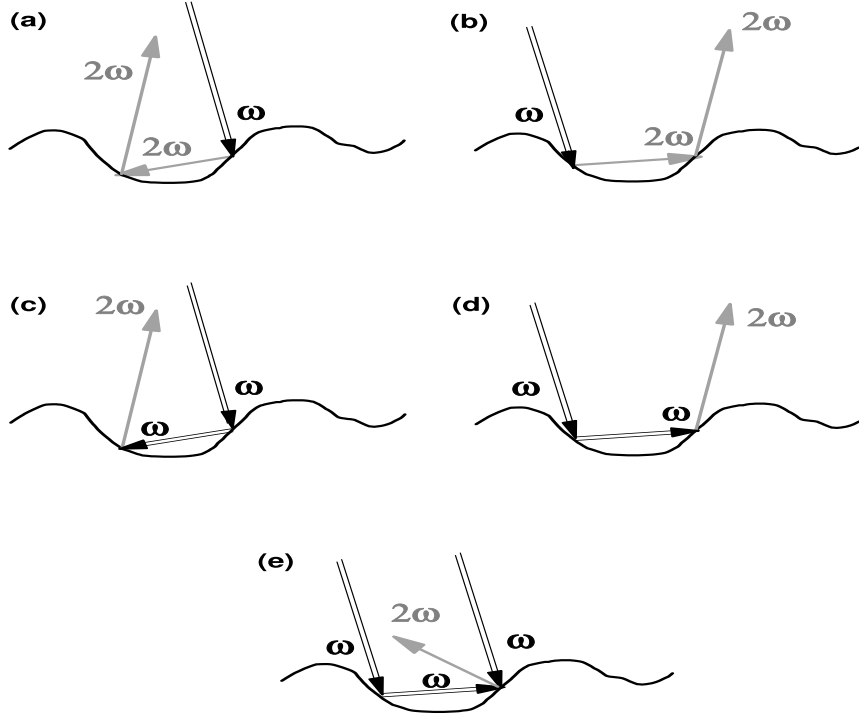


FIG. 32: Diagrams illustrating some of the multiple scattering processes that produce the second harmonic scattered light. The double line black arrows represent light of frequency  $\omega$ , while the thick gray arrows represent light of frequency  $2\omega$ . (After Ref. [96].).

The numerical results presented so far seem to indicate that the behavior in the backscattering direction is affected by interference between the paths of either type I or type II. In the backscattering direction, there is no phase difference due to optical path difference between the two type I paths say. Similar argument hold for the type II paths. Hence any phase difference between the two paths has to come from phase shifts during the reflection. In the linear multiple-scattering processes giving rise to enhanced backscattering the phase shifts due to reflection will be the same for the two processes because the local Fresnel coefficients are *even* functions of the angle of incidence. Hence, the two paths in the backscattering direction will for the full linear problem both have the same phase and hence interfere constructively giving rise to the celebrated enhanced backscattering peak. However, for multiple scattering processes involving second harmonic generated light the situation is quite different. The reason for this is that the local nonlinear Fresnel coefficient is not an even, but an *odd* function of the angle of incidence [96]. Hence, the phase difference between the two type I paths, say, will not be zero any more in general since the phases for these two paths will add instead of subtract. If this phase shift is positive in Fig. 32a, say, then it will be negative for the path shown in Fig. 32b since the local incident angles in the two cases have different signs and the local nonlinear Fresnel reflection coefficient is an odd function of the incident angle. Hence in the nonlinear case the phase difference in the backscattering direction is different from zero for the paths that seem to interfere. From the numerical results shown in this section they in fact seem to be close to  $\pi$  out of phase resulting in destructive interference, or a dip as compared to its background at the backscattering direction.

## 2. Weakly Rough Surfaces

So far in this section we have presented both experimental and numerical results for the second harmonic generated light scattered from strongly rough surfaces. There has also been conducted experiments for weakly rough surfaces [102]. The results are quite similar to the experimental results presented in Fig. 29. In particular, also for

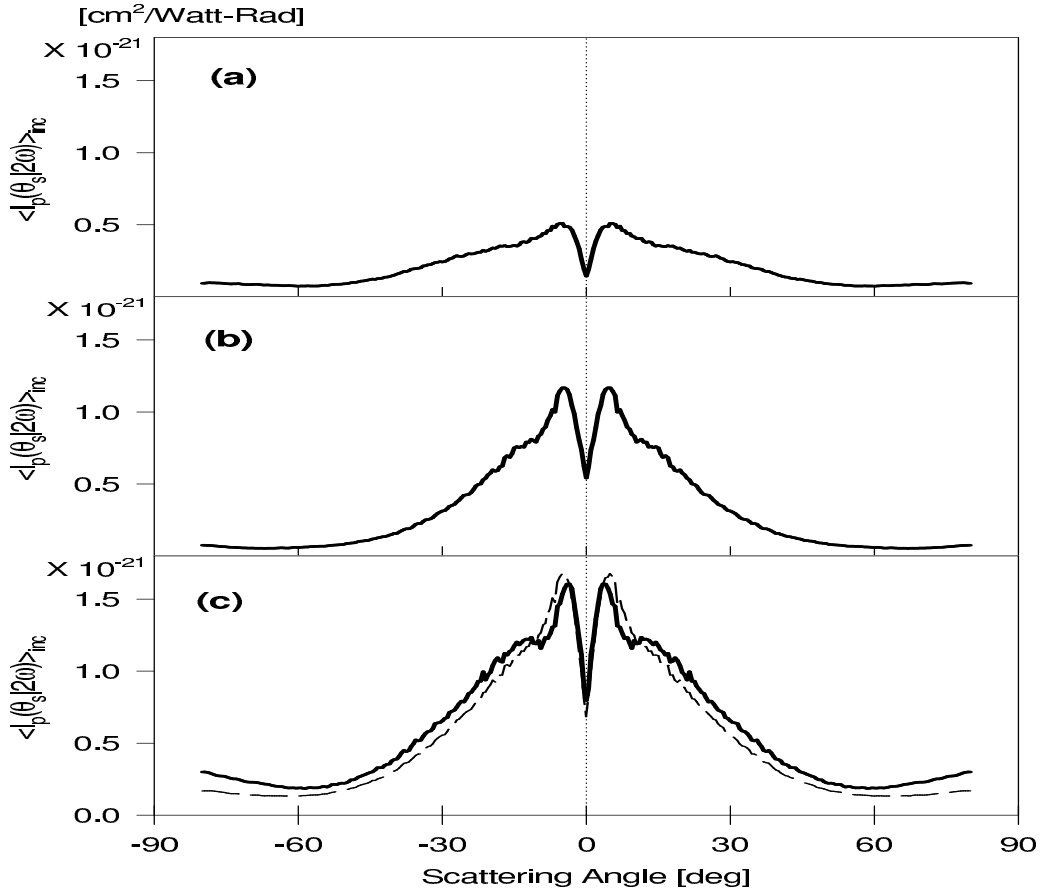


FIG. 33: Calculations of the mean normalized second harmonic intensity as a function of the scattering angle  $\theta_s$  for the scattering of  $p$ -polarized light from a random silver surface where the linear part of the problem was solved by iteration. The incident angle of the light was  $\theta_0 = 0^\circ$  and the other parameters of the simulation were as in Fig. 29. The curves have, (a) the single scattering contributions in the linear scattering and all contributions at the harmonic frequency, (b) pure double scattering contributions in the linear scattering and all contributions at the harmonic frequency, and (c) the single and double scattering contributions in the linear scattering and all contributions at the harmonic frequency. In (c), the curve shown with the dashed line represents the sum of the curves shown in (a) and (b). (After Ref. [96].)

these weakly rough surfaces the second harmonic generated light scattered diffusely showed a dip in the backscattering direction. However, in theoretical studies [103–105] both dips as well as peaks in the backscattering direction have been predicted. If it is a peak or dip depends on the values used for the nonlinear phenomenological constants. Even though predicted theoretically, only dips have so far been seen in experiments.

For weakly rough surface the scattering processes giving rise to these dips (or peaks) are believed to be different for weakly and strongly rough surfaces. This situation resembles quite a bit the origin of the enhanced backscattering peak for weakly and strongly rough surfaces. Indeed, for weakly rough surfaces the origin of the dip in the intensity of the diffusely scattered light at frequency  $2\omega$  is intimately related to the excitation of surface plasmon polaritons at this frequency [104, 105]. Thus such dips are not to be expected for the second harmonic light generated in  $s$ -polarization from weakly rough surfaces.

## V. DIRECTIONS FOR FUTURE RESEARCH

We have in the introduction to this review tried to give some glimpses of the many multiple scattering phenomena that may take place when electromagnetic waves are scattered by a randomly rough surface separating two media of different dielectric properties. Even though much is understood today when it comes to the rough surface scattering

problem, there are still, after a century of research efforts, many questions that have not been addressed and answered properly. Below we will therefore try to sketch out some directions for further research.

We have exclusively considered one-dimensional surfaces. Naturally occurring surfaces are mostly two-dimensional. Thus, the advance most needed in the field are techniques, either numerical or analytical, that accurately and fast can handle electromagnetic wave scattering from two-dimensional surfaces of varying RMS-height. Two-dimensional weakly rough surfaces can be treated by perturbation theory [108, 109], but if the surface is not weakly rough this approach is not adequate any more. In principle a general solution of the scattering problem can be formulated on the basis of a vector version of the extinction theorem [8, 11]. However, the resulting system of linear equations that needs to be solved in order to calculate the source functions is so big, and therefore require so much computer memory, that it for the moment is not practical in general [110]. Thus, one has to come up with new and more efficient methods for solving this kind of problems, or, the less appealing approach, to wait for advances in computer technology to make the extinction theorem approach tractable from a computational point of view.

The scientific community dealing with wave scattering from disordered systems, seems to be divided into two separate groups: (i) those that deal with surface disordered systems and (ii) those that concentrate on systems with volume disorder. In the future these two “groups” have to be unified to a much higher degree than what is the case today in order to deal with scattering systems consisting of bulk disorder materials bounded by a random surface. Strictly speaking there has already been published some works for such “dual” disordered systems [111–114], but still more work, and in a more general framework, need to be done for such problems.

An area that needs to be addressed further in the future is the *inverse scattering problem* [115] in contrast to the forward scattering problem that is the one that has received the most attention in theoretical studies of wave scattering from randomly rough surfaces. In the inverse scattering problem one has information, *e.g.* from experiments, about the angular dependence of the scattered light and one is interested in trying to reconstruct the surface profile function or its statistical properties. This problem is quite difficult and huge research efforts have been spent on it in related fields like remote sensing and seismic in order to try to find its solution. So far a general solution to the problem has not been found.

### Acknowledgement

It is a pleasure to acknowledge numerous fruitful discussion with Alex Hansen, Ola Hunderi, Jacques Jupille, Rémi Lazzari, Tamara A. Leskova, Alexei A. Maradudin, Eugenio R. Méndez, Stéphane Roux, and Damien Vandembroucq. This research was supported in part by The Research Council of Norway (Contract No. 32690/213), Norsk Hydro ASA, NTNU, Total Norge ASA, Centre National de la Recherche Scientifique (CNRS), and the Army Research Office (DAAD19-99-1-0321).

### APPENDIX A: MATRIX ELEMENTS

In this Appendix, some calculational details are presented for the matrix elements appearing in the matrix equations (132) used to determine the source functions needed in the rigorous numerical simulation approach given in Sect. III.

From this section, Eqs. (133), we recall that these matrix elements are defined as

$$\begin{aligned} \mathcal{A}_{mn}^{\pm} &= \int_{\xi_n - \Delta\xi/2}^{\xi_n + \Delta\xi/2} dx'_1 A_{\pm}(\xi_m | x'_1), \\ &= \int_{-\Delta\xi/2}^{\Delta\xi/2} du A_{\pm}(\xi_m | \xi_n + u), \end{aligned} \tag{A1a}$$

$$\begin{aligned} \mathcal{B}_{mn}^{\pm} &= \int_{\xi_n - \Delta\xi/2}^{\xi_n + \Delta\xi/2} dx'_1 B_{\pm}(\xi_m | x'_1), \\ &= \int_{-\Delta\xi/2}^{\Delta\xi/2} du B_{\pm}(\xi_m | \xi_n + u) \end{aligned} \tag{A1b}$$

where we in the last transition have made a change of variable  $u = x_1 - \xi_n$  and where the kernels, according to

Eqs. (125) and (130), are given by

$$A_{\pm}(x_1|x'_1; \omega) = \lim_{\eta \rightarrow 0^+} \frac{1}{4\pi} \gamma(x'_1) \partial_{n'} G_{\pm}(\mathbf{r}|\mathbf{r}'; \omega) \Big|_{\substack{x_3 = \zeta(x_1) + \eta \\ x'_3 = \zeta(x'_1)}}, \quad (\text{A2a})$$

$$B_{\pm}(x_1|x'_1; \omega) = \lim_{\eta \rightarrow 0^+} \frac{1}{4\pi} G_{\pm}(\mathbf{r}|\mathbf{r}'; \omega) \Big|_{\substack{x_3 = \zeta(x_1) + \eta \\ x'_3 = \zeta(x'_1)}}, \quad (\text{A2b})$$

with  $\mathbf{r} = (x_1, x_3)$  and a similar expression holds for  $\mathbf{r}'$ , and

$$\xi_n = -\frac{L}{2} + \left(n - \frac{1}{2}\right) \Delta\xi, \quad n = 1, 2, 3, \dots, N, \quad (\text{A3})$$

with  $\Delta\xi = L/N$ . In the above expressions  $G_{\pm}(\mathbf{r}|\mathbf{r}'; \omega)$  denote the free-space Green's functions for the Helmholtz equation. In 2-dimensions, as we will be considering here, it can be written as [56]

$$G_{\pm}(\mathbf{r}|\mathbf{r}'; \omega) = i\pi H_0^{(1)}\left(\varepsilon_{\pm} \frac{\omega}{c} |\mathbf{r} - \mathbf{r}'|\right), \quad (\text{A4})$$

where  $H_0^{(1)}(z)$  is the Hankel function of the first kind and zeroth-order [39, 56]. By substituting this expression for the Green's function into Eqs. (A2) for the kernels, one gets

$$A_{\pm}(x_1|x'_1; \omega) = \lim_{\eta \rightarrow 0^+} \left(-\frac{i}{4}\right) \varepsilon_{\pm} \frac{\omega^2}{c^2} \frac{H_1^{(1)}(\chi_{\pm}(x_1|x'_1))}{\chi_{\pm}(x_1|x'_1)} \times [(x_1 - x'_1)\zeta'(x'_1) - (\zeta(x_1) - \zeta(x'_1) + \eta)], \quad (\text{A5a})$$

$$B_{\pm}(x_1|x'_1; \omega) = \lim_{\eta \rightarrow 0^+} \left(-\frac{i}{4}\right) H_0^{(1)}(\chi_{\pm}(x_1|x'_1)), \quad (\text{A5b})$$

where we have defined

$$\chi_{\pm}(x_1|x'_1) = \sqrt{\varepsilon_{\pm}(\omega)} \frac{\omega}{c} \sqrt{(x_1 - x'_1)^2 + (\zeta(x_1) - \zeta(x'_1) + \eta)^2}. \quad (\text{A5c})$$

Notice that since the Hankel functions are divergent for vanishing argument [39, 56], so are the kernels  $A_{\pm}(x_1|x'_1; \omega)$  and  $B_{\pm}(x_1|x'_1; \omega)$ . However, fortunately these singularities are integrable, so the matrix elements  $\mathcal{A}_{mn}^{\pm}$  and  $\mathcal{B}_{mn}^{\pm}$  are in fact non-singular everywhere and in particular when  $\xi_m = \xi_n$ . We will now show this and obtain explicit expressions for these matrix elements.

We start by considering the off-diagonal elements where the kernels are non-singular. In this case, one may approximate the integrals in Eqs. (A1) by for example the midpoint method [40] with the result that ( $m \neq n$ )

$$\mathcal{A}_{mn}^{\pm} = \Delta\xi A_{\pm}(\xi_m|\xi_n; \omega), \quad (\text{A6a})$$

$$\mathcal{B}_{mn}^{\pm} = \Delta\xi B_{\pm}(\xi_m|\xi_n; \omega), \quad (\text{A6b})$$

where the expressions for the kernels are understood to be taken in the form Eqs. (A5).

So now what about the diagonal elements where the kernels are singular? In order to calculate these elements, we start by noting that  $\chi_{\pm}(\xi_m|\xi_m + u)$ , needed in order to evaluate the matrix element, can be written as

$$\begin{aligned} \chi_{\pm}(\xi_m|\xi_m + u) &= \sqrt{\varepsilon_{\pm}} \frac{\omega}{c} \sqrt{u^2 + \left(\zeta'(\xi_m)u + \frac{1}{2}\zeta''(\xi_m)u^2 + \dots + \eta\right)^2}, \\ &= \sqrt{\gamma(\xi_m)u^2 - 2\eta\zeta'(\xi_m)u + \eta^2 + \dots} \\ &= \sqrt{\varepsilon_{\pm}} \frac{\omega}{c} \gamma(\xi_m)|u| + \dots \end{aligned} \quad (\text{A7})$$

where we have Taylor expanded  $\zeta(\xi_m + u)$  and where we recall from Eq. (120b) that  $\gamma(x_1) = \sqrt{1 + \zeta'^2(x_1)}$ . Furthermore, by advantage of the following (small argument) asymptotic expansions for the Hankel functions [39]

$$H_0^{(1)}(z) = \frac{2i}{\pi} \left(\ln \frac{z}{2} + \gamma\right) + 1 + \mathcal{O}(z^2 \ln z), \quad (\text{A8a})$$

$$\frac{H_1^{(1)}(z)}{z} = -\frac{2i}{\pi} \frac{1}{z^2} + \frac{i}{\pi} \left(\ln \frac{z}{2} + \gamma + \frac{1}{2}\right) - \frac{1}{2} + \mathcal{O}(z^2 \ln z), \quad (\text{A8b})$$

where  $\gamma = 0.5772157\dots$  is the Euler constant.

With these expressions, it is now rather straight forward to derive, to obtain the matrix elements by integrating the resulting expressions term-by-term. To demonstrate this we start with the  $\mathcal{B}_{mm}^\pm$  matrix element. With Eqs. (A7) and (A8a) and passing to limit  $\eta \rightarrow 0^+$  whenever no singularities results and one gets

$$\begin{aligned}
\mathcal{B}_{mm}^\pm &= 2 \int_0^{\Delta\xi/2} du B_\pm(\xi_m|\xi_m + u) \\
&\simeq -\frac{i}{2} \int_0^{\Delta\xi/2} du H_0^{(1)} \left( \sqrt{\varepsilon_\pm} \frac{\omega}{c} \gamma(\xi_m) u \right) \\
&= -\frac{i}{2} \int_0^{\Delta\xi/2} du \left[ \frac{2i}{\pi} \left\{ \ln \left( \sqrt{\varepsilon_\pm} \frac{\omega}{c} \gamma(\xi_m) u \right) + \gamma \right\} + 1 + \dots \right] \\
&= -\frac{i}{2} \frac{\Delta\xi}{2} \left[ \frac{2i}{\pi} \left\{ \ln \left( \sqrt{\varepsilon_\pm} \frac{\omega}{c} \frac{\gamma(\xi_m) \Delta\xi}{2e} \right) + \gamma \right\} + 1 + \dots \right] \\
&\simeq -\frac{i}{4} \Delta\xi H_0^{(1)} \left( \sqrt{\varepsilon_\pm} \frac{\omega}{c} \frac{\gamma(\xi_m) \Delta\xi}{2e} \right). \tag{A9}
\end{aligned}$$

Here in the last transition we have Eq. (A8a) one more.

Furthermore, for the leading term of the diagonal elements of  $\mathcal{A}$  one gets in a similar way from Eqs. (A8b) and (A7)

$$\begin{aligned}
\mathcal{A}_{mm}^\pm &= \int_{-\Delta\xi/2}^{\Delta\xi/2} du A_\pm(\xi_m|\xi_m + u) \\
&= \frac{i}{4} \varepsilon_\pm \frac{\omega^2}{c^2} \lim_{\eta \rightarrow 0^+} \int_{-\frac{\Delta\xi}{2}}^{\frac{\Delta\xi}{2}} du \left[ -\frac{2i}{\pi} \frac{1}{\chi_\pm^2(\xi_m|\xi_m + u)} + \dots \right] \\
&\quad \times \left[ \eta + \frac{1}{2} \zeta''(\xi_m) u^2 + \dots \right] \\
&= \lim_{\eta \rightarrow 0^+} \frac{1}{2\pi} \int_{-\frac{\Delta\xi}{2\eta}}^{\frac{\Delta\xi}{2\eta}} du \frac{1}{\gamma^2(\xi_m) u^2 - 2\zeta'(\xi_m) u + 1} \\
&\quad + \frac{1}{4\pi} \frac{\zeta''(\xi_m)}{\gamma^2(\xi_m)} \int_{-\frac{\Delta\xi}{2}}^{\frac{\Delta\xi}{2}} du \\
&= \frac{1}{2\pi} \lim_{\eta \rightarrow 0^+} \left[ \tan^{-1} (-\zeta'(\xi_m) + \gamma(\xi_m) u) \right]_{u=-\frac{\Delta\xi}{2\eta}}^{\frac{\Delta\xi}{2\eta}} + \Delta\xi \frac{\zeta''(\xi_m)}{4\pi\gamma^2(\xi_m)} \\
&= \frac{1}{2} + \Delta\xi \frac{\zeta''(\xi_m)}{4\pi\gamma^2(\xi_m)} \tag{A10}
\end{aligned}$$

To sum up we have for the matrix elements

$$\mathcal{A}_{mn}^\pm = \begin{cases} \Delta\xi A_\pm(\xi_m|\xi_n), & m \neq n, \\ \frac{1}{2} + \Delta\xi \frac{\zeta''(\xi_m)}{4\pi\gamma^2(\xi_m)}, & m = n, \end{cases} \tag{A11}$$

and

$$\mathcal{B}_{mn}^\pm = \begin{cases} \Delta\xi B_\pm(\xi_m|\xi_n), & m \neq n \\ -\frac{i}{4} \Delta\xi H_0^{(1)} \left( \sqrt{\varepsilon_\pm} \frac{\omega}{c} \frac{\gamma(\xi_m) \Delta\xi}{2e} \right), & m = n. \end{cases} \tag{A12}$$

In these equations  $A_\pm(\xi_m|\xi_n)$  and  $B_\pm(\xi_m|\xi_n)$  are given by Eqs. (A2)

## APPENDIX B: THE $\chi$ -FUNCTIONS USED IN SMALL AMPLITUDE PERTURBATION THEORY

In this appendix some of the lengthy formulae found in small amplitude perturbation theory, Sect. III F, are given. In particular we here give the first few  $\chi$ -functions found in Eqs. (88). We will now in the next two subsection explicitly give these functions for  $p$  and  $s$ -polarization. All explicit reference to the frequency  $\omega$  has been suppressed. We have also for completeness used  $\varepsilon_0$  for the dielectric constant of the upper medium. In the case of vacuum this constant is  $\varepsilon_0 = 1$ .

### 1. P-polarization

The three first functions in the set  $\{\chi_p^{(n)}\}$  are [46]:

$$\chi_p^{(1)}(q|k) = i \frac{\varepsilon_0 - \varepsilon}{\varepsilon\alpha_0(q) + \varepsilon_0\alpha(q)} [\varepsilon_0\alpha(q)\alpha(k) - \varepsilon qk] \times \frac{2\alpha_0(k)}{\varepsilon\alpha_0(k) + \varepsilon_0\alpha(k)}, \quad (\text{B1a})$$

$$\begin{aligned} \chi_p^{(2)}(q|p_1|k) &= \frac{\varepsilon_0 - \varepsilon}{\varepsilon\alpha_0(q) + \varepsilon_0\alpha(q)} \left\{ \varepsilon\alpha(q) [\alpha_0^2(k) - qk] + \varepsilon_0\alpha(k) [\alpha^2(q) - qk] \right\} \frac{2\alpha_0(k)}{\varepsilon\alpha_0(k) + \varepsilon_0\alpha(q)} \\ &+ 2 \frac{(\varepsilon_0 - \varepsilon)^2}{\varepsilon\alpha_0(q) + \varepsilon_0\alpha(q)} \frac{\alpha(q)\alpha_0(p_1) + qp_1}{\varepsilon\alpha_0(p_1) + \varepsilon_0\alpha(p_1)} \frac{2\alpha_0(k) [\varepsilon_0\alpha(p_1)\alpha(k) - \varepsilon p_1k]}{\varepsilon\alpha_0(k) + \varepsilon_0\alpha(k)} \end{aligned} \quad (\text{B1b})$$

$$\begin{aligned} \chi_p^{(3)}(q|p_1|p_2|k) &= -i \frac{\varepsilon_0 - \varepsilon}{\varepsilon\alpha_0(q) + \varepsilon_0\alpha(q)} \left\{ 2\varepsilon\alpha^2(q)\alpha_0^2(k) + [\alpha^2(q) + \alpha_0^2(k)] [\varepsilon_0\alpha(q)\alpha(k) - \varepsilon qk] \right. \\ &\quad \left. - 2\varepsilon_0qk\alpha(q)\alpha(k) \right\} \frac{2\alpha_0(k)}{\varepsilon\alpha_0(k) + \varepsilon_0\alpha(k)} \\ &- 3i \frac{\varepsilon_0 - \varepsilon}{\varepsilon\alpha_0(q) + \varepsilon_0\alpha(q)} [\alpha(q)\alpha_0(p_1) + qp_1] \frac{\varepsilon_0 - \varepsilon}{\varepsilon\alpha_0(p_1) + \varepsilon_0\alpha(p_1)} \\ &\quad \times \left\{ \varepsilon\alpha(p_1) [\alpha_0^2(k) - p_1k] + \varepsilon_0\alpha(k) [\alpha^2(p_1) - p_1k] \right\} \frac{2\alpha_0(k)}{\varepsilon\alpha_0(k) + \varepsilon_0\alpha(k)} \\ &- i \left\{ 3 \frac{\varepsilon_0 - \varepsilon}{\varepsilon\alpha_0(q) + \varepsilon_0\alpha(q)} [\alpha(q)\alpha_0(p_2) + qp_2] [\alpha(q) - \alpha_0(p_2)] \right. \\ &\quad \left. + 6 \frac{\varepsilon_0 - \varepsilon}{\varepsilon\alpha_0(q) + \varepsilon_0\alpha(q)} [\alpha(q)\alpha_0(p_1) + qp_1] \right. \\ &\quad \left. \times \frac{\varepsilon_0 - \varepsilon}{\varepsilon\alpha_0(p_1) + \varepsilon_0\alpha(p_1)} [\alpha(p_1)\alpha_0(p_2) + p_1p_2] \right\} \\ &\times \frac{\varepsilon_0 - \varepsilon}{\varepsilon\alpha_0(p_2) + \varepsilon_0\alpha(p_2)} [\varepsilon_0\alpha(p_2)\alpha(k) - \varepsilon p_2k] \frac{2\alpha_0(k)}{\varepsilon\alpha_0(k) + \varepsilon_0\alpha(k)}, \end{aligned} \quad (\text{B1c})$$

### 2. S-polarization

Here follows the corresponding expressions for  $s$ -polarization [46]:

$$\chi_s^{(1)}(q|k) = -i \frac{\omega^2}{c^2} \frac{\varepsilon_0 - \varepsilon}{\alpha_0(q) + \alpha(q)} \frac{2\alpha_0(k)}{\alpha_0(k) + \alpha(k)}, \quad (\text{B2a})$$

$$\chi_s^{(2)}(q|p_1|k) = -\frac{\omega^2}{c^2} \frac{\varepsilon_0 - \varepsilon}{\alpha_0(q) + \alpha(q)} \left( \alpha(q) + \alpha(k) + 2 \frac{\omega^2}{c^2} \frac{\varepsilon_0 - \varepsilon}{\alpha_0(p_1) + \alpha(p_1)} \right) \frac{2\alpha_0(k)}{\alpha_0(k) + \alpha(k)} \quad (\text{B2b})$$

$$\begin{aligned} \chi_s^{(3)}(q|p_1|p_2|k) &= i \frac{\omega^2}{c^2} \frac{\varepsilon_0 - \varepsilon}{\alpha_0(q) + \alpha(q)} \left\{ \alpha^2(q) + 2\alpha(q)\alpha(k) + \alpha_0^2(q) + 3 \frac{\omega^2}{c^2} \frac{\varepsilon_0 - \varepsilon}{\alpha_0(p_1) + \alpha(p_1)} [\alpha(p_1) + \alpha(k)] \right. \\ &\quad \left. + 3 [\alpha(q) - \alpha_0(p_1)] + 2 \frac{\omega^2}{c^2} \frac{\varepsilon_0 - \varepsilon}{\alpha_0(p_1) + \alpha(p_1)} \frac{\omega^2}{c^2} \frac{\varepsilon_0 - \varepsilon}{\alpha_0(p_2) + \alpha(p_2)} \right\} \frac{2\alpha_0(k)}{\alpha_0(k) + \alpha(k)} \end{aligned} \quad (\text{B2c})$$

With these expressions we close this appendix.

---

[1] Lord Rayleigh, Proc. R. Soc. London Ser. A **79**, 399 (1907).

- [2] Lord Rayleigh, *The theory of sound*, (Dover, New-York, 1945).
- [3] L. I. Mandel'shtam, *Ann. Physik* **41**, 609 (1913).
- [4] S. O. Rice, *Commun. Pure Appl. Math.* **4**, 351 (1951).
- [5] P. Beckmann and A. Spizzichino, *The scattering from electromagnetic waves from rough surfaces*, (Artech House, 1963).
- [6] J. A. Ogilvy, *Theory of wave scattering from random rough surfaces*, (IOP Pub., Bristol, UK, 1991).
- [7] A. G. Voronovich, *Wave scattering from rough surfaces*, (Springer Verlag, 1994).
- [8] M. Nieto-Vesperinas, *Scattering and diffraction in physical optics*, (John Wiley & Sons, New York, 1991).
- [9] C. S. West and K. A. O'Donnell *J. Opt. Soc. Am. A* **12**, 390 (1995).
- [10] M. Born and E. Wolf, *Principles of optics : electromagnetic theory of propagation, interference and diffraction of light*, 7th (expanded) edition, (Cambridge University Press, Cambridge, 1999).
- [11] J. A. Kong, *Electromagnetic Wave Theory*, 2nd edition (John Wiley & Sons, New York, 1990).
- [12] S. Ross, *Introduction to Probability Models*, 6th edition, (Academic Press, San Diego, 1997).
- [13] W. Feller, *an Introduction to Probability Theory and its Applications* Vol. 1, 3rd edition (John Wiley & Sons, New York, 1968).
- [14] W. Feller, *an Introduction to Probability Theory and its Applications* Vol. 2, 2nd edition (John Wiley & Sons, New York, 1971).
- [15] E. Parzen, *Stochastic processes*, (Holden-Day, San Francisco, 1962).
- [16] A. Papoulis, *Probability, random variables, and stochastic processes*, 2nd edition, (McGraw-Hill, New York, 1984).
- [17] A. Papoulis, *Probability and statistics*, (Prentice Hall, Englewood Cliffs, NJ, 1990).
- [18] A. Mendaza-Suárez and E. R. Méndez, *Opt. Commun.* **134**, 241 (1997).
- [19] A. A. Maradudin and T. Michel, *J. Stat. Phys.* **58**, 485 (1990).
- [20] S. West and K. A. O'Donnell, *J. Opt. Soc. Am. A* **12**, 390 (1995).
- [21] A. A. Maradudin, T. Michel, A. R. McGurn, and E. R. Méndez, *Ann. Phys.* **203**, 255 (1990).
- [22] V. Freilikher, E. Kanzieper, and A. A. Maradudin, *Phys. Rep.* **288**, 127 (1997).
- [23] P. Meakin, *Phys. Rep.* **235**, 189 (1993).
- [24] L. Barabasi and H. E. Stanley, *Fractal Growth Models* (Cambridge University Press, Cambridge, 1995).
- [25] P. Meakin, *Fractals, scaling and growth far from equilibrium*, (Cambridge University Press, 1998).
- [26] E. Bouchaud, G. Lapasset and J. Planès, *Europhys. Lett.* **13**, 73 (1990).
- [27] J. Schmittbuhl, Ph.D. thesis, Université Paris 6, (1994).
- [28] A. Hansen and O. M. Nes, *IKU Report*, unpublished, 1997.
- [29] F. Plouraboué and M. Boehm, *Trib. Int.* **32**, 45 (1999).
- [30] T. Vicsek, M. Cserző and V. K. Horváth, *Physica A* **167**, 315 (1990).
- [31] T. Vicsek, *Fractal growth phenomena*, 2nd edition, (World Scientific, Singapore, 1992).
- [32] J. Feder, *Fractals* (Plenum, New York, 1988).
- [33] B. B. Mandelbrot, *The fractal geometry of nature*, (Freeman, 1975).
- [34] J. D. Jackson, *Classical electrodynamics*, 3rd edition, (John Wiley & Sons, New York, 1999).
- [35] O. Keller (ed.), *Nonlinear optics in solids*, Springer-Verlag, Berlin, 1990.
- [36] A. A. Maradudin, in *Surface Polaritons—Electromagnetic Waves at Surfaces and interfaces*, ed. V. M. Agranovich and D. L. Mills, (North-holland Publishing Company, 1982).
- [37] A. A. Maradudin, R. F. Wallis, and L. Dobrzynski, *Handbook of Surfaces and interfaces, Volume 3: Surface Phonons and Polaritons*, (Garland STPM Press, 1980).
- [38] C. Kittel, *Introduction to solid state physics*, 7th edition, (John Wiley & Sons, New York, 1996).
- [39] M. Abramowitz and I. A. Stegun, *Handbook of Mathematical Functions*, (Dover, New York, 1964).
- [40] W. H. Press, S. A. Teukolsky, W. T. Vetterling and B. P. Flannery, *Numerical Recipes in fortran*, 2nd edition, (Cambridge University Press, Cambridge, 1992).
- [41] G. H. Golub and C. F. Van Loan, *Matrix Computation* 3rd edition (The John Hopkins University Press, Baltimore, 1996).
- [42] A. Madrazo and A. A. Maradudin, *Opt. Commun.* **134**, 251 (1997).
- [43] N. R. Hill, V. Celli, *Phys. Rev. B* **17**, 2478 (1978).
- [44] F. Toigo, A. Marvin, V. Celli, and N. R. Hill, *Phys. Rev. B* **15**, 5618 (1977).
- [45] T. A. Leskova, A. A. Maradudin, M. Levay-Lucero, and E. R. Méndez, *Multiple-scattering effects in the second harmonic generation of light in reflection from a randomly rough metal surface* (To appear *Ann. Phys.*).
- [46] A. Shchegrov, Ph.D. thesis, University of California, Irvine, (1998).
- [47] R. Newton, *Scattering Theory of Waves and Particles*, 2nd edition, (Springer-Verlag, Heidelberg, 1982).
- [48] G. C. Brown, V. Celli, M. Coopersmith, and M. Haller, *Surf. Sci.* **129**, 129 (1983).
- [49] G. C. Brown, V. Celli, M. Haller, and A. Marvin, *Surf. Sci.* **136**, 381 (1984).
- [50] G. Brown, V. Celli, M. Haller, A. A. Maradudin, and A. Marvin, *Phys. Rev. B.* **31**, 4993 (1985).
- [51] K. A. O'Donnell, C. S. West, and E. R. Méndez, *Phys. Rev. B* **57**, 13207 (1998).
- [52] J. A. Sánchez-Gil, A. A. Maradudin, and E. R. Méndez, *J. Opt. Soc. Am.* **12**, 1547 (1995).
- [53] T. N. Antsygina, V. D. Freylikher, S. A. Gredeskul, L. A. Pustur, and V. A. Slusarev, *Journal of Electromagnetic Waves and Applications* **5**, 873 (1991).
- [54] A. R. McGurn, A. A. Maradudin, and V. Celli, *Phys. Rev. B* **31**, 4866 (1985).
- [55] A. A. Maradudin and E. R. Méndez, *Appl. Opt.* **32**, 3335 (1993).
- [56] P. M. Morse and H. Feshbach, *Methods of Theoretical Physics*, Part 1 and 2, (McGraw-Hill, New York, 1953).
- [57] E. I. Thorsos and D. R. Jackson, *J. Ac. Soc. Am.* **66**, 261 (1989).

- [58] M. F. Chen, S. C. Wu, A. K. Fung, *J. Wave-Material Interaction* **2**, 9 (1987).
- [59] M. C. W. van Rossum and Th. M. Nieuwenhuizen, *Rev. Mod. Phys.* **71**, 313 (1999).
- [60] A. Lagendijk and B. A. van Triggelen, *Phys. Rep.* **270**, 143 (1996).
- [61] A. R. McGurn, A. A. Maradudin, *Opt. Commun.* **72**, 279 (1989).
- [62] E. R. Méndez and K. A. O'Donnell, *Opt. Comm.* **61**, 91 (1987).
- [63] K. A. O'Donnell and E. R. Méndez, *J. Opt. Soc. Am. A* **4**, 1194 (1987).
- [64] M. Nieto-Vesperinas and J. M. Soto-Crespo, *Opt. Lett.* **12**, 979 (1987).
- [65] V. Freilikher, M. Pustilnik, and I. Yurkevich, *Phys. Lett. A* **193**, 467 (1994).
- [66] V. Freilikher, M. Pustilnik, I. Yurkevich, and A. A. Maradudin, *Opt. Commun.* **110** 263 (1994).
- [67] A. R. McGurn, A. A. Maradudin, and R. F. Wallis, *Waves in Random Media* **1**, 43 (1991).
- [68] Jun Q. Lu, A. A. Maradudin, and T. Michel, *J. Opt. Soc. Am. B* **8**, 311 (1991)
- [69] J. A. Sánchez-Gil, A. A. Maradudin, Jun Q. Lu, V. D. Freilikher, *Phys. Rev. B* **51**, 17100 (1995).
- [70] J. A. Sánchez-Gil, A. A. Maradudin, Jun Q. Lu, V. D. Freilikher, M. Pustilnik, and I. Yurkevich, *Phys. Rev. B* **50**, 15353 (1994).
- [71] J. A. Sánchez-Gil, A. A. Maradudin, Jun Q. Lu, and V. R. Freilikher, *J. Mod. Opt.* **43**, 435 (1995).
- [72] P. W. Anderson, *Phys. Rev.* **109**, 1492 (1958).
- [73] P. Sheng, *Introduction to Wave Scattering, Localization, and Macroscopic Phenomena* (Academic Press, New York, 1995).
- [74] P. Sheng, *Scattering and Localization of classical Waves in Random Media*, (World Scientific, Singapore, 1990).
- [75] N. Mott, *Metal-insulator transitions*, (Taylor and Francis, London, 1990).
- [76] A. Lagendijk and B. van Tiggelen, *Phys. Rep.* **270**, 143 (1996).
- [77] D. S. Wiersma, P. Bartolini, A. Lagendijk, and R. Righini, *Nature* **390**, 671 (1997).
- [78] J.C. Dainty (Ed.), *Laser Speckle and Related Phenomena* (Springer-Verlag, Berlin 1975).
- [79] S. Feng, C. Kane, P. A. Lee, and A. D. Stone, *Phys. Rev. Lett.* **61**, 834 (1988).
- [80] I. Freund and M. Rosenbluh, *Optics Commun.* **82**, 362 (1991).
- [81] M. P. van Albada, J. F. de Boer, and A. Lagendijk, *Phys. Rev. Lett.* **64**, 2787 (1990).
- [82] F. Scheffold and G. Maret, *Phys. Rev. Lett.* **81**, 5800 (1998).
- [83] B. Shapiro, *Phys. Rev. Lett.* **57**, 2168 (1986).
- [84] N. Garcia and A. Z. Genack, *Phys. Rev. Lett.* **63**, 1678 (1989).
- [85] R. Kubo, *Phys. Soc. Japan* **17**, 1100 (1962).
- [86] R. K. Pathria, *Statistical Mechanics*, 2nd editiod, (Butterworth-Heinemann, Oxford, 1996)
- [87] A. Arsenieva and S. Feng, *Phys. Rev. B* **47**, 13047 (1993).
- [88] L. B. Felsen and N. Marcuvitz, *Radiation and Scattering of Waves*, (Prentice-Hall, Inc., Engelwood Cliffs, New Jersey, 1973).
- [89] C. S. West and K. A. O'Donnell, *Phys. Rev B* **59**, 2393 (1999).
- [90] V. Malyshkin, A.R. McGurn, T.A. Leskova, A.A. Maradudin, and M. Nieto-Vesperinas, *Opt. Lett.* **22**, 946 (1997).
- [91] V. Malyshkin, A. R. McGurn, T. A. Leskova, A. A. Maradudin, and M. Nieto-Vesperinas, *Waves in Random Media* **7**, 479 (1997).
- [92] A. R. McGurn and A. A. Maradudin, *Opt. Commun.* **155**, 79 (1998).
- [93] J. W. Goodman, *Statistical Optics* (Wiley, New York, 1985).
- [94] J. W. Goodman, *Optics Commun.* **14**, 324 (1975).
- [95] K. A. O'Donnell and R. Torre, *Opt. Comm.* **138**, 341 (1997).
- [96] M. Leyva-Lucero, E. R. Méndez, T. A. Leskova, and A. A. Maradudin, *Opt. Commun.* **161**, 79 (1999).
- [97] E. R. Méndez, A. G. Navarrete and R. E. Luna, *J. Opt. Soc. Am. A* **12**, 2507 (1995).
- [98] N. Bloembergen, R. K. Chang, S. S. Jha, and C. H. Lee, *Phys. Rev.* **174**, 813 (1968).
- [99] D. Maystre and M. Nevière, *Appl. Phys. A* **39**, 115 (1986).
- [100] E. G. Liska and J. J. McCoy, *J. Acoust. Soc. Am.* **71**, 1093 (1982).
- [101] A. Sentenac and A. A. Maradudin, *Waves in Random Media* **3**, 343 (1993).
- [102] K. A. O'Donnell, R. Torre, and C. S. West, *Opt. Lett.* **21**, 1738 (1996).
- [103] A. R. McGurn, V. M. Agranovich, and T. A. Leskova, *Phys. Rev. B* **44**, 11441 (1991).
- [104] M. Leyva-Lucero, E. R. Méndez, T. A. Leskova, A. A. Maradudin, and J. Q. Lu, *Opt. Lett.* **21**, 1809 (1996).
- [105] T. A. Leskova, A. A. Maradudin, M. Leyva-Lucero, and E. R. Méndez, *Phys. Rev. B* (in preparation).
- [106] J. A. Sánchez-Gil and M. Nieto-Vesperinas, *J. Opt. Soc. Am. A* **8**, 1270 (1991).
- [107] A. Sommerfeld, *Optics*, (Academic Press, 1954).
- [108] A. R. McGurn and A. A. Maradudin, *Waves in Random Media* **6**, 251 (1996).
- [109] A. R. McGurn and A. A. Maradudin, *J. Opt. Soc. Am. B* **4**, 910 (1987).
- [110] P. Tran and A. A. Maradudin, *Opt. Commun.* **110**, 269 (1994).
- [111] J. M. Elson, *Phys. Rev. B* **30**, 5460 (1984).
- [112] J. M. Elson, J. M. Bennett, and J. C. Stove, *Appl. Opt.* **32**, 3362 (1993).
- [113] K. Pak, L. Tsang, and C. H. Chan, *Radio Science* **28**, 331 (1993).
- [114] J. M. Elson, *Waves in Random Media* **7**, 303 (1997).
- [115] M. Pascual, W. Zierau, T. Leskova, and A. A. Maradudin, *Opt. Commun.* **155**, 351 (1998).
- [116] N. W. Ashcroft and N. D. Mermin, *Solid State Physics*, (Saunders College, Philadelphia, 1976).
- [117] A. V. Tutov, A. A. Maradudin, T. A. Leskova, A. P. Mayer, and J. A. Sánchez-Gil, *Phys. Rev. B* **60**, 12692 (1999).
- [118] A. A. Maradudin, I. Simonsen, T. A. Leskova, and E. R. Méndez, *Physica B* **296**, 85 (2001).



- [119] T. A. Leskova, I. Simonsen, and A. A. Maradudin, *Waves Random Media* **12**, 307 (2002).
- [120] I. Simonsen, A. A. Maradudin, and T. A. Leskova, *SPIE* **3784**, 218 (1999).
- [121] I. Simonsen and A. A. Maradudin, *Opt. Commun.* **162**, 99 (1999).
- [122] I. Simonsen, T. A. Leskova, A. A. Maradudin, and O. Hunderi, *SPIE* **4100**, 65 (2000).